RIIKKA MIKKONEN

Studies of Low Surface Energy Materials for Printed Electronics Applications

RIIKKA MIKKONEN

Studies of Low Surface Energy Materials for Printed Electronics Applications

ACADEMIC DISSERTATION
To be presented, with the permission of
the Faculty of Information Technology and Communication Sciences
of Tampere University,
for public discussion in the auditorium TB109
of the Tietotalo, Korkeakoulunkatu 1, Tampere,
on 17 June 2022, at 12 o'clock.

ACADEMIC DISSERTATION
Tampere University, Faculty of Information Technology and Communication Sciences
Finland

Responsible supervisor and Custos	Professor Matti Mäntysalo Tampere University Finland	
Pre-examiners	Associate professor Wai Yee Yeong Nanyang Technological University Singapore	Associate professor Johan Sidén Mid Sweden University Sweden
Opponent	Associate professor Wim Deferme Hasselt University Belgium	

The originality of this thesis has been checked using the Turnitin OriginalityCheck service.

Cover design: Roihu Inc.

PREFACE

The initial spark for this work came from my supervisor, Professor Matti Mäntysalo, who first introduced me to the fascinating field of printed electronics all those years ago when he supervised my B.Sc. thesis. Later, he offered me an opportunity to prepare my M.Sc. thesis in his group, and there was no turning back. Thus, I would like to express my gratitude to him for this opportunity, not forgetting his guidance and support throughout all these years.

I am also profoundly grateful for all the co-authors, especially for M.Sc. Paula Puistola and D.Sc. Anastasia Koivikko: million thanks for those seemingly never-ending hours in the lab. D.Sc. Mari Honkanen and D.Sc. Turkka Salminen from the Tampere Microscopy Center always worked miracles with my challenging samples; thank you for that.

The ups and downs of the journey should be shared with someone, and I feel privileged for having been able to do that with the most amazing co-workers (and friends). Special thanks to D.Sc. Tiina Vuorinen, D.Sc. Juha Niittynen, D.Sc. Mika-Matti Laurila, D.Sc. Milad Mosallaei, D.Sc. Behnam Khorramdel, D.Sc. Suvi Lehtimäki, D.Sc. Marika Janka, D.Sc. Jari Keskinen, M.Sc. Teemu Salo, M.Sc. Hanna Christophliemk, M.Sc. Anna Railanmaa, M.Sc. Karem Lozano Montero, and M.Sc. Vänni Panula.

Lastly, I want to thank my family, friends, and my dearest, Pentti, for their love and unfaltering support. This would not have been possible without you. Kiitos.

Tampereella 4.5.2022

Riikka Mikkonen

ABSTRACT

Printed electronics have gained steadily increasing attention due to the attractive simplicity and straightforwardness of the processes. The processes are also compatible with various flexible and stretchable materials. Thus, they can be used to create lightweight, unobtrusive, and conformable devices. However, there are certain challenges related to material compatibility. For example, hydrophobic materials with low surface energies tend to repel liquid coatings, prohibiting straightforward manufacturing. Therefore, substrate materials with beneficial properties like chemical inertness, elasticity, optical transparency, or robustness may be neglected because processing can become exhaustively complicated.

In this thesis, two water-repelling polymers, a poly(phenylene ether) (PPE) based polymer blend and poly(dimethylsiloxane) (PDMS) were studied. Furthermore, their applicability in printed electronics was investigated. These studies began with surface characterization. In addition, conductive tracks were printed and evaluated on PPE and PDMS substrates by screen printing silver (Ag) flake inks and inkjet printing silver nanoparticle (Ag NP) inks, respectively. The performance of the screen-printed Ag patterns was evaluated on both the native and surface-treated substrates, and the endurance against environmental stress was studied in accelerated aging tests. After developing an inkjet printable PDMS ink, alternative approaches for multilayer fabrication on this substrate were proposed. First, direct layer-by-layer inkjet deposition of conductive and dielectric layers on PDMS was studied. In the second approach, conductive and dielectric layers were printed separately on mesh-like electrospun poly(vinyl alcohol) (PVA) nanomesh substrates to form self-standing layers, which were sandwiched to create capacitive pressure sensor elements.

The results indicate that conductive tracks can be printed on both substrates relatively straightforwardly. Highly conductive lines could be screen printed with only a single pass, the resulting sheet resistance being only 8-10 $m\Omega \cdot \square^{-1}$. However, a comprehensive understanding of ink composition and printing parameters is required to minimize the prints' surface roughness and edge roughness. In addition, as new screens are needed for each new pattern, prototyping with this method is time-consuming. Finally, the environmental reliability of the screen printed patterns was

heavily dependent on the used materials, and the results emphasize the need for proper encapsulation.

In comparison, prototyping was relatively easy by inkjet printing the functional materials directly on PDMS, and sheet resistances below 0.5 $\Omega \cdot \square^{-1}$ were obtained, even though print thickness was less than 2 μm. Although the sheet resistance of the porous, PVA-based conductive layers was higher (3 $\Omega \cdot \square^{-1}$) despite the high layer thickness of 10 μm, the obtained adhesion between the ink and the substrate was excellent. Intermediate surface treatments and curing steps of the direct layer-by-layer multilayer deposition approach made the printed patterns susceptible to deformation already during the fabrication process, requiring a new patterning strategy and curing condition optimization to prevent the defects. The integrated PVA layer made the self-standing dielectric easy to handle despite its low thickness. The capacitive sensors had linear sensitivity of up to 4 Mpa^{-1} with low hysteresis (< 8.5 %), remained functional over 2000 cycles, and were capable of sensing physical interactions with the surroundings.

It was shown that simple processes could be used to print electronics even on hydrophobic substrates. Moreover, multilayered device configurations can be prototyped using just one material printer, either by a direct, layer-by-layer deposition or using separately printed functional layers to build devices, such as sensors. The presented results provide a reference point to further studies, which should determine the full potential and usability of the proposed materials and methods in complex printed electronic applications where both circuits and sensor elements are used in various device configurations.

CONTENTS

List of Tables

ABBREVIATIONS AND SYMBOLS

3D	Three-dimensional
AgCl	Silver chloride
C	Capacitance
C_r	Relative capacitance
CIJ	Continuous inkjet
CTE	Coefficient of thermal expansion
CNT	Carbon nanotube
d	Density
D	Nozzle diameter
DI	Deionized
DIW	Direct ink writing
DoD	Drop-on-demand
dpi	Dots per inch
E-jet	Electrohydrodynamic jetting
E-skin	Electronic skin
FDM	Fused deposition modeling
FIB	Focused ion beam
IBA	Isobutyl acetate
IC	Integrated circuit
IoT	Internet of Things
KOH	Potassium hydroxide
l	length
LCP	Liquid crystal polymer
MID	Molded interconnect device
MPTMS	(3-mercaptopropyl)trimethyl siloxane
N_2	Nitrogen
NaCl	Sodium chloride
NIR	Near-infrared
NP	Nanoparticle
O_2	Oxygen

OA	Octyl acetate
OFET	Organic field-effect transistor
Oh	Ohnesorge number
OLED	Organic light-emitting diode
OPV	Organic photovoltaic
PCB	Printed circuit board
PDMS	Poly(dimethylsiloxane)
PANI	Polyaniline
PEDOT: PSS	Poly(3,4-ethylene dioxythiophene: poly(styrene sulfonate))
PET	Poly(ethylene terephthalate)
PEN	poly(ethylene naphthalate)
PI	Polyimide
PPE	Poly(phenylene ether)
PS	Polystyrene
PU	Polyurethane
PVA	Poly(vinyl alcohol)
R2R	Roll-to-roll
R_q	Root-mean-square roughness
R_s	Sheet resistance
R_t	Peak-to-peak roughness
Re	Reynolds number
RH	Relative humidity
RFID	Radio-frequency identification technology
RMS	Root-mean-square
S	Sensitivity
SAM	Self-assembled monolayer
SEM	scanning electron microscopy
t	Thickness
T_g	Glass transition temperature
TENG	triboelectric nanogenerator
TFT	Thin-film transistor
UV	Ultraviolet
UVO	Ultraviolet/Ozone
v	Velocity
wt%	Weight percentage
w	Width

We	Weber number
Z	Z-number
γ_l	Surface tension of a liquid
γ_s	Surface energy of a solid
ε_r	Relative permittivity
η	Viscosity
θ	Contact angle
ρ	Resistivity

ORIGINAL PUBLICATIONS

Publication I   Mikkonen, R. & Mäntysalo, M., 2018, "Benchmark study of screen printable silver inks on a PPE based substrate" in 2017 21st European Microelectronics and Packaging Conference (EMPC) & Exhibition [189] IEEE.

Publication II   Mikkonen, R. & Mäntysalo, M., 2018, "Evaluation of screen printed silver trace performance and long-term reliability against environmental stress on a low surface energy substrate", Microelectron. Reliab., vol. 86, pp. 54-65.

Publication III   Mikkonen, R., Puistola, P., Jönkkäri, I. & Mäntysalo, M., 2020, "Inkjet printable polydimethylsiloxane for all-inkjet-printed multilayered soft electrical applications", ACS Appl. Mater. Interfaces, vol. 12, no. 10, pp. 11990-11997.

Publication IV   Mikkonen, R. & Mäntysalo, M., 2020, "Inkjettable, polydimethylsiloxane based soft electronics" in FLEPS 2020 - IEEE International Conference on Flexible and Printable Sensors and Systems [9239558] IEEE.

Publication V   Mikkonen, R., Koivikko, A., Vuorinen, T., Sariola, V. & Mäntysalo, M., 2021, "Inkjet-printed, nanofiber-based soft capacitive pressure sensors for tactile sensing", IEEE Sens. J., vol. 21, no. 23, pp. 26286-26293.

1   INTRODUCTION

In the modern world, we are enjoying such a generosity of electrical devices and artificial intelligence solutions that it is almost too easy to forget how only a few decades ago, some of these innovations were regarded merely as science fiction [1]–[3]. This rapid evolution of electronics is thanks to miniaturization and would have been impossible without: first, the industrial printed circuit board (PCB) manufacturing that began in the 1940s; second, the silicon-based semiconductor transistors and integrated circuits (ICs), which were invented in the 1950s [4], and third, the advanced processes like lithography, where the achieved minimum feature size is only a few nanometers [5], [6]. Even though the conventional technologies have gotten us so far, their era, at least at the current scale, might be soon over for several reasons.

First, these conventional processes are often rather complex, employing a multitude of process steps [7]. These subtractive methods require the usage of hazardous etching chemicals and produce a large amount of waste material. Furthermore, the suitability of the conventional PCBs for the new Internet of Things (IoT) devices in a digitalized, intelligent environment is limited since they often are rigid and brittle. Thus, they lack conformability, which is required to integrate the electronics seamlessly to our surroundings, rather than just piling up new portable devices with different functions.

Truly conformable, i.e., flexible, stretchable, and easily moldable electronics could have great potential in many applications, such as wearable devices, display technology, or molded interconnect devices (MID). For example, form-fitting wearable solutions could make patient monitoring more unobtrusive, easily affordable, and better available. Alternatively, in the case of MIDs, conformable structures could be used to create custom-made modules, which also help reduce the electrical devices' weight and required space. Furthermore, setting up traditional production facilities requires tremendous effort and investments, and the space for competition and innovations is limited. Scaling up new, less expensive technologies could spark rapid development of entirely new electrical applications, which, in their turn, may sound like mere science fiction today.

For all these reasons, academia and industry are looking for alternative fabrication methods and materials to realize future electronics applications. One solution could be printed electronics, where electronics are merged with various printing technologies. Even though the minimum feature sizes are still several orders of magnitude higher than those of the conventional methods (> 100 nm) [8], [9], printing methods allow large-area fabrication of conformable electronics to the degree that is not possible with the traditional, wafer-based technologies. These alternative processes aid in expanding the variety of material options. They also provide a technological platform for fabricating individual, highly customizable devices and even for roll-to-roll (R2R) mass production.

1.1   Aims and scope of the thesis

The printed electronics fabrication relies on direct patterning of circuit layouts on a substrate. Since patterning is done by depositing the functional materials to the target substrate in a liquid ink form, the inks must be post-processed to obtain coatings with the desired functionalities. This approach sets some basic requirements for the used materials, such as sufficient ink flow on the substrate to enable patterning. In addition, the thermal properties, chemical compatibility, level of softness, and thickness of the substrate should fit the process requirements. These restrictions become essential, especially in flexible and stretchable electronics, where polymers are often used to make the devices conformable.

Polymers like poly(tetrafluoroethylene) (PTFE) and poly(dimethylsiloxane) (PDMS) possess various attractive characteristics for conformable electronics, such as low flammability, chemical inertness, optical transparency, elasticity, low dielectric constant, and triboelectricity – to name a few. These materials' perhaps the most characteristic property is the low surface energy, making them attractive for self-cleaning or barrier coatings. However, it limits their use in printed electronics applications because the hydrophobic surface is challenging to coat without exhaustive pre-treatment steps. Intrinsically, these substrates will repel water (and many other liquids), causing it to bead up on the polymer surface instead of spreading. This thesis seeks to offer new solutions for straightforward printed electronics fabrication on hydrophobic substrates: first, on a poly(phenylene ether) (PPE) based polymer blend (Preperm® L260), and second, on PDMS (Sylgard 184).

The first research question is related to the material compatibility in general: can these hydrophobic substrates be coated using functional inks in a simple process, i.e.,

what would be the minimum of the required process steps (**Publications I–V**)? It is known that some hydrophobic surfaces tend to recover their native surface characteristics over time, despite the initial modification of the surface by a specific treatment. However, it is also possible to weaken or permanently damage the substrate surface if the used surface treatment is too harsh. Moreover, as the aim of printing methods is to simplify the device fabrication, there is no point in utilizing exhaustingly complex processes. The poor ink adhesion on phobic substrates is a well-known, serious issue. Without a sufficient level of adhesion, the patterns will delaminate from the substrate, and thus the functionalities are lost. Maintaining the desired level of adhesion in various environments and use conditions can be more difficult than maintaining the electrical properties. Therefore, one of the research questions here is maintaining sufficient ink adhesion (**Publications I–V**). Secondly, is it possible to retain good adhesion even in a harsh environment (**Publication II**)?

Preperm® L260 can be shaped by injection molding or extrusion, both of which, in a sense, are methods that could be applied in all-printed electronics as such, but the options for printing PDMS were very limited by the time this work began. Therefore, the next main question lies in the processing options of PDMS: can it be patterned additively using an existing printing machine (**Publication III–V**)? Additive printability of various functional materials is of the essence in all-printed electrical applications since the on-demand deposition of the material layers will help to reduce device thickness and allows material layering without additional molds, masks, or punching tools. Ideally, material compatibility with the existing printing machines would enable simple and straightforward multi-material processing within a single printer.

The related research questions extend the previous questions: is it possible to use PDMS as a dielectric in all-inkjet-printed electrical applications (**Publications III–V**)? The topic is complex, and the issues of interest here begin with optimizing the patterning strategy: how to add layers to the device when direct printing of functional layers on top of the PDMS dielectric is assumed to require a surface treatment in each phase? Furthermore, how might the intermediate curing steps affect the process (**Publications III and IV**)? Alternatively, can some other strategy be used to make self-standing, multilayered, fully printed PDMS-based electronics (**Publication V**), and what would be the advantages or limitations of the different approaches? Below a summary of the presented research questions is given:

- Is it possible to print electronics onto PPE and PDMS substrates in a simple, straightforward manner, and what would be the minimum of process steps required?
- Do the prints adhere to the substrate?
- Do harsh environmental conditions (humidity and salt) affect the performance?
- Can PDMS be patterned additively using an electronics printer?
- Is it possible to use PDMS as a dielectric in all-inkjet-printed electrical applications?
- How to add layers to the device when printing other functional layers on top of the PDMS dielectric is assumed to require a surface treatment in each phase?
- Do the intermediate curing steps affect the process?
- Is it possible to fabricate self-standing PDMS sheets by inkjet printing?
- Would another strategy enable fabrication without the previous concerns?
- What are the advantages and limitations of the different approaches?

1.2   Structure of the thesis

This thesis consists of a summary, three peer-reviewed journal publications, and two peer-reviewed conference articles. The summary is divided into four chapters and a conclusion. Chapter 1 gives a brief introduction to the broader context and the aims and scope of the thesis, presents the thesis structure and states the author's contribution to all publications. Chapter 2 is dedicated to printed electronics: fabrication technologies and materials, and lastly, the thesis' aims and scope are discussed in reflection on the background survey. Moving forward, Chapter 3 briefly explains the material choices and methods used in this thesis, and in Chapter 4, the obtained main results are presented and discussed. Finally, Chapter 5 will conclude the work done, summarizing the main findings, and placing them in a broader context. The original publications are appended at the end of the thesis.

1.3 The author's contribution

Publication I. The author was the main contributor, designed and performed the experiments related to substrate surface analysis, printing, and characterization of the printed structures. In addition, the author analyzed the measurement data. M. Mäntysalo supervised the research and participated in experiment design and data analysis. The manuscript and figures were prepared by the author. Both the author and M. Mäntysalo participated in writing and improving the manuscript.

Publication II. The author was the main contributor who designed and performed the experiments related to substrate surface analysis, printing, and characterization of the printed structures. The author designed and executed the reliability tests with Janne Kiilunen and Juha Pippola. In addition, the author analyzed the measurement data. M. Mäntysalo supervised the research and participated in experiment design and data analysis. The author prepared the article, which was improved together with M. Mäntysalo.

Publication III. The author was the main contributor and designed the experiments for the dielectric ink preparation and characterization. The author and I. Jönkkäri executed ink characterization experiments: the author measured the surface tension of the inks, and I. Jönkkäri performed the viscosity measurements. The author designed the test structures, which the author fabricated and characterized with P. Puistola. The Raman and FIB-SEM imaging were conducted at the Tampere Microscopy Center (TMC). The author analyzed the data and wrote the manuscript, which was revised and improved by other writers.

Publication IV. The author was the main contributor and designed, fabricated, and measured the test structures with the assistance of P. Puistola. The manuscript was written and revised by the author and M. Mäntysalo.

Publication V. The author was the main contributor who designed and fabricated the test structures together with T. Vuorinen, who was responsible for electrospinning and wrote a chapter about this topic for the manuscript. The author was also responsible for the characterization of the prints. A. Koivikko and the author conducted the sensor measurements and analyzed the results with other writers. FIB-

2 PRINTED ELECTRONICS

Printed electronics is a family of technologies merging electronics fabrication and traditional graphics or textile printing methods: the functional ink is deposited on a substrate to create interconnected electrical devices. Even though this method has been mentioned already in the earliest PCB patents at the beginning of the 20th century [10], and some consumer electronics applications already exist, the large-scale development started only at the end of the 20th century. After the discovery of conductive polymers and the resulting innovations of organic field-effect transistors (OFETS) [11], organic photovoltaics (OPVs) [12], and organic light-emitting diodes (OLEDs) [13], researchers started to attempt solution processing of these new materials, since they could easily be used in ink form. Thus, inexpensive electronics could be produced on a massive scale simply by printing [14]–[17].

The potential of this new technology family did not go unnoticed, and printed electronics started to emerge as an independent field following the development of inorganic nanomaterials. These nanoscale materials could be used in ink formulations, and thus, for example, conductive, semiconductive, and dielectric materials were merged with printing methods [18]–[24], and the printed electronics became a reality. Since then, the number of annual publications has been increasing tremendously, and several fields have adopted these fabrication technologies [7], [25].

This popularity in both industry and academia is thanks to the advantageous key features of this technology family, including large-area manufacturing capabilities, freedom of substrate choice, the additive nature, and low processing temperatures. Since the earliest innovations in the field, the development has been rapid. The latest advances include electronic skin (E-skin) for bioelectronics, nanogenerators, and self-healing electronics [26]–[28].

2.1 Fabrication technologies

In **Table 1**, PE methods gravure, (reverse) offset, flexographic, screen, inkjet, electrohydrodynamic jetting (E-jet), aerosol, and three-dimensional (3D) printing are presented together with their key characteristics. The key elements here are line width,

thickness, printing speed, and ink viscosity. All techniques are of a different nature, and therefore, the compatible materials are unique for each method. Thus, the distinct process characteristics also lead to different process outputs. Therefore, the technique selection is dependent on both the desired outcome and the used materials.

For example, most traditional printing techniques are contact methods, where a patterned printing plate (flexo, gravure, offset) or a stencil (screen) is first tinted with ink, and the desired image is pressed on the substrate. There are some variations in the contact time and the required pressure. For example, in gravure printing the pattern is engraved on the printing plate. This characteristic enables high printing speed with rather thin inks, and the resolution is relatively high compared to the other printing methods [29]. However, the plate must be in contact with the substrate for the entire printing cycle, and high pressure is required for good image formation. This high pressure limits the choice of substrate materials because, for example, the stretchable or soft materials might deform.

In flexographic printing, the printing plate pattern is a relief raised above the plate. This technique does not require as high pressure as the former, but it compromises speed and accuracy [30]. The principle of the conventional offset printing method is somewhat similar, but the image is first printed to a blanket cylinder with the help of oil or water and then pressed to the target substrate [31]. In reverse offset printing, a semidry process is used to create the pattern on the blanket cylinder [32]. There, fine features comparable to gravure are within reach, but the speed remains low in comparison.

Of the contact methods, screen printing offers the most freedom of choice for the substrate materials. Here, the ink is forced through a patterned screen using a squeegee. The main benefit is the high aspect ratio, primarily due to the high paste viscosity. Thus, screen printing can be used for easy patterning of highly porous or rough surfaces [33]. The method is discussed in further detail below (Section 2.1.1.).

In contrast to the techniques mentioned above, inkjet printing can be regarded as a purely additive, digital printing method, where the printhead never comes to contact with the substrate, and ink is deposited as single droplets, strictly based on a digital image file that is given to the printer [29]. This technique offers more freedom for substrate selection, as they can be as soft and stretchable as demanded [30]. Even patterning of 3D-shaped objects is possible to some extent, but low ink viscosity sets some limits to the substrate curvature. Further explanation of the method is given in Section 2.1.2. Although this additive technique offers the benefit of reduced waste material compared to the previous ones, it is significantly slower, therefore, not as good an option for mass production of printed electronics.

Other digital printing techniques include E-jet printing and aerosol printing. The former relies on an external electrical field for droplet ejection [8], [34], and the latter uses aerosol to atomize functional inks [35]. These methods can be used to obtain more delicate features than the inkjet systems, and they offer a wider variety of printable materials due to the higher viscosity range. Still, the devices are rather complex, and the printing speed is also limited.

3D printing is becoming an increasingly popular method for electronics manufacturing because the interest in additively manufactured applications like MIDs is increasing [36]–[38]. Especially the extrusion-based techniques, such as fused deposition modeling (FDM) and direct ink writing (DIW), are of interest because they would allow rapid prototyping of new device configurations, possibly using just one multi-material printer. However, the current limitations of extrusion-based 3D printed electronics include resolution, scalability, and lack of multi-material printers.

Table 1. Common printing methods and their essential characteristics. [9], [34], [35], [39]–[43]

Printing method	Minimum line width (µm)	Line thickness (µm)	Printing speed (m·min^{-1})	Ink viscosity (mPa·s)
Gravure	10	0.1–1	1000	10–1000
Offset	1–10	1–10	< 1000	5–100000
Reverse-offset	0.5	0.02–1	3	1–5
Flexo	20	< 1	500	50–500
Screen	30	0.1–100	150	500–10000
Inkjet	15	0.2–10	1–500	5–50
E-jet	0.7	0.2–1.5	< 1	1000–10000
Aerosol	10	0.01–3	< 0.6	1–1000
Extrusion 3D printing	1–250	> 1	< 1	100–300000

In addition to printing methods, fabrication of the electrical devices often also requires other techniques because several functional layers are needed, and not all materials can be directly printed. These techniques can include but are not limited to: spray coating, spin coating, and electrospinning [44]–[46]. Another useful fabrication technique, which applies to the above-mentioned printing methods, is transfer printing, i.e., printing on a donor substrate, which is then used to transfer the print to the target substrate. It can be done to avoid printing directly on the target substrate, if there are compatibility issues between the materials, or if the substrate material is extremely temperature-sensitive [47]. These supportive coatings can be used, for example, to fabricate protective layers for the encapsulation of the printed devices, or they can be used to prime the substrate before printing. Moreover, these thin layers

can also be used to modify other materials, giving them additional functionalities, such as improved mechanical stability or lower resistivity.

2.1.1 Screen printing

As already shortly described above, a patterned screen is used for image formation in screen printing. The screen mesh (polyester or steel) is tensioned between the screen frames and is then covered with an emulsion to expose only the areas where the ink should be pushed through the mesh. As shown in **Figure 1**, a squeegee is used to press the ink through the screen, which shortly comes to contact with the substrate due to the applied pressure. Once the squeegee moves further on the screen and the pressure is released, the screen detaches from the substrate, now covered with fresh ink.

The final resolution (line width), print thickness, and print quality can be adjusted by manipulating both the thickness and density of the mesh threads and the emulsion properties. In addition, fabrication parameters like snap-off distance and squeegee speed significantly affect the print quality [48]–[50]. To prevent the inks from flooding through the screen before any pressure is applied, screen printing inks are highly viscous (**Table 1**), although they usually are also shear-thinning, meaning that an applied shear will thin the ink so that it can be pushed through the screen. The ink viscosity and other ink characteristics are discussed further in Section 2.3. Ink composition.

The thickness of the screen printing inks offers additional advantages. As seen in **Table 1**, the aspect ratio, i.e., the thickness of the print versus line width, is very high. It is an advantageous feature in such applications, requiring high conductivity because the large ink volume is likely to yield a low resistance. Moreover, the quality of the thick prints is less likely to suffer from substrate roughness, making it an attractive option for paper-based devices or other electronics, where a porous substrate material is needed [52]. The final aspect ratio is dependent on the ink thickness and screen properties.

There are also some limitations to this printing method. Since the screen mesh and the process parameters are of great importance for the final pattern formation, they also affect the print quality significantly [53], [54], and optimization of the process may be rather tedious. At high frequencies, the current flows nearer the conductor surface, and both edge smoothness and surface roughness become increasingly important in addition to material resistivity. However, it has been shown that this method can be

effectively used in high-frequency applications through careful parameter optimization and material selection [53], [55].
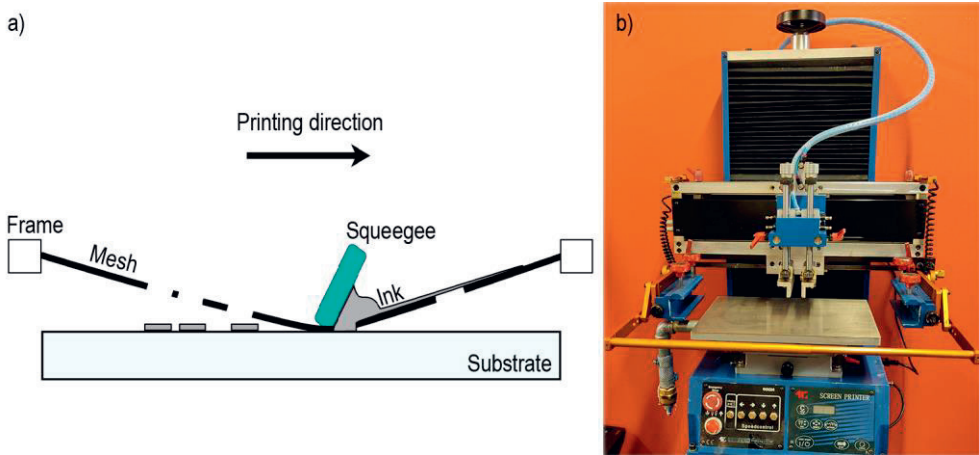
Figure 1. a) Schematic illustration of screen printing process (adapted from [51]), b) a screen printer (TIC SCF-300, DE Eickmeyer).

One disadvantage of this method is that even though it offers freedom of design compared to other contact printing methods, each new pattern configuration will require a new stencil design. Thus, the method is not necessarily as sufficient for prototyping stages as the digital methods. Therefore, the attractiveness of screen printing comes from the suitability for mass-production of large-area applications, where high conductivity is essential, but the resolution does not necessarily have to be very high (**Table 1**).

2.1.2   Inkjet printing

Since inkjet printing, like other digital and additive methods, generally allows additive on-demand fabrication and rapid modification of pattern files, the process is highly customizable. These features are highly beneficial, for example, in rapid prototyping. Inkjet printing technologies can be divided roughly into two categories: continuous inkjet (CIJ) and Drop-on-demand inkjet (DOD) printing [56]. In CIJ printing, droplets are formed continuously, and the unused droplets may be collected for reuse. The main benefits of this technique are the rapid speed and wide variety of solvents.

However, this technique cannot yield a high resolution, requires a tremendous amount of maintenance, and the use of volatile solvents makes its environmental friendliness questionable [56]. Furthermore, aggressive solvents are not compatible with sensitive polymer substrates, limiting the applicability of this technique.

In DOD printing, droplets are ejected only when instructed, based on the digital image file with the patterning information. Droplet ejection is based on a pressure pulse created in the print head. There are several methods for pulse generation, including, for example, thermal, electrostatic, and piezoelectric inkjet [56]. In thermal inkjet, droplet formation is based on the vaporization of heated ink, while electrostatic inkjet uses an electrical field.

In this work, a piezoelectric inkjet was used. Here, a piezo actuator undergoes distortion based on an applied electrical field, mechanically forming the pressure pulses that cause the droplet ejection. The principle of this method is shown in **Figure 2**. It offers freedom of material selection and long head life. However, the main drawbacks are the high expense compared to thermal inkjet and the resolution, limited by the nozzle diameter [56].
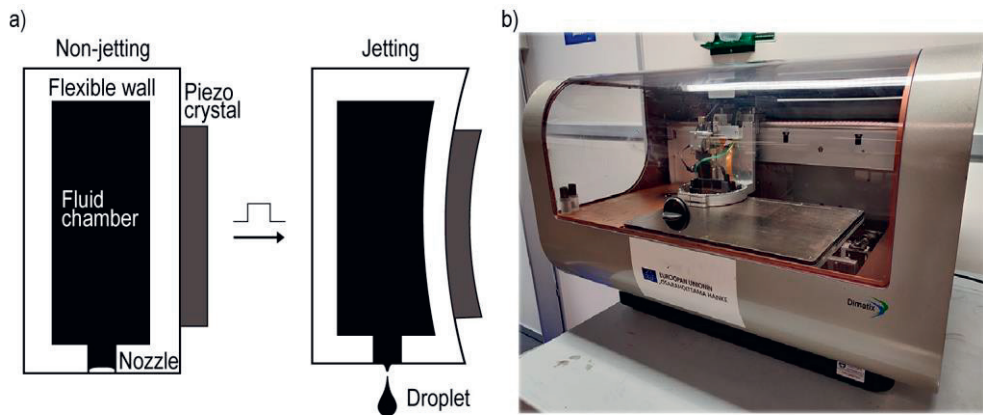
Figure 2. a) Working principle of piezoelectric printheads, b) a desktop inkjet printer (Dimatix DMP-2831, FujiFilm).

2.2   Printable materials

As interconnects form the base of all electrical circuits, tremendous effort has been put into developing electrically conductive printable materials. As a result, a wide

variety of inks and pastes is available nowadays, even commercially. Other basic materials for printed electrical devices include semiconductive materials, dielectrics, and magnetics. In addition, other functional materials such as electroactive polymers [57], [58] are used.

Since metals are known for their excellent thermal and electrical conductivity in contrast to other materials, they are widely used as the base material of the conductive printing inks. The most common metals used in the conductive printing inks are gold (Au) and silver (Ag) [59], [60]. Ag has been perhaps the most popular choice for fabricating the interconnects and electrodes of the printed devices, first, for its superior conductivity, second, for its low cost in comparison to Au, and third, for its air stability in an atmospheric environment, in comparison to some alternatives, such as aluminum (Al) or copper (Cu). However, metal oxides have their uses as semiconductors and even as dielectrics in, for example, thin-film transistors (TFTs) and gas sensors [61], [62]. To widen the variety of usable materials, alternative processes, like reactive printing, have been developed [63]–[65].

The metals in the conductive inks are often synthetized nanoparticles (NPs) or ionic precursors, as in metal-organic decomposition (MOD) inks. Low resistivities close to that of bulk material are within reach for both ink types, although there are some characteristic differences. For example, the metal load of the NP ink is typically higher, resulting in thicker, more uniform layers. In contrast, MOD inks can be used to avoid complex and exhaustive nanoparticle synthesis because the final structure is formed through a reduction reaction in the curing process [66], [67]. Other advantages of particle-free MOD inks are the simpler ink formulation without the need for additives and avoidance of nozzle clogging due to particle agglomerates. However, the substantial volume loss of the curing MOD inks makes the prints susceptible to large voids and disconnection [66], [67]. The reader should check Section 2.3.5. for further details about the post-processing step.

Even though metallic nano-inks offer superior conductivity in contrast to other printable materials, the end-applications of printed metallic films are limited due to their intrinsically dense yet brittle structure: in the more mechanically demanding applications, like stretchable electronics, where high stresses are applied to the devices, the rigidity and brittleness of the conductive structure are intolerable. Therefore, different metal compositions like nanowires (NWs), flakes, liquid metals, and metal-elastomer composites have been developed, and various engineering strategies have been utilized to improve the deformability of the printed conductive films [68]–[77]. Moreover, organic conductive materials, such as carbon nanotubes (CNTs), graphene, graphite, carbon black, and conductive polymers like polyaniline (PANI) and

Poly(3,4-ethylene dioxythiophene: poly(styrene sulfonate)) (PEDOT: PSS) have been extensively studied [77]–[80]. Often, the final properties compromise the desired conductivity and flexibility. A summary of the most used conductive (printable) materials and their key properties is given in **Table 2**.

The key properties here include material resistivity, particle size, layer thickness, and sheet resistance. The sheet resistance R_s describes the resistivity of a uniformly thick conductive coating per specific area, and can be written as:

$$R_s = \frac{\rho}{t}, \tag{1}$$

where ρ is the material's resistivity, and t is the conductive film thickness. If the film thickness is uniform and the lateral dimensions of the conductive line are known, the sheet resistance can be derived from the total resistance R:

$$R_s = R\frac{w}{l}, \tag{2}$$

where w is the line width, and l is the length of the tracks. In other words, the conductive track is divided into squares, and the total resistance is then divided by the number of squares to obtain the sheet resistance information.

Table 2. Printable conductive materials and their key properties. [81]–[88]

Conductive material	Resistivity ($\mu\Omega\cdot$cm)	Particle size	Layer thickness (μm)	Sheet resistance ($\Omega\cdot\square^{-1}$)
Au NPs	11	5–10 nm	0.5	> 0.22
Ag NPs	5–300	80 nm	0.24	> 0.02
Ag NWs	> 90	20–40 μm	0.24	> 3.75
Ag flakes	70	7 μm	10	0.07
Ag MOD	12	< 50 nm	0.2	0.59
Cu	260	3 nm–3 μm	4	0.7
PEDOT: PSS	840	10–15 nm	1	8.4
PANI	$1.6\cdot10^6$	60–100 nm	0.3	50000
CNT	270	48 μm	4–10	> 0.3

In the past, solution-processable TFTs have been strongly at the center of attention, meaning that great effort has been paid to the printing of both organic and inorganic, conductive and semiconductive materials. In contrast, the dielectric

materials may have been deposited by other methods like spin-coating instead of actual printing [89], [90]. Recently, an increasing effort has been directed towards the development of fully printed electronics, where also the dielectric layers, protective coatings, and even the substrate would be printed [75], [91], [92].

2.3 Ink composition

Inks often consist of several components to achieve the prints' desired functionalities and meet the requirements of the chosen fabrication equipment. The basic elements of the liquid ink medium include the functional part, solvent(s), polymer binders, and perhaps some additives like surfactants [93].

There are several characteristics and requirements to consider when ink is formulated. Most importantly, the viscosity and surface tension of the ink should be optimized. These characteristics affect ink's printability and compatibility with the chosen substrate material. In addition, the ink composition and material choices also impact the post-processing options, which again affect the compatibility with the substrates. Therefore, the careful formulating of ink is essential for developing printed electronics.

2.3.1 Viscosity

Understanding a liquid's flow and deformation behavior is critical when determining ink's use and applications. Viscosity η, the resistance of flow, is of great importance for coatings and inks, as it describes the shape-change of liquids subjected to a force [94]. It is a ratio of shear stress, a force applied to a certain area in a liquid, and shear rate, the mechanical energy applied to the liquid [95]. Both the type of ink components and their concentration affect the viscosity. If an ink or coating liquid were Newtonian, its viscosity would remain unaltered over time, despite the shear rate [93].

Inkjet printing inks are typically aimed to be Newtonian, so that the viscosity would not be affected by the forces in the fluid chambers of the printhead, where the shear rate can reach values around 10^6 s^{-1}, and that the printing parameters would not have to be adjusted over time [95]. Manipulation of ink viscosity in the printhead is possible by heating the printhead (lower viscosity), and printing parameters like firing voltage can be adjusted to jet inks with various viscosities.

However, the viscosity of liquids is often dependent on the applied shear. Especially, shear-thinning behavior, where the liquids' viscosity decreases under

applied force, is common [96]. This tendency to shear-thinning is advantageous in, for example, screen printing, where the printing paste should be highly viscous to prevent it from spontaneously flowing through the mesh while still allowing an external force from a squeegee to press the ink through the screen to form the desired pattern [49]. In addition, the thixotropic tendency of ink viscosity to change over time, yield stress (the minimum stress required for liquids to flow), and viscoelasticity (the ability of materials to show both viscous and elastic tendency) are of interest in the screen printing process [97].

2.3.2   Surface tension

The molecules in a liquid are attracted to surrounding molecules, whereas surface molecules are attracted only to each other and the molecules beneath them. Therefore, liquids aim to minimize their surface area and tend to form spherical shapes in a suspended space [98]. The surface tension γ_l is a measure of these attractive forces. Liquids with high surface tension, such as water, have stronger molecular bonds than liquids with lower surface tension. Thus, they are less likely to be affected by external forces, prone to form spheres instead.

The surface chemistry of inks and other liquids can be manipulated to change their tendency to bead up. In inkjet printing, the surface tension of the liquid is closely related to the drop formation at the nozzle tip, to the consequent droplet size, and finally, to the droplet behavior on a substrate surface. In addition, the liquid meniscus in the nozzle will be greatly affected by the liquid's surface tension (and viscosity). Low surface tension can cause ink flooding, possibly even preventing droplet formation, whereas high surface tension can cause improper priming of the nozzle, and nothing will be jetted [99]. Moreover, both viscous and capillary forces affect the droplet pinch-off from the meniscus. On the other hand, the surface tension of the screen printing inks (together with the viscous forces) influences the separation mechanism of the screen mesh from the print after the passing of the squeegee. It thus affects ink spread on the substrate and the overall print quality.

2.3.3   Drop formation in inkjet printing

In addition to the viscosity and surface tension, ink's printability is also dependent on other characteristics, such as density d and the size of the printing orifice D (nozzle diameter). Especially the jettability of inkjet inks can be sensitive to even the slightest

variations of the ink composition, and a thorough understanding of material characteristics is crucial. A so-called Z-number, a reciprocal of the Ohnesorge number, can evaluate the printability of the inkjet ink solutions by approximating the droplet's tendency to stay together or fly apart. The Ohnesorge number is dependent on Weber number We, which describes the balance between the inertial and capillary forces of the liquid, and Reynolds number Re, the ratio of inertial and viscous forces [100], [101]. So, first, We is calculated:

$$We = \frac{v^2 D d}{\gamma_l},\tag{3}$$

and Re is as follows:

$$Re = \frac{v D d}{\eta}.\tag{4}$$

Here, v is the droplet velocity, D is the nozzle diameter, d is the ink density, η is the ink viscosity, and γ_l is the ink surface tension. Now the Ohnesorge number Oh can be derived from (3) and (4):

$$Oh = \frac{\sqrt{We}}{Re} = \frac{\sqrt{\frac{v^2 D d}{\gamma_l}}}{\frac{v D d}{\eta}} = \frac{\frac{\sqrt{D d}}{\sqrt{\gamma_l}}}{\frac{D d}{\eta}} = \frac{\eta}{\sqrt{D d \gamma_l}},\tag{5}$$

and as the Z-number is an inverse of the Ohnesorge-number:

$$Z = \frac{1}{Oh} = \frac{\sqrt{\gamma_l D d}}{\eta}.\tag{6}$$

Some target values for the Z-number have been presented in the literature [101]–[104]. In general, it should be high enough so that viscous dissipation will not prevent the droplet ejection, but too high of a Z might lead to the formation of satellite droplets. Therefore, the targeted range is often $1 < Z < 10$. However, several other fluid properties will affect the jettability of the inks, such as the solvent's vapor pressure, particle size, or molecular weight of the polymer [105]. Furthermore, the waveform of the applied electrical pulse in the printhead can be tuned, and therefore, the ink jetting is a sum of several variables.

Once the droplet formation has been optimized, attention needs to be paid to the printing parameters. For example, as demonstrated in **Figure 3**, the delay between the

ejected droplets and drop spacing (the physical distance between the droplets) significantly affect the subsequent line morphology. Therefore, careful optimization of the printing parameters, such as the firing voltage, waveform, and frequency, are essential to ensure sufficient print quality and performance.
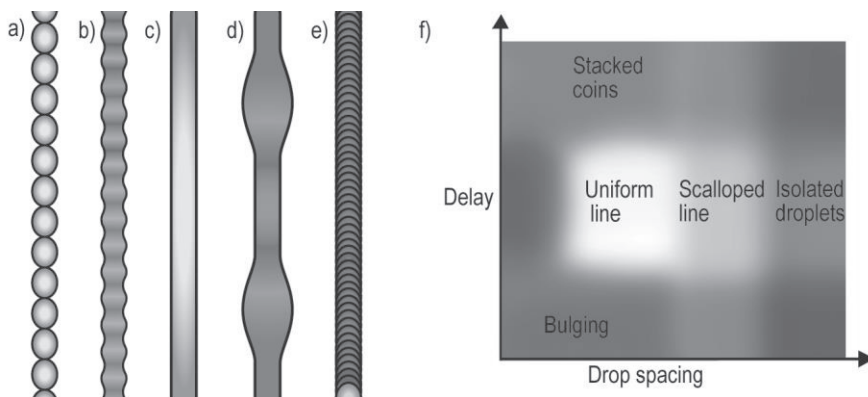
Figure 3. Line formation in inkjet printing: a) isolated droplets, b) scalloped line, c) uniform line, d) bulging line, e) stacked coins, and f) the relationship between drop spacing, delay, and line formation. Adapted from [106] with permission.

Moreover, several printers come with the option to heat either the printhead or the substrate, which can be used to manipulate ink composition (printhead heating) or the behavior of the droplet on the substrate, and thus, line formation (substrate heating). However, at elevated temperatures, inks tend to coalesce at the droplet edges instead of the center due to the accelerated solvent evaporation and the resulting outwards capillary flow [106]. This phenomenon is known as the coffee-ring effect. It can be problematic in, for example, dielectric layers or highly conductive tracks, where uniformity of the lines is of the essence.

2.3.4   Ink transfer mechanism in screen printing

The ink transfer mechanism onto the substrate in screen printing differs from inkjet printing immensely, as the ink is first applied on a stencil, after which the ink is pressed onto the substrate through the mesh openings. The pursuit for an improved printing resolution and edge definition has led to extensive studies of the screen printing

parameters, ink composition, and their effects on the print result. It has been shown that many of the quality issues of the process are related to the match (or rather a mismatch) between the printing ink chemistry and the printing parameters [49].

However, the relationship between these parameters is not simple, and proper process optimization requires a deep understanding of the chosen materials. Recently, studies relying on high-speed imaging of the area between the screen and the substrate have been conducted [48], [97], [107]–[109]. They seem to confirm that four phases take place during screen printing: first, *pre-injection* occurs when the paste in front of the squeegee is pushed through the mesh openings, after which there is a *contact*, as the squeegee presses the mesh against the substrate, followed by a *cling zone*, which is determined as the time that is needed for the screen to be slowly separated from the substrate before *snap-off* when the screen retreats to its original distance from the substrate. A visual presentation of these phases is offered in **Figure 4**.
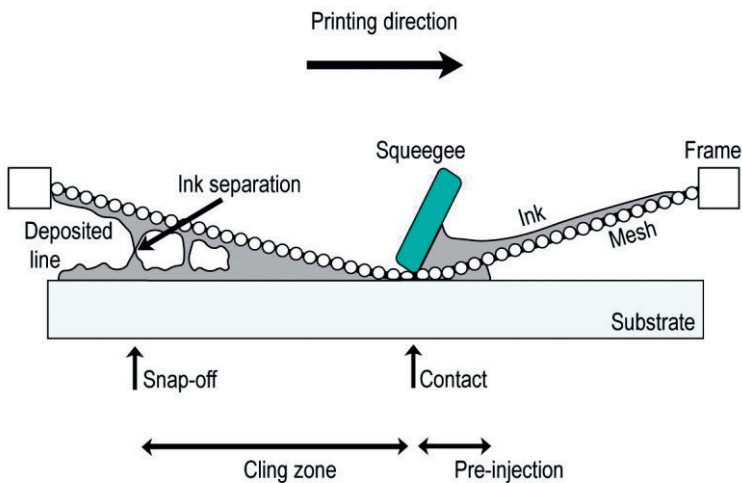
Figure 4. Ink transfer mechanism in screen printing. Adapted from [48].

As shown in **Figure 4**, the pre-injection and the cling zone have quite remarkable effects on the final properties of the printed film. If the ink is pushed through the screen before the squeegee contact takes place, there is an excess volume of the ink on the screen, which can cause the print quality to suffer if the ink is pushed outside the targeted pattern area, though the ink does retract a little during the last phases. The emulsion, squeegee pressure, and ink chemistry also affect the ink spread at the cling

zone. After the contact, the screen slowly retreats, and some of the deposited ink is removed. Before the separation, ink first forms filaments, which begin to thin and finally break during the snap-off. Here, menisci are formed on the print surface. The ink's surface roughness may be higher than the print thickness unless the printing parameters are adjusted to prevent filament formation. It can be concluded that the snap-off distance, printing speed, and the squeegee pressure can be tuned to improve printing quality. However, the relationship might not be linear, and these parameters are highly dependent on both ink chemistry and mesh properties [48], [97], [107]–[109].

2.3.5   Post-processing

Since the inks consist of several components, it is necessary to remove the solvents from the print, decompose the binders, and activate the functional material, whether to sinter metal particles together, start the reduction reaction of MOD inks, or cross-link a polymer, for example. Traditionally, a thermal post-process is used. In **Figure 5**, the basic principle of the NP sintering is shown. First, the solvent of the ink is removed by heating. After that, the bonds of the polymer binders are broken, and the adjacent particles start to form physical contact with each other (neck formation). Thus, a conductive percolation network is created.
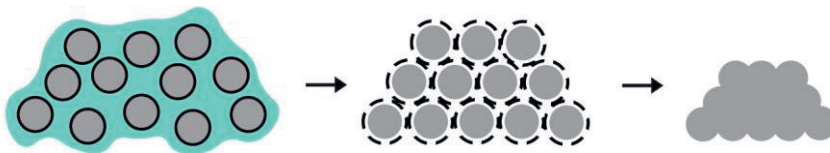
Figure 5. Nanoparticle ink sintering stages.

Here, minimization of particle size is advantageous: for example, the metallic nanoparticles can be sintered at low temperatures: Ag NP ink can be annealed already at the temperature of approximately 150 ˚C, whereas the melting temperature of bulk silver is close to 1000 ˚C [110]. The low curing temperature is a highly beneficial process feature considering, for example, the fabrication of flexible devices, where temperature-sensitive materials like polymers are often used. However, heating the

substrate to the required temperature in some applications is not possible, and other methods should be considered.

Examples of alternative post-processing methods include photonic, electrical, microwave, and plasma sintering [7]. The family of photonic sintering tools consists of ultraviolet (UV) radiation, near-infrared (NIR), laser, and pulsed light or flashlight methods. The printed pattern is exposed to light radiation, and the print is cured due to the photonic heat. Electrical sintering is based on Joule heating: an applied voltage is used to heat and sinter the pattern. Other methods include microwave and plasma sintering, based on the absorption of electromagnetic energy or exposure to plasma irradiation, respectively. Each method has its advantages and shortcomings, and the appropriate tool selection is application-specific.

The curing mechanism is different for other materials, such as flake inks or dielectrics. The flake particles are often larger than the NPs, flake size being up to a few micrometers instead of tens of nanometers. The required sintering temperatures are thus significantly higher than for the NP inks. However, keeping the flake inks' curing temperature low is often beneficial for highly flexible applications because the non-melted particles can slide past each other during elongation. Good conductivity can be maintained even in the stretched state (as long as a contact between the flakes remains). Moreover, the non-rigid structure is less likely to crack and permanently lose the connection between the adjacent particles during a stretch, being advantageous in stretchable applications.

In reactive printing processes, where the final material layer, such as metal particles (MOD inks) or polymers, are formed as a reaction of the ink components, the post-processing step is needed to trigger the synthesis or polymerization of the materials [111], [112]. These reactions can be initiated by light or heat, and the steps include evaporation of the solvents, followed by the reaction between the functional components. This principle is shown in **Figure 6**, where PDMS crosslinking is activated in the presence of a platinum (Pt) catalyst.
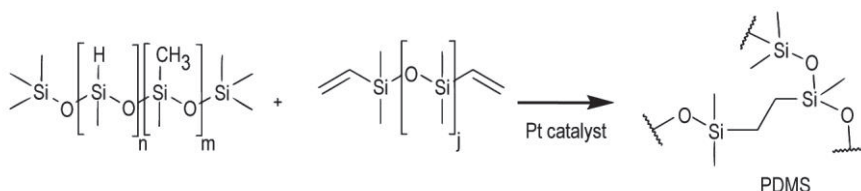
Figure 6. Catalyst-assisted PDMS cross-linking. Adapted from [113] with permission from the Royal Society of Chemistry.

2.4 Substrates

The substrate has a significant role in electronics fabrication since it provides a building platform and supports and protects the electrical circuits. Moreover, the selected substrate influences devices' signal attenuation, thermal stability, heat dissipation, breathability, and biodegradability. The interest in alternative materials and methods beyond the traditional silicon wafer manufacturing has enabled the development of large-area devices, for which inexpensive but relatively sensitive polymer materials are used, even commercially. Some of the commonly used printed electronics substrates, and their selected properties are shown and compared to the chosen substrates (silicones and PPE) in **Table 3**.

One important property of conformal electronics is flexibility. There are several degrees of flexibility, each equally significant for the conformability of electronics. Flexibility without stretchability may be enough depending on the material choices and end applications. Some of the widely used flexible substrate materials include poly(ethylene terephthalate) (PET) [33], [114]–[118], poly(ethylene naphthalate) (PEN) [119]–[121] and polyimide (PI) [122]–[128]. They are attractive choices in such flexible applications, where moisture resistance and robustness are required. The latter options also provide excellent thermal resistance at a higher expense, and the optical transparency may suffer [129]–[131]. A significant benefit of these materials is the wide thickness range.

In some E-skin applications or human-machine interfaces, the free deformability of the devices is essential. In other words, materials should allow free stretching, compression, twisting, and other such deformations. In addition to elasticity, these materials should also be soft to improve user comfort. The skin's elastic modulus is lower than 1 MPa, and thus, the previously mentioned substrate materials, let alone rigid conductive materials, cannot provide the softness required here [132]. Other attractive characteristics include biocompatibility and inertness, again, to improve user comfort and avoid undesirable chemical reactions of the implanted materials and devices within the human body [133].

Common examples of these soft materials include silicone elastomers and polyurethane (PU) compounds [27], [28]. These materials possess interesting characteristics: silicones have a pleasant feel, repel water, are inert, and absorb shock and sound. Therefore, they are widely used in various industries, from the cosmetics and food industry to the automotive industry [134]. On the other hand, polyurethanes can be either thermoset or thermoplastic elastomers. The latter possess rubbery properties, while they can be molded in consecutive heating-cooling processes. PU

materials also have various industrial and domestic applications, such as foams, shoe soles, and vehicle body parts [134].

Table 3. Selected substrate materials and their properties. [9], [131], [139-149]

Substrate	Thickness (μm)	T_g (˚C)	Elastic modulus (GPa)	CTE (ppm·˚C^{-1})	Surface energy (mN·m^{-1})
PET	1–356	80–150	2–3	33	40–43
PI	0.5–125	360–410	2–3	8–20	50
PEN	1–250	120–200	2–4	20	45
Silicone elastomers	4–3000	120–150	< 0.002	325	10–24
PU	25–500	30–40	< 0.001	148	31–42
Paper	20–250	80	0.5–3.5	-	42–70
PPE (Preperm® L260)	10^3	160–180	2–3	-	30–32

To further improve user comfort, nanomesh materials can be used. Mesh-like nanoscale substrate materials have certain advantages over dense substrates, such as improved breathability. In addition, they are even more lightweight and unobtrusive than the polymer foils that are often used as flexible electronics substrates [135], [136].

In addition to the conformability aspects of the novel electronics applications, the high-frequency properties of the substrates are also of great interest. After all, the substrate material has a significant role in the signal attenuation at high frequencies. As the number of wireless applications increases, the demand for device operations at high frequencies increases. Examples of these applications include wireless networks, radars, satellite and spacecraft communications, spectroscopy, remote sensing, and keyless entry systems – to name a few. For example, in radio frequency identification (RFID) tags, cost minimization is essential for the mass-scale production of the devices. Paper has been proposed as a substrate choice for its light weight, flexibility, cheapness, and biodegradability [137]. However, the main issues of paper-based fabrication include the limited thermal resistance and high porosity of the substrate, although primer coatings can be applied to improve the substrate characteristics [137], [138].

From the fabrication point of view, some of the most critical substrate properties include chemical resistance, thermal properties like glass transition temperature T_g and the coefficient of thermal expansion (CTE), surface characteristics, optical transparency, and lastly, expense. These characteristics affect the material compatibility, suitable fabrication process, and end applications.

2.4.1 Wetting

Wetting describes the interaction between a liquid (ink) and solid (substrate) when the printed ink meets the substrate surface, i.e., the ink's spread on a particular substrate. This relationship can be approximated using Young's equation:

$$\gamma_{lv} \cos \theta = \gamma_{sv} - \gamma_{sl}, \tag{7}$$

where contact angle θ is dependent on interfacial tensions between phases: γ_{lv} is the liquid's surface tension in equilibrium with its saturated vapor, γ_{sv} is the surface energy of the solid in equilibrium with the saturated vapor of the liquid, and γ_{sl} is the interfacial tension between the solid and the liquid [150]. Since the vapor density, which is usually air, is negligible compared to the liquid and the solid densities, its effect on the interfacial tensions can be excluded. Therefore, γ_{lv} may be replaced with the liquid's surface tension γ_l, and γ_{sv} may be reduced to the solid surface energy γ_s.

As seen in **Figure 7**, there are four wetting states; in a non-wetting state ($\theta = 180$ °), the liquid completely beads up on the substrate surface. Wetting is poor already when the contact angle θ equals or exceeds 90 °. Thus, for the ink to wet the substrate surface, the surface tension of the ink must be lower than the substrate's surface energy ($0 \leq \theta \leq 90$ °). On the other hand, if the contact angle is very low ($\theta = 0$ °), wetting is complete without any restrictions, and the liquid spreads freely.

Surface tension and wetting are often of interest even before the ink meets the substrate. When the ink and the substrate interact, an equilibrium between the coating and the coated material must be found, as printed electronics performance relies on sufficient coating quality. Since the surface tension of the liquid must be smaller than that of the substrate for wetting to occur, printing ink surface tensions should match the low substrate surface energies of the polymers (**Table 3**). Substrates that intrinsically repel water or oil are hydrophobic or oleophobic, whereas substrates attracting these substances are hydrophilic or oleophilic. The suitability of the inks on different substrates can be changed by modification of ink formulations. Other methods for manipulating ink wetting on the substrate will be further discussed in Section 2.4.3.
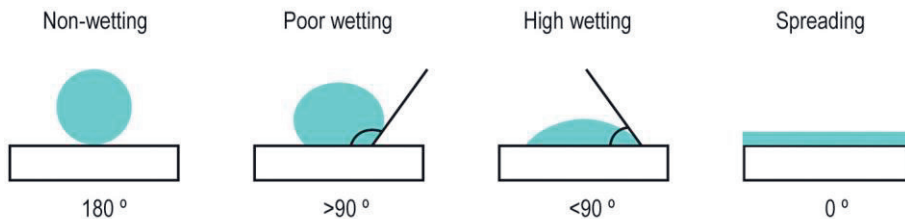
Figure 7. Contact angle and levels of wetting.

2.4.2 Adhesion

Adhesion, the bonding mechanism between two phases (the ink and the substrate), and its strength are a sum of several factors. First, a sufficient level of wetting is required since there will be more contact area between the two materials if ink wets the substrate well and no air bubbles or cavities remain between them. In addition, the bonds between the materials affect the adhesion strength.

The bonding mechanism can generally be divided into physical, chemical, and electrostatic bonds, occurring from atomic to macroscopic levels [151]. Furthermore, these mechanisms are highly dependent on the bonding surfaces. For example, different bonds are likely to form in a polymer-polymer interface than in a metal-metal interface [151].

In the physical bonding theory, the coating penetrates the substrate surface's pores, cavities, and irregularities, and so-called mechanical interlocking occurs. It has been shown that roughening the adherend surface (substrate) improves adhesion, but this may also be a result of a simultaneous cleaning of the surface, formation of a reactive surface, or an increment of the contact area between the two phases, enhancing other bonding mechanisms [151]. This hypothesis is supported by the fact that roughening can also be used to transform the already hydrophobic surfaces into even less wettable, super-hydrophobic surfaces [98].

In addition to the physical mechanisms, chemical forces impact adhesion. Strong chemical forces like covalent and ionic bonds occur within materials with polar groups. In contrast, nonpolar materials tend to form weaker bonds, such as hydrogen bonding or van der Waals forces. The diffusion theory assumes that the interfacial molecules are both mobile and miscible, and the materials can thus merge, forming concentration gradients [151], [152]. The level of this interdiffusion is dependent on the time, pressure, and temperature of contact [152]. This phenomenon is of

particular interest in nanoparticle ink sintering since the diffusion mechanism directly impacts the neck growth between the particles, thus affecting the densification and the final conductivity of the printed films [153].

Good adhesion between the substrates and the printing inks is essential since the bonding strength directly determines the mechanical stability of the prints: if the ink does not adhere to the substrate, the printed structure will be highly susceptible to mechanical damage and delamination, and thus, the lifetime of the device will be short. Therefore, understanding the adhesion strength is of the essence when new printed electronics applications are developed.

There are standardized test methods for adhesion strength determination, such as the crosscut and pull-off tests [154]. The former is a qualitative test and, thus, more suitable for the initial states of prototyping, where a rough estimation of the adhesion level might be enough. The latter test is quantitative and better suited for accurately comparing different materials. However, the existing test methods are not necessarily compatible with the soft substrates, and obtaining reliable data on the adhesion strength might be tricky. In flexible applications, bending tests can give valuable information about the adhesion between the materials.

2.4.3   Modification of the surface properties

If the wetting or the adhesion of the coatings is poor on a particular substrate, it is often advisable to alter the surface characteristics of the substrate material. Alteration can be achieved by applying an additional, thin material layer on the surface, and it could serve as an adhesion promoter between the coating and the substrate [155]. Other strategies include treating the substrate surface with, for example, plasma. It is a well-known and versatile surface-treatment method that can utilize different gases. Depending on the intensity of the treatment, it can either increase or decrease the surface energy of polymers, to clean and even etch surfaces [156]. Another effective dry treatment is UV/ozone (UVO) [157].

It is also possible to use chemical treatments, where the substrate surface is etched with acids or bases to alter the surface properties [158], [159]. To prime sensitive materials, self-assembling monomer (SAM) layers can be deposited onto the target surface by methods like electroless plating or vapor deposition [160], [161]. It is also possible to manipulate material properties by additives: for example, an adhesive silicone elastomer can be structured by adding other polymers to the mixture before cross-linking [162].

Often, the surface treatments aim to make materials more hydrophilic or enhance the adhesion of the ink to the substrate. Sometimes, however, it is preferable to use low surface energy materials or manipulate surfaces to make them more hydrophobic. Hydrophobic surfaces have valuable properties, like self-cleaning and anti-fogging abilities, and they can be used as barrier coatings to enhance corrosion resistance [163], [164]. These hydrophobic features can be obtained by plasma treatment, chemical treatment, or coating. In printed electronics, even though ink spread is desired to some extent, it is possible that wetting needs to be controlled. Even though the native substrate may be too porous or hydrophilic for a specific process, a hydrophobic treatment can modify the substrate material for improved resolution or enhanced fabrication process versatility [137], [165]. A selective surface modification based on consecutive hydrophilic and hydrophobic areas can be used to manipulate print resolution even below the nozzle diameter [137].

2.5 Low surface energy materials and their applications in electronics

A material is considered hydrophobic when its contact angle equals or exceeds $90°$, and the water droplets tend to bead up on the substrate surface instead of spreading. Water surface tension is approximately 73 mN·m^{-1}, and a contact angle of $90°$ is often obtained on substrates with surface energies less than or equal to about 35 mN·m^{-1} [166], [167]. However, the material's hydrophilic or phobic tendency is also dependent on the ratio of the polar and non-polar surface energy components rather than just the total energy.

Polymers that are commonly considered to be hydrophobic include examples like polystyrene (PS), PTFE, and PDMS [161], [163], [164]. These materials lack polarity, and the absence of functional groups on the surface weakens the adhesion between the substrate and the coating materials. Even though there are methods for modifying the surface characteristics, additional steps will complicate the process. In addition, they may add some extra concerns, like the need for harsh chemicals or processing at elevated temperatures. Another concern is the hydrophobic recovery, which means that the treatment effect fades over time when the modified surface is left in ambient conditions [170].

Some printing processes, like inkjet printing, are susceptible to the slightest adjustments in the ink composition, substrate characteristics, and printing parameters.

Therefore, several issues must be addressed when a hydrophobic substrate is used [170]. First, the required intensity of surface modification should be determined: if the substrate is not hydrophilic enough, the ink tends to bead up rather than form a continuous line. To some extent, the drop spacing can be decreased to aid line formation. However, when small drop spacings are used and the ink volume on the substrate is very high, the hydrodynamic instability may lead to line bulging, shown in **Figure 3**.

Again, this behavior can be prevented to some extent. Substrate heating will enable rapid solvent evaporation and thus allow continuous line printing. However, as noted earlier, the rapid evaporation of the solvents at elevated temperatures can lead to the coffee-ring effect, and the final functionalities may suffer as the ink coalesces at the edges of the printed pattern. Moreover, too harsh a surface treatment can damage the substrate surface instead of activating it, making it brittle and fragile, causing deformations like surface cracking [170]. In addition, the general concerns related to polymer materials, such as challenging thermal properties and chemical resistance, are also present here. However, hydrophobic polymers are often less sensitive to chemical exposure.

Hydrophobic polymer materials can offer exciting features for conformable electronics applications despite all these challenges. For example, PDMS, PS, and PTFE all are attractive nanogenerator materials due to their electron-attracting ability (triboelectricity) and flexibility [171], [172]. Moreover, elasticity, optical transparency, inertness, and biocompatibility are attractive features for various industries [173].

In addition to the barrier coatings and wetting manipulation, the hydrophobic polymers have found their way into electronics fabrication. They can be used as flexible foils, and layer deposition in liquid form is possible by employing, for example, spin coating. In addition to the issues related to the liquid-repelling tendency, flexible and stretchable electronics fabrication may prove challenging due to the mismatch in the elastic properties of the more rigid functional materials and the flexible substrates.

To tackle the elasticity mismatch, selective surface activation has been used to form so-called out-of-plane structures. One strategy for achieving this geometry is a pop-up structure. The conductive coating literally pops up from the pre-strained substrate that is not activated by surface treatment once the pre-strain is released [174]. Controlled buckling is obtained as the coating layer adheres to the substrate in those regions where the surface activation was used. The amplitude of the pop-up structure can be controlled by changing the distance between the activated areas. Unfortunately, this and the other out-of-plane approaches suffer from the fact that the structure is

nearly impossible to utilize in multilayered devices because stacking multiple layers while maintaining the geometry is dreadfully challenging.

The capability of multilayer fabrication is essential, first, for PCB manufacturing since most PCBs consist of at least two functional layers. Second, deposition of several functional layers is needed to make, for example, simple passive components, supercapacitors, and more complex devices with multiple functions [175]–[178]. Third, when electronics printing on hydrophobic surfaces is demonstrated, the focus often is on printing just a single material layer like conductive tracks [179]–[182]. Finding a suitable coating strategy for the hydrophobic substrate is an essential step toward printed electronics fabrication, but a deeper understanding of material interfaces and the ability to print multiple material layers are needed to create printed, multi-functional electrical systems instead of just the interconnect layers.

To avoid the direct coating of the hydrophobic surfaces and remove the need for geometry engineering, approaches have been presented for merging the functional patterns to the liquid polymer matrix before curing [59], [183]. As the print is either transferred to the surface of the liquid polymer with the aid of a donor substrate or it is directly printed onto the liquid polymer matrix, multilayer fabrication is enabled. However, as each pattern is sealed by the polymer that crosslinks upon curing, these layers can only be connected if additional molds and punching tools are used to enable via fabrication. Recently, an advanced process, where vias were also printed to connect the functional layers inside the polymer matrix, was used [184]. Despite the recent advantages, these approaches still suffer from the limitations of polymer casting instead of printing: pouring new layers over the whole structure builds up the device's thickness, weakening its conformability.

Direct coating methods without additional geometrical engineering, where selective surface treatments have been used for high-resolution patterning of multilayer electronics, have been presented [137], [185]. However, despite the benefits of the room temperature processing capability, the need for several fabrication steps, including screen printing, inkjet printing, drop-casting, spin coating, and mask-based surface treatments, makes the process exhaustingly complex scalability remains questionable.

Further studies on hydrophobic materials and their application potential in printed electronics are needed for all these reasons. The remaining Chapters will introduce the reader to the work that has been carried out in this thesis and discuss the findings in the provided scope.

3 MATERIALS AND METHODS

In this chapter, a summary of the used materials, fabrication methods, and characterization tools is given. First, the chosen substrates are briefly discussed, and their selection is justified in Section 3.1. After that, the surface modification approaches and printing strategies for coating the substrates are presented in Section 3.2. and 3.3., followed by steps toward dielectric ink development (Section 3.4.) Finally, the strategies for multilayer fabrication of stacked conductive circuits and capacitive sensor elements are presented in Section 3.5.1. and Section 3.5.2., respectively.

3.1   Chosen substrates

In **Publications I** and **II**, the material characteristics of a high frequency-compatible substrate with low surface energy, a polyphenylene ether (PPE) based polymer blend, were studied before and after surface treatments. As the substrate (Preperm® L260) has a relative permittivity ε_r of 2.6 and a controlled dissipation factor *tan δ* of only 0.0025 at 60 GHz frequency, it is an attractive option for various low loss antenna structures [186]. In comparison, popular high-frequency substrates such as PI, PET, or FR4 come with ε_r/*tan δ* of 3.5/0.001 (10 GHz), 2.0/0.03 (10 GHz), and 4.5/0.015 (7 GHz), respectively. In addition, as a thermoplastic material, it can be shaped at elevated temperatures using both injection molding and extrusion; it could be used to create 3D-shaped, printed high-frequency electronics for MID applications. In addition to the material studies, conductive patterns were printed on this substrate. The prints were characterized: first, right after printing and post-processing, and secondly, their long-term reliability against environmental stress was evaluated in accelerated aging tests (**Publication II**).

The second part of the thesis (**Publications III-V)** focuses on PDMS-based electronics, where the silicone elastomer was used both as a substrate and a dielectric. The aim was to investigate additive fabrication strategies of multilayered soft electronics. This elastomer was selected based on the reasons that were stated earlier in Chapter 2: it is used in multiple industries, and characteristics like optical

transparency, biocompatibility, thermal stability, stretchability, breathability, and triboelectricity make it an attractive material choice for many printed electronics application areas, such as E-skin applications, soft robotics, or microfluidics. However, properties like hydrophobicity and processing by mold-casting have limited the approaches for simple and straightforward manufacturing.

For straightforwardness, all silicone-related studies were conducted using just one silicone elastomer, a well-known PDMS (Sylgard 184, Dow). This PDMS is a two-component product, requiring a catalyst to activate the crosslinking process of the silicone compound. It can be cured either at room temperature or by heating, after which it has good flexibility and moderate tear resistance.

It is sometimes argued that this specific type of silicone is not necessarily the best choice, for example, for stretchable electronics, due to the limitations of the mechanical properties (max. stretchability approx. 100 %). However, it was still chosen for several reasons. First, this level of stretchability is sufficient for many flexible applications, such as skin-like electronics or robotics [160], [187]. Moreover, this silicone is convenient to process and mold. Its viscoelastic properties are easily tunable simply by changing the crosslinking ratio of the material or by adjusting the curing conditions [188], [189]. It is also inexpensive and readily available. In addition to the other advantages, this material is also optically transparent. Transparency provides additional benefits in, for example, optometric applications, where devices need to be imperceptible [190].

3.2   Screen printing of conductive tracks on PPE

In **Publications I** and **II**, conductive patterns were printed on the PPE substrate. Screen printing was chosen as the printing method due to the high aspect ratio that enables high layer thickness. Thus, the resistivity of the printed lines can be minimized easily. As mentioned already in Section 2.1.1., the edge and surface smoothness of the prints can be adjusted so that they become smooth enough even for high-frequency applications, despite the notably high print thickness. Second, as the resolution of printed lines does not have to be very high, even in the high-frequency applications, the maximum resolution of screen printing was judged to be sufficient here, especially when considering the mass manufacturing options of large-area applications. Since the quality of screen-printed lines is not highly dependent on the substrate roughness, this method also allows freedom for surface modification of the substrate material.

First, five commercial Ag flake inks were chosen based on the existing literature and manufacturer recommendations. The inks and their key properties are presented in **Table 4**. These inks were used to print two conductive patterns on the native and modified PPE substrates: 1.3 mm wide, 32 mm long tracks with measurement pads, and square patterns (2 mm x 2 mm) for adhesion studies. Finally, the native, hydrophobic PPE substrate was compared to PPE substrates whose surface was modified before printing with physical or chemical treatment.

First, the native substrates' surface characteristics were studied. There were two different substrates: injection-molded ones with a 10 cm x 10 cm area and 3 mm thickness. The other substrates were extruded with the same size but only 1 mm thickness. Since the surface energy is rather low, it could prohibit good wetting, and especially any sufficient adhesion between the printing inks and the substrate. Therefore, several surface treatments, both dry and wet, and their effects on both wetting and adhesion were studied. Oxygen (O_2) plasma (RIE 100, Oxford Instruments) and pyrolytic silicating were applied as dry alternatives. The chemical treatments included etching with potassium hydroxide (KOH) and sulfuric acid (H_2SO_4) and spray coating with tri(ethylene glycol) monoethyl ether. A summary of the used surface treatments is given in **Table 5**. These methods were chosen because they have been either effectively used to prime polymer surfaces for metallization [156], [158], [159], [191], or were recommended by ink manufacturers (tri(ethylene glycol) monoethyl ether).

The surface energies of the native and treated substrates were measured with a set of test pens (MaxiPack, Dyne test), ranging from 30 mN·m^{-1} to 60 mN·m^{-1}. The substrate surfaces were imaged with an optical profilometer (Wyko N1100, Veeco). The first surface parameter of interest was the root-mean-square (RMS)-roughness R_q, which is used to describe the roughness deviation from the mean and is calculated as follows:

$$R_q = \sqrt{\frac{1}{n}\sum_{i=1}^{n} y_i^2}. \tag{8}$$

Here, y is the deviation over the roughness mean, and n is the number of samples. This parameter describes the standard deviation of height distribution on the surface, and it is significantly affected by the variations from the surface mean line. Therefore, it is a suitable measurement parameter for rough substrates with many deviations. In addition, peak-to-peak roughness R_t (the difference between the highest peak and the deepest valley of the surface) was measured.

In addition to substrate studies, Ag ink compatibility with the substrate was evaluated in printing trials and consecutive performance characterization. The screen printing method was used here because of its high aspect ratio and the excellent availability of highly conductive inks. A screen printer (TIC SCF-300, DE Eickmeyer) was used in all printing experiments, together with an aluminum screen holding a polyester mesh (UX79-45, NBC: opening 81 μm, theoretical wet thickness 27.7 μm). Conductive lines with measurement pads were printed for the resistance measurements, and square patterns were used in the adhesion tests. After printing, the samples were cured in an oven according to datasheet recommendations: HPS-021LV at 150 °C for 30 min, HPS-FG32 at 140 °C for 10 min, CRSN2442 at 150 °C for 30 min, LS411AW at 150 °C for 20 min, and 5064H at 130 °C for 20 min.

Table 4. Key properties of the inks used in **Publications I** and **II**.

Ink, manufacturer	Ag content (%)	Viscosity (mPa·s)	Solvent	Sheet resistance (mΩ·□$^{-1}$ at specified t)
CRSN2442, SunChemical	69–71	2000–3000	Propylene diacetate	10 at 25 μm
5064H, DuPont	63–66	10000–20000	C11-ketone	< 14 at 25 μm
LS411AW, Asahi	65–75	20000–30000	Butyl cellosolve acetate, isophorone	< 40 at 10 μm
HPS-FG32, Novacentrix	75	8000	Butyl carbitol	25 at 25 μm
HPS-021LV, Novacentrix	75	2600	Water	< 14 at 25 μm

Table 5. Summary of PPE surface treatments.

Substrate	Surface treatment	Specifications
Injection-molded, 3 mm thick	None	-
	O$_2$ plasma	1 min exposure at 75 W power, gas flow 30 sccm, Chamber pressure 56 mTorr
	Pyrolytic silicating	propane-butane-organosilicon gas mixture
	Airbrush-coating	Tri(ethylene glycol) monoethyl ether at 1.1 bar pressure + 15 cm distance
	H$_2$SO$_4$ etching	5 min exposure, 98 % concentration
	Potassium hydroxide etching	5 min exposure, 30 % concentration
Extruded, 1 mm thick	None	-

In the initial stage, the line widths of the prints were measured using an optical microscope to evaluate ink wetting, and the line surface was imaged with an optical profilometer to determine the surface roughness. Again, the profile range R_t and the RMS-roughness R_q were of interest since they offer information on the print thickness and the roughness deviations of the surface. Next, the resistance R of the samples was measured with a 4-wire sensing mode of a source measure unit (Keithley SMU 2425) to eliminate the effect of contact resistance on the results, and sheet resistance was calculated using equation (2).

In addition to the resistance measurement, the adhesion of the square pattern samples was evaluated according to the ASTM-D3359-17 standard [192]. Here, a crosscut pattern was cut onto the surface of the conductive square, after which an adhesive tape was applied. After waiting for approximately 90 s, the tape was peeled off. The level of ink removal was determined visually by estimating the surface area of the ink remaining on the substrate and the ink that was removed by the adhesive tape. These areas were compared to the total surface area of the crosscut pattern, and the adhesion was rated accordingly. A scanning electron microscope (SEM) was used to inspect the flake composition of the inks.

The resistance measurements and adhesion test results were compared, and the best material combinations were selected for further testing. Finally, new square pattern samples were fabricated on the injection-molded substrates, either left to the native state or treated with selected surface treatments to investigate environmental reliability. As this thermoplastic material would be an exciting substrate option in, for example, MIDs in demanding applications like offshore radars or wireless marine security systems, the aging tests were selected to simulate a humid environment, with and without salt exposure.

In the first aging test, one set of samples was placed in a Weiss C340 chamber and kept in an 85 % relative humidity (RH) at an 85 °C temperature for 500 hours, according to a JEDEC JESD22-A101C standard [193]. In the second test, another set of samples was exposed to a salty, humid environment in an Ascott S450XP chamber, according to IEC 60068 2-52 standard [194]. First, the samples were exposed to sodium chloride (NaCl) mist at a 35 °C temperature for two hours, after which they were kept in 93 % RH at 40 °C temperature for 168 h. This cycle was then repeated. The sample placement in the chamber was random to minimize possible bias due to an uneven salt spray. After the test, the samples were rinsed with deionized (DI) water to remove the excess salt and, thus, suspend any corrosive reactions. After the

environmental aging tests were finished, the samples were again characterized using the ASTM-D3359-17 crosscut test, and SEM was used for imaging the samples.

3.3   Inkjet printing conductive lines on PDMS

Inkjet was selected as the printing method of the additively fabricated PDMS-based devices due to its maturity, simplicity, speed, and low cost compared to aerosol and E-jet printing. The obtained resolution is lower than the alternatives but high enough for these experiments.

Before printing, surface treatments were applied to modify the surface characteristics of the hydrophobic PDMS surfaces. The utilized treatments were: nitrogen (N_2) plasma (Diener Atto, Diener Electronic GmbH), which was first used in **Publication III**, and later compared to a flame-pyrolytic silicating method (Nanoflame NF02 pistol), and coating of the plasma-treated PDMS with a (3-mercaptopropyl) trimethyl siloxane (MPTMS) solution in **Publication IV**. A summary of the surface treatment methods for PDMS is given in **Table 6**. N_2 plasma and the chemical treatment were chosen because they have been used earlier for the effective modification of PDMS surfaces [161], [195]–[199]. The results of [196] and [197] suggest that the effect of N_2 plasma would be more resilient to the substrate's hydrophobic recovery than that of oxygen plasma. The MPTMS treatment can be applied as a coating onto a plasma-treated PDMS surface without swelling or degrading effects on the substrate. NanoFlame treatment (pyrolytic silicating) was chosen based on the results obtained in **Publications I** and **II**.

Table 6. Summary of PDMS surface treatments.

Method	Specifications
N_2 plasma	Exposure power of 100 W for 1 min at a chamber pressure of 0.6 mbar, gas flow 700 sccm.
MPTMS	(on plasma-treated PDMS) 6 wt% in ethanol, spin coating for 2 min at 1600 rpm, baking at 120 ˚C for 30 min
Pyrolytic silicating	propane-butane-organosilicon gas mixture

All conductive tracks on PDMS were fabricated by inkjet printing (Dimatix DMP-2831, Fujifilm) using a commercial Ag NP ink (DGP 40LT-15C, Advanced Nano Products) and 10-pl DMC-11610 printheads. The ink selection was based on several

factors: first, the particle size had to be sufficient for the printhead nozzles (< 200 nm), limiting the choice of conductive materials. Second, the DGP 40LT-15C ink resistivity is low (11 μΩ·cm), despite the low-temperature curing at 120-150 ˚C. Other advantages include long shelf-life and stability, and good compatibility with PDMS [200]–[203]. Here, the ink was cured at 120˚C for 30 minutes. The resistance of the conductive tracks was recorded after post-processing using a 4-wire sensing mode of a source measure unit (Keithley 2425), after which the sheet resistance was calculated using equation (2). An adhesive tape was used for a peel off-test, and adhesion was evaluated based on the level of ink removal.

3.4   Dielectric ink development

Traditionally, to pattern and shape PDMS (or other silicone elastomers), it is first mold-cast in a liquid form and then cured to achieve the desired shape. Another alternative is to create flat PDMS layers using methods like spin coating or bar coating, sometimes together with physical masks for patterning. Unfortunately, these fabrication methods are somewhat limited considering printed electronics applications, where only a small volume of material might be needed in one layer. Still, deposition of several material layers is often necessary. For example, if this material would be used as a dielectric between conductive layers, the traditional methods would require first coating the whole circuit with PDMS. Then, punch tools would be needed to connect the conductive layers after curing. In another scenario, an application-specific, physical mask could be used to apply the dielectric coating on demand, but the process would still be material-wasting, time-consuming, and inconvenient.

To avoid these laborious processes, an inkjet printable PDMS ink was developed in this thesis. A desktop printer (Dimatix DMP-2831, Fujifilm) was used in all inkjet printing experiments. Therefore, the developed PDMS ink solution was optimized for this printer type, although the solution is also tunable for other printers. Here, 10-pl liquid crystal polymer (LCP) cartridges (DMCLCP-11610) were used. First, the ink solvents were selected. The aim was to use as non-hazardous ink solvents as possible and to compare solvents with high and low boiling points. Thus, based on earlier works [113], [204]–[206], isobutyl acetate (IBA) and octyl acetate (OA) were selected as the two alternatives.

Solution rheology was studied and optimized to achieve a printable solution by measuring the viscosity as a temperature and shear rate function. All viscosity studies were carried out using a rotational rheometer (MCR301, Anton Paar). The

temperature measurements were conducted to determine how printhead heating (up to 70 °C) would affect the liquid viscosity, thus estimating printability and cartridge functionality over time. Since the crosslinking of the used PDMS (Sylgard 184, Dow) is faster at elevated temperatures, the cartridge should remain functional longer if the temperature is kept as low as possible.

The shear rate measurements were used to evaluate viscosity stability at higher shear rates, as the shear rate in the printhead is highly dependent on the piezoelectric actuator's motion. In addition to the viscosity measurements, surface tensions of the inks were measured using a pendant drop method (Drop Shape Analyzer DSA100, Krüss GmbH). The surface tension was calculated from the extracted droplet profile using the software's Young-Laplace equation.

Raman spectroscopy (532 nm, inVia Qontor, Renishaw) was used to determine whether the printed ink would resemble the cast, native PDMS and whether there would be solvent residues. An optical profilometer (Wyko NT1100, Veeco) was used to measure the thicknesses of the PDMS patterns when 1–8 layers were printed and cured. A thin carbon coating was sputtered onto the surface (JEOL-530, JEOL) to enable the imaging of the otherwise transparent samples.

3.5   Demonstrator applications of multilayer fabrication

The use cases of the developed PDMS ink as a dielectric were studied when applied to electrical circuits: first between two layers of conductive tracks when all layers were deposited directly on top of each other. This application demonstrator was built on a glass carrier with a PTFE coating, and the PDMS substrate was applied on top of the carrier using a spin coater. The spinning speed was 1600 rpm, and the duration was 60 s. The functional layers were printed on the substrate, which could be peeled from the carrier and attached to the target surface (skin).

In the second approach, PDMS was used in soft capacitive sensors as the dielectric material. The free-standing functional layers were printed separately on a supporting electrospun PVA substrate. Then, the layers were attached with the previously developed PDMS ink solution to form a sandwiched metal-insulator-metal structure.

3.5.1   Conductive circuits

In **Publication III**, devices with two overlapping conductive layers, insulated by a PDMS dielectric, were fabricated on a PDMS substrate. The fabrication process and

the final device are presented in **Figure 8**. Since the PDMS surface is hydrophobic and thus conductive layer printing was not possible on the native PDMS; a surface treatment was used to make the substrate more hydrophilic. Here, N_2 plasma treatment was chosen based on the results obtained in the previously conducted printing trials of the Ag NP ink (DGP 40LT-15C, Advanced Nano Products).
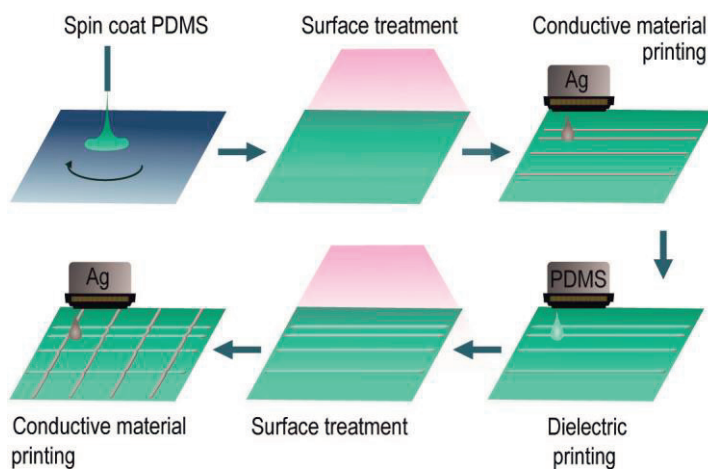
Figure 8. Process flow of multilayer printing **in Publications III and IV.** Adapted from **Publication III.**

The printer platen temperature was kept at 60 °C to let the inks dry and settle before curing. The first two-layered Ag NP print was then annealed at 120 °C for 30 minutes, followed by the printing of the PDMS ink. Next, up to eight layers of the dielectric ink were printed directly on the underlying surfaces, without any additional surface treatments. The printer platen temperature was again kept at 60 °C to prevent the excessive spread of the wet ink. Finally, when all layers had been printed, a hot plate was used to cure the elastomer ink at 120 °C for 20 minutes.

After the dielectric printing, the structure was again treated with the N_2 plasma. A PET foil was used as a temporary protective mask during the surface treatment to prevent oxidation of the uncovered conductive areas. Then, the topmost Ag tracks were printed perpendicular to the first silver layer, thus making the PDMS an electrically insulating layer of the multilayered lattice structure. After that, the whole system was again cured at 120 °C for 30 min to anneal the topmost Ag NPs.
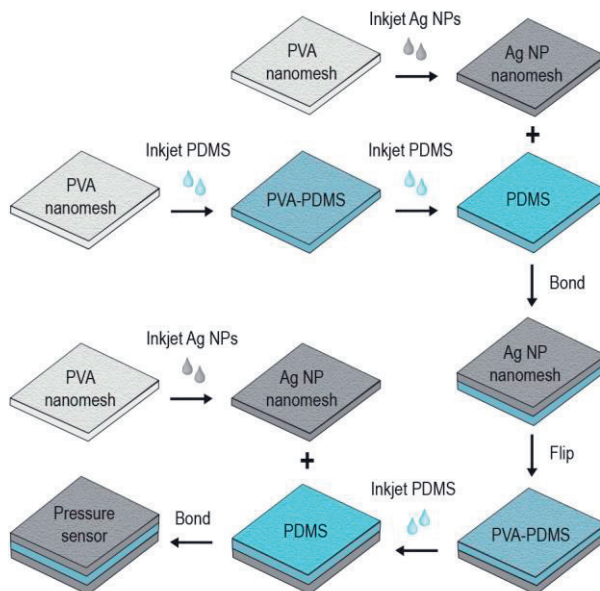
Cross-section samples of the circuits were fabricated with a focused ion beam (FIB), and the material layers were imaged with SEM (Crossbeam 540, Zeiss). Furthermore, after each curing step, microscope images were taken to monitor the print quality. The resistance of the conductive tracks was recorded after each curing step using a 4-wire sensing mode of a source measure unit (Keithley 2425) to check the possible changes in conductivity. The values were converted to sheet resistance using equation (2). These measures were taken to evaluate the suitability of the applied process for multilayer fabrication. In **Publication IV**, further studies on PDMS surface treatments and jetting were conducted.

3.5.2   Capacitive pressure sensors

An alternative fabrication strategy and its suitability for PDMS-based printed electronics manufacturing were studied in **Publication V**. The first aim was to improve the adhesion of the PDMS dielectric and the conductive layers. The second aim was to make the structures mechanically resilient, thus better suitable for soft electronics applications. Here, a PVA nanomesh was fabricated as the substrate material for two reasons. First, it served as a template for fabricating mesh-like, thin, and flexible conductive layers. Secondly, it was used to print self-standing PDMS layers with additional mechanical support. Then, the different material layers could be merged simply by stacking the layers on top of each other, using the earlier developed PDMS ink solution as a bonding medium. To demonstrate the applicability of this new method to printed electronics manufacturing, soft, fully inkjet-printed capacitive pressure sensors were built and characterized.

The capacitive sensors were built, as shown in **Figure 9**. First, the PVA nanomesh was electrospun using a syringe infusion pump (KDS 100, KdScientific) and a voltage supply (Chargemaster, SIMCO). A 2 ml·h^{-1} feeding speed was used at a 25 cm distance and 25 kV voltage between the needle and the substrate. After peeling the PVA sheets off the foil carrier, both the conductive and dielectric layers of the sensors were inkjet-printed on the PVA sheets using a commercial Ag NP silver ink (DGP 40LT-15C, Advanced nanoproducts), and the house-made PDMS-octyl acetate ink, respectively. Two curing agent-to-base ratios of PDMS (1:10 & 1:20) were used to study whether the cross-linking density of the silicone would affect the performance. These printed layers were cured, Ag NPs at 120 °C for 60 min and PDMS at 120 °C for 25 min, after which the dielectric was covered with the PDMS ink to attach the first conductive layer of the sensor. The layers were pressed together and heated to seal the bond (120

°C for 25 min). The device was flipped, and the other conductive plate was bonded similarly. Reference sensors were fabricated for comparison. A spin-coated dielectric was used instead of printed ones, with the same cross-linking densities.

Figure 9. Schematics of the sensor fabrication process. Adapted from **Publication V**.

SEM imaging was used to inspect the structure of the different layers: cross-section samples of the sensors were fabricated with FIB, and the material layers of both the printed sensors and the reference ones were imaged (Crossbeam 540, Zeiss). To investigate mesh resistivity, conductive tracks with varying layer counts (1–6 layers) were printed, and the resistance was measured for the sheet resistance calculation.

The sensor performance was characterized by measuring the capacitance C as a function of the applied pressure P. Copper tape connected the sensor electrodes to an LCR meter (ST2827A, Sourcetronics). A mechanical tester (TA.XTplus, Stable Micro Systems) was used to apply force, and a small piece of silicone rubber (Ecoflex™ 00-50, Smooth-On Inc.) was attached to the tester's cylindrical probe tip to mimic a tissue-like force source.

The capacitances were recorded when loads equaling 0.1–50 kPa pressure were applied to the sensor. First, the load was maintained for 1 s, then 10 s. The latter test

results were used to calculate the sensitivity of the sensors. First, the relative change in capacitance C_r was calculated as follows:

$$C_r = \frac{C-C_0}{C_0},$$

(9)

where C is the measured capacitance, and C_0 is the initial capacitance when no load is applied. Sensitivity S is the ratio of the changing capacitance and changing pressure:

$$S = \frac{\Delta C_r}{\Delta P}.$$

(10)

Furthermore, the hysteresis of the sensors was measured by slowly applying a load on the sensor and then slowly removing the load. The maximum load applied was 6.4 kPa. The repeatability of the devices was investigated by measuring the dynamic sensor response in a cyclic test, where an approximately 20 kPa peak-to-peak sinusoidal load was applied for 2000 cycles. The frequency of the loading cycle was 0.5 Hz.

4 RESULTS AND DISCUSSION

In this Chapter, the principal results and findings of the thesis are presented and discussed. First, the options for conductive pattern printing are discussed in Section 4.1. and 4.2. that focus on the ink compatibility and reliability on the native and treated PPE substrates (Section 4.1.), and inkjet printing of Ag NP ink on PDMS (Section 4.2.). Next, the developed PDMS ink properties are shown and discussed in Section 4.3. Finally, the focus moves to the multilayer fabrication in Section 4.4. The first part (4.4.1.) is dedicated to the direct layer-by-layer deposition, followed by a discussion of the mesh-based approach and the fabricated capacitive sensors in Subsection 4.4.2. The approaches are further discussed and compared in the last Subsection of this Chapter (4.4.3.)

4.1   Screen-printed tracks on PPE

The measured surface energies and surface roughness values (RMS-roughness R_q and peak-to-peak roughness R_t) are shown in **Table 7**. The surface energy of both substrates was measured to be 30-32 mN·m^{-1}, and the extruded substrate surface was relatively rough (R_q 380–1150 nm, R_t 3–6 μm) in comparison to the injection-molded ones (R_q 28–56 nm, R_t 0.3–1 μm). The surface treatments had different effects on the substrate, both on the surface energy and the roughness parameters.

The results of the electrical and mechanical tests, shown in **Table 8**, indicate that the surface roughness of the hydrophobic, relatively rough surface of the extruded substrate affected the adhesion between the ink and the substrate negatively, as the ink removal was markedly greater (5–100 %) than that on the injection-molded substrate (0–15 %). The results obtained in **Publication I** suggested that the H$_2$SO4 etching may improve ink adhesion on the substrate, whereas the KOH etching treatment did not affect the adhesion. However, no definitive conclusions can be made about the effects of these etching treatments. Instead, O$_2$ plasma treatment could significantly improve the ink adhesion, decreasing the ink removal of all samples to 0% from the original, up to 15 % removal.

Therefore, O_2 plasma treatment was also used in **Publication II**. It was compared to new, alternative treatments, including flame-based silicating treatment (NanoFlame) and airbrush coating of the injection-molded substrates that were either native or previously etched with the acid. The results indicate that the direct airbrush coating of the native PPE did not affect the adhesion of the inks on the substrate. In contrast, the combined acid-etching with coating and NanoFlame treatments positively affected ink adhesion.

Table 7. A summary of the measured surface energies and roughness values of the native and modified PPE surfaces.

Substrate	Surface energy (mN·m^{-1})	Rq (nm)	Rt (µm)
PPE	30-32	28–56	0.3–1.0
O_2 plasma	≥ 60	75–93	1.3–2
H_2SO_4	56–58	32–58	0.4–1.6
KOH	32–34	32–56	0.6–1.7
H_2SO_4 + coating	58–60	53–110	1.2–1.7
Coating	33–39	45–115	0.7–1.6
NanoFlame	≥ 60	42–65	0.8–1.6
Extruded PPE	30–32	380–1150	3.0–6.0

Table 8. A summary of the used materials' measured sheet resistances and adhesion rates.

Ink	Sheet resistance (mΩ·□$^{-1}$)	Ink removal on the substrate (%)							
		PPE	Plasma	H_2SO_4	KOH	Acid + coating	Coating	Nano-Flame	Extruded PPE
CRSN2442	8-28	5–15	0	0–15	5–15	0–5	5–15	0	15–65
5064H	10-25	0–5	0	0	0–5	0	5	0–5	5–100
LS411AW	14-30	0	0	-	-	0-5	0	0	0
HPS-021LV	10-20	0	0	-	-	0	0–5	0	0

The results indicate that the increment of surface energy plays a vital role in ink adhesion. The treatments likely affect the functional groups on the substrate surface [207]. Moreover, the roughened surface may increase the contact area between the materials, allowing stronger adhesion simply because there is more space for bonding between the functional groups [208]. In general, it looks like both higher surface

energy ($\geq$ 58 mN·m^{-1}) and roughening of the surface are required to promote ink adhesion on the substrate. However, there is some variation in the roughness parameters. For example, the combined acid-etching with coating results in a relatively rough surface compared to Nanoflame treatment, assumingly because the former coating layer is thicker. Still, the surface energy of the NanoFlame-treated substrate is higher. Despite these differences, the adhesion rate was somewhat similar, although the treatments seem to work better with different inks.

No significant difficulties in wetting were observed even with the water-based HPS-021LV ink, although the lines tend to be narrower than the rest. As the screen printing inks are highly viscous and the ink volume transferred through the screen is relatively high, the print quality is less sensitive to the substrate's surface properties. Nevertheless, significant variation was seen in the prints' obtained line width, thickness, and surface roughness values. Since the used screen printer relies on manual adjustment of the squeegee pressure and the snap-off distance, it is hard to explicitly determine whether the differences relate to material properties or the process.

As prints with sufficiently low sheet resistance and good adhesion were obtained with 5064H, LS411AW, and HPS-021LV inks, these materials were chosen for the accelerated aging tests. There, we also compared the effects of wet and dry surface treatments, and thus, patterns were printed on the native PPE (reference), on the acid-etched and coated PPE (wet treatment), and on the O$_2$ plasma-treated PPE (dry treatment). A summary of the material combinations is given in **Table 9**. The results of the crosscut peel-off test after the aging tests indicate that most material combinations survived the 85 % RH/85 °C test tolerably, even though various failure types started to occur. In contrast, the salt mist test led to severe adhesion and material degradation, as shown in **Figure 10**.

Table 9. Fabricated test samples for the accelerated aging tests.

Ink	Substrate	85/85	Salt mist
LS411AW	Native PPE	1a	1b
	O$_2$ plasma-treated	2a	2b
	Acid-etched + coated	3a	3b
5064H	Native PPE	4a	4b
	O$_2$ plasma-treated	5a	5b
	Acid-etched + coated	6a	6b
HPS-021LV	Native PPE	7a	7b
	O$_2$ plasma-treated	8a	8b
	Acid-etched + coated	9a	9b

In a sense, this result was expected. The former test is used to evaluate the moisture resistance of the devices at elevated temperatures and can be very harsh for temperature-sensitive polymers like PET. Because the temperature was well below the softening point of PPE, this test should not be as severe for it. The salt mist test simulates an even harsher marine environment where devices are exposed to high relative humidity and cyclic salt mist. The likelihood for corrosive reactions of Ag is higher in the presence of NaCl.
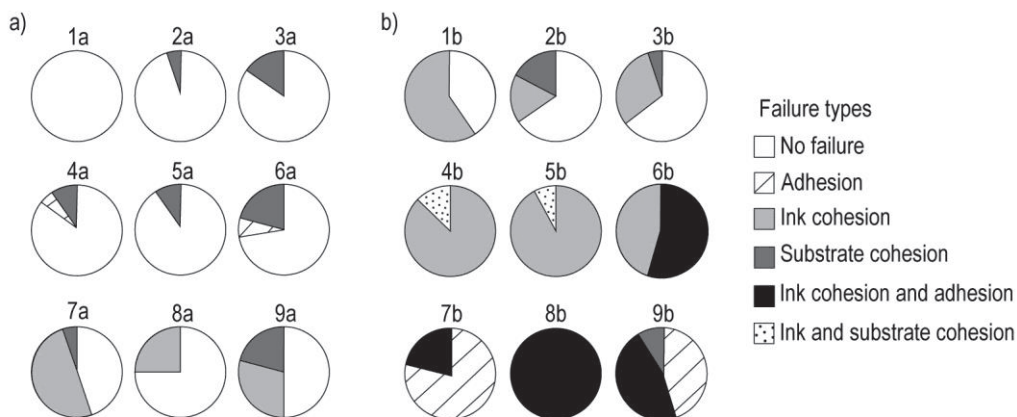

Figure 10. Failure types of the aged samples after a) 85/85 test and b) salt mist test. Redrawn from **Publication II**.

Corrosion products were detected only on the surface of the LS411W and 5064H prints. In the peel-off test, ink cohesion failed on the corroded areas, while the rest of the ink remained intact, except for the observed adhesion failures. Judging from the particle size of the suspected corrosive compounds, variating from tens of nanometers to several micrometers, several corrosion products may have been formed, even though most of them are likely to be forms of silver chloride (AgCl) [209]–[211]. These corroded areas were focused on the edges of the prints (**Figure 11**), and the print surface on edge may have been rougher, allowing the anchoring of the NaCl particles.

As noted above, no visible corrosion marks were seen on the surface of HPS021LV prints. Still, both the adhesion and ink cohesion degradation was dramatic compared to the other inks. The corrosion products may have been dissolved in the chamber at some point, but Ag corrosion still took place. It is suspected that the wetting and adhesion of the aqueous HPS021LV may be poorer than those of the solvent-based

inks despite the excellent initial test results, and the loose flake structure may enhance the absorption of corrosive compounds. The interaction of the ink solvents with the substrate was not studied, but the low surface tensions of the 5064H ink and LS411AW ink solvents could improve wetting and, thus, strengthen adhesion. Substrate swelling of other significant material degradation mechanisms were not detected in the presence of inks or treatment chemicals. However, no conclusion about the solvent-substrate interaction mechanisms or their impact cannot be made.

Interestingly, the native PPE substrate was found to be somewhat sensitive to moisture, as the substrate cohesion began to fail during the adhesive tape peel-off after the environmental aging tests. Based on just these results, it cannot be determined whether the surface treatments provide protection against moisture or if they weaken the moisture resistance instead. However, the results emphasize the need for further studies with different encapsulation strategies to improve reliability. Encapsulation or cover films could protect the substrate and the prints, improve the mechanical resilience of the samples in general, and hinder the corrosion of the devices [212]–[214]. Cover films would also aid in embedding the smart structures into the surroundings in an indistinguishable manner. Options for adding a cover include printing, other chemical deposition methods like spray coating, or laminating a cover sheet on top of the structure.
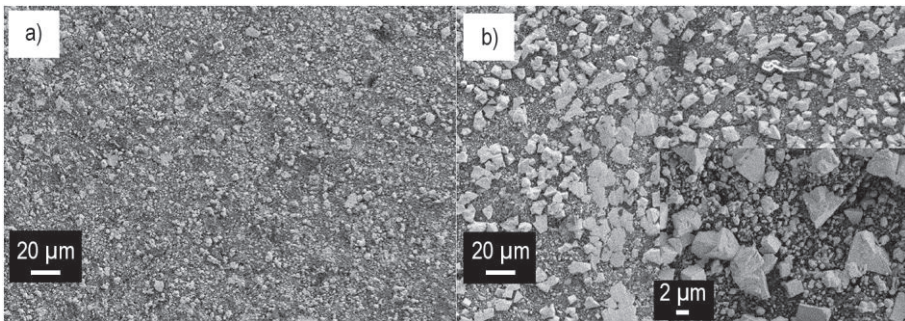
Figure 11. SEM image of the corroded Ag flake surface after the salt mist test a) in the middle and b) around the edge of the print. Adapted from **Publication II.**

Considering high-frequency applications, it would be essential to study the effects of the surface treatments on the substrate characteristics further to determine whether the modification of the substrate would affect, for example, the loss tangent of the material and thus, signal attenuation. It would also be of interest to determine the print reliability against environmental stress in natural marine surroundings, as it has been

pointed out that the chamber tests exclude some real-life corrosion contributors like ozone and UV radiation [209]–[211]. Even though the high-frequency applicability could not be studied in the scope of this thesis, the findings were utilized in a study where three-band, monopole-like antennas were designed and fabricated by screen printing on a thin and flexible, high permittivity substrate [215].

4.2   Inkjet printing on PDMS

As ink deposition on the native PDMS surface is impossible, different dry and wet surface treatments and their effects on printed patterns were studied in **Publications III** and **IV**. The microscopic images of the initial test prints on the used substrates are shown in **Figure 12**. The best print quality was obtained using the N_2 plasma treatment (**Figure 12**a&c), and the adhesion was good in the tape peel-off test: no visible ink removal was observed. However, the wetting of the Ag NP ink on the NanoFlame-treated substrate was not as good (**Figure 12**b), and print edges sometimes looked somewhat rough compared to the lines on plasma-treated PDMS (**Figure 12**e).

As the handheld device-based treatment relies heavily on the user, the coating may be uneven since the movement of the tool cannot be accurately controlled. However, the adhesion was comparable to that of the plasma-treated surface in the tape test, suggesting that this method can effectively manipulate the PDMS surface. A significant advantage of this method is simplicity. The only equipment needed is the handheld device filled with the functional gas, without masking and pre- or post-treatments.

Lastly, the ink wetting on the MPTMS-treated substrate was comparable to that of the N_2 treatment, but the surface was uneven, and the print quality suffered on this substrate. As seen in **Figure 12**c&f, the conductive patterns' edges are highly rough compared to the other material combinations. Moreover, the peel-off adhesion was poorer on this substrate, as the adhesive tape partially removed the ink. These results agree with those of [161], where MPTMS was used for surface modification of PDMS: ink adhesion was improved to some extent from that of the inks on a native substrate, but obtaining good print quality was challenging. However, with further optimization, this coating could be used for additive surface modification by printing and, thus, for selective patterning of Ag prints on PDMS [198]. In addition, screen printing could

be of interest with this treatment as the thick pastes can be used effectively even on rough surfaces, as noted earlier.
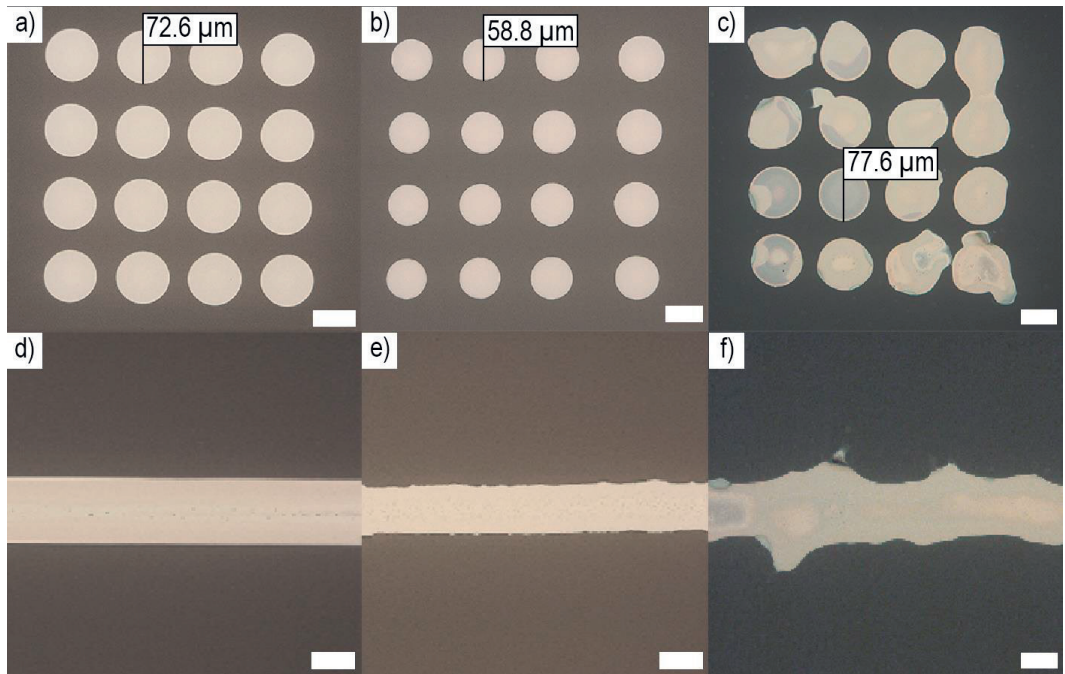
Figure 12. Microscope images of the conductive patterns on PDMS substrates: drop matrix on a) N_2 plasma-treated PDMS, b) NanoFlame treated PDMS, c) MPTMS-treated PDMS, and line on d) N_2 plasma-treated PDMS, e) NanoFlame treated PDMS, and f) MPTMS-treated PDMS. Scale bar 50 µm. Adapted from **Publication IV**.

After these initial tests, resistance measurements were conducted for the samples on N_2 plasma-treated, and NanoFlame treated PDMS as the print quality and adhesion seemed promising for the further trials. The obtained sheet resistance values were 250 m$\Omega\cdot\square^{-1}$ (mean) with a standard deviation of 25 m$\Omega\cdot\square^{-1}$ for the N_2 plasma samples and 321 m$\Omega\cdot\square^{-1}$ with a standard deviation of 63 m$\Omega\cdot\square^{-1}$ for the NanoFlame samples (**Publication IV**). Although the mean values do not differ significantly, there is more variation in the latter values. However, these results were expected as deviations in print quality can affect the conductivity of the samples, and further optimization of the flame-based treatment is required.

The inkjet-printed conductive tracks on PDMS were susceptible to wrinkling and cracking (**Publications III** and **IV**). This behavior is assumed to be a result of several

factors: first, the CTE value of this polymer is relatively high, and the thermal expansion may disturb the sintering process (**Table 3**). Secondly, even though silicones are resistive to most chemicals, they do swell in the presence of certain organic solvents, and thus, ink solvents may cause deformation. These issues were tackled mainly by optimizing the patterning strategy: first, the outlines of the conductive tracks were printed and dried, after which the created shape was filled with the Ag NP ink. This strategy helped to improve the print quality significantly.

4.3   Dielectric PDMS ink

The viscosity of all ink solutions remained relatively stable in the shear rate tests, indicating Newtonian behavior (**Figure 13**a). On the other hand, the temperature tests revealed that the faster evaporating IBA affected the results at high temperatures: in general, the viscosity decreases as the temperature increases, but the viscosity of the two IBA inks increased at the most elevated temperatures, indicating that the solvent evaporation rate may not be sufficient for these inks to function appropriately (**Figure 13**b). In addition, the viscosity slope of the PDMS-OA ink with a 1:2 concentration seemed to saturate at the high temperatures, suggesting that high PDMS concentration might affect the result.

The targeted minimum surface tension was 20 mN·m^{-1}, which was reached only with the octyl-acetate-based solutions (**Figure 13**c). However, the Z-numbers, often used to evaluate inkjet inks' printability, were all in the range of $1 < Z < 3$ for our ink solutions. Thus, all alternatives were selected for the initial jetting trials. However, it was observed that the solutions containing IBA could not be printed, or printing was possible only for a short time before nozzle clogging and the subsequent, exhaustive nozzle cleaning process.

This behavior is assumed to be a result of several factors. First, low volume printheads (droplet size 10 pl) and narrow nozzles (diameter 21 μm) are sensitive to slight variations in solution characteristics and printing parameters. Moreover, the solvent vapor pressure, which is not considered in calculating Z-numbers, dramatically impacts the inkjet. It has been shown that polymer ink solutions are also affected by, for example, the polymer's molecular weight and concentration [103]. The hypothesis about the significance of the solvent vapor pressure is supported by the results obtained with the OA-containing inks: all of them could be jetted effortlessly. Also, the jetting velocity, which is not considered in the calculated Z-numbers, affects both

the Weber and Reynolds numbers and, thus, plays a part in the droplet jetting. So, several parameters could cause the non-jetting tendency of the IBA inks.

Since the OA-inks could be jetted and OA is a less hazardous solvent than IBA, these inks were studied further. The inks containing at most 25 % PDMS functioned better, and to maximize the polymer content of the final prints, 1:3 (PDMS to OA) ink was chosen for the actual printing trials. The obtained Raman spectra indicate that the developed ink solution could be cured, so that cross-linking of PDMS takes place and that the solvent evaporates thoroughly in the process (**Figure 13**d). The thickness of one layer was approximately 3–5 μm with a drop spacing of 30 μm, equal to an 847–dpi resolution when printed on a PDMS (Sylgard 184) substrate. The resulting minimum linewidth of the prints was 45 μm. This resolution is relatively high [113], [205], [206], [216], [217] and valuable in such applications where accurate deposition of small dielectric ink volumes is needed. The lower layer thickness and higher resolution are assumed to be primarily a result of the smaller deposition volume of the used printer. Higher deposition volume would be beneficial for 3D fabrication, which has been demonstrated in [113], [204], [218].

In addition to jetting and print quality, the shelf life of the prepared inks was examined in **Publication IV**. All inks have a so-called shelf-life, which defines how long the inks will last functional after manufacturing. When stored in a refrigerator at approx. 5°C temperature, the ink solution remained functional for several weeks, depending on the curing agent-to-base ratio of the PDMS and the solvent concentration. The loaded printheads could be kept operational for 3–5 days when stored in the refrigerator overnight between the printing sessions. These findings agree with those of Peng et al. [205], who monitored the viscosities of the PDMS solutions stored at controlled temperatures. In addition, the printhead could be heated to keep it functional longer. However, eventually, the heating of the ink will accelerate the cross-linking process of the polymer and cause nozzle clogging.

It is also possible to print PDMS separating the polymer components, having them in their own printheads and depositing them in turn, based on the targeted mixing ratio and droplet volume to avoid the crosslinking process from disturbing printing [113], [206], [218]. This approach could be more advantageous in such procedures, where the printing of the PDMS must be done over a long time.

Although the composition of the printed PDMS layers was observed to resemble the cast reference, the electrical or mechanical properties of the prints were not studied or compared to the reference material here. However, good reports have been presented, for example, by McCoul et al. [206], who studied the behavior of inkjet-printed PDMS dielectric in dielectric elastomer actuators (DEA). The results suggest

that the inkjet-printed PDMS would be mechanically and electrically comparable to the cast reference dielectric. However, further studies are required to confirm the properties and material differences.
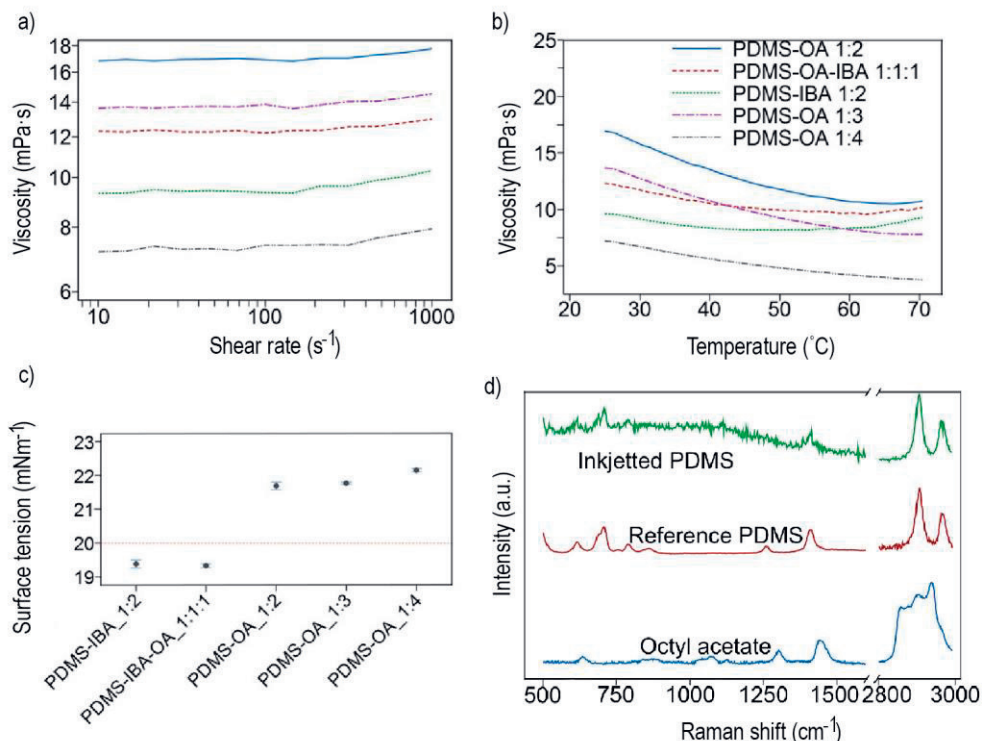

Figure 13. Properties of the dielectric inks: a) viscosity as a function of shear rate and b) temperature, c) measured surface tensions, and d) Raman spectra of the cured PDMS-OA 1:3 ink. Adapted from **Publication III**.

4.4   Applications of multilayer fabrication

Once the approaches for conductive track printing were selected, and the dielectric ink had been developed, experiments were moved to the multilayer fabrication phase. First, the options for a direct layer-by-layer deposition approach were studied, and the applicability of the selected method was demonstrated by building a 2-layer conductive circuit on a carrier substrate. The circuit consisted of stacked conductive lines separated by a printed PDMS dielectric. The proposed device structure is shown in **Figure 14**a, and the main findings are presented in Subsection 4.4.1. The alternative,

nanomesh-based approach and the obtained results are presented in Subsection 4.4.2. The device configuration is shown in **Figure 14**b. Finally, the main advantages and limitations of the two approaches are discussed in further detail (Subsection 4.4.3).
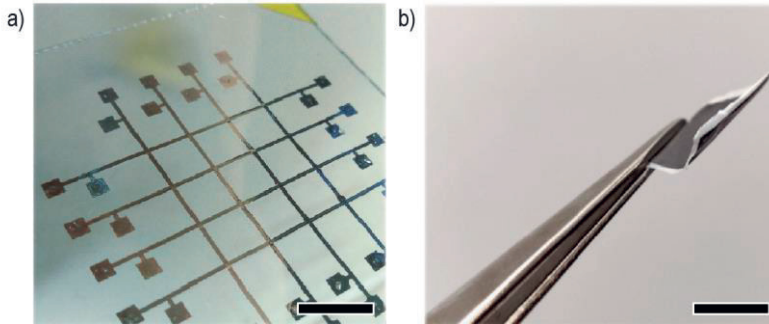

Figure 14. Photographs of the multilayered, PDMS-based electrical structures as-fabricated: a) stacked conductive circuits **(Publications III and IV)** and b) printed capacitive sensors **(Publication V).** Scale bar 1 cm.

4.4.1   Conductive circuits

The multilayer demonstrator circuits were fabricated once the promising surface treatments for improved ink wetting on PDMS were determined (N2 plasma and NanoFlame). The earlier optimized patterning strategy, where pattern outlines are printed before filling the pattern with ink, was used to print the dielectric and the conductive lines. This strategy helped to pin the PDMS ink to the underlying conductive layer. Thus, building a relatively thick (25 µm) dielectric was possible when eight printing passes (wet layers) were used. As seen in **Figure 15**, the chosen patterning strategy allowed the printing of crack-free conductive lines and control over ink spread at the topmost layer.

Unfortunately, not all wrinkles could be removed from the bottommost layers, and during the process, these wrinkles transformed into cracks. It is suspected that this behavior is a sum of several factors. First, there is a mismatch of CTE values between the materials, which may affect material deformation during the curing steps. Second, the adhesion of the ink on the substrate may not be strong enough to prevent the conductive layer from deforming, and third, the PDMS may react with the organic solvent of the ink and swell. However, no evident polymer swelling was observed.
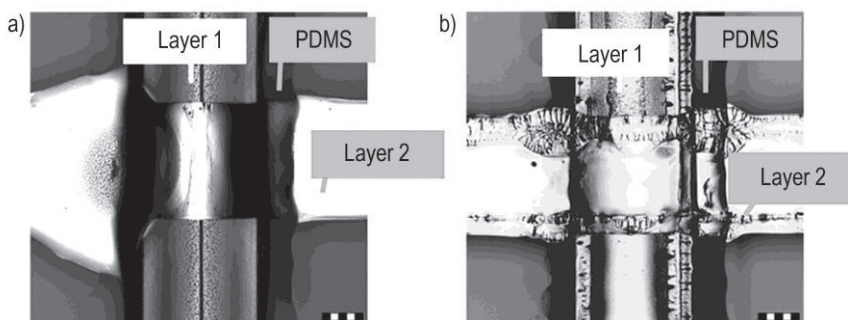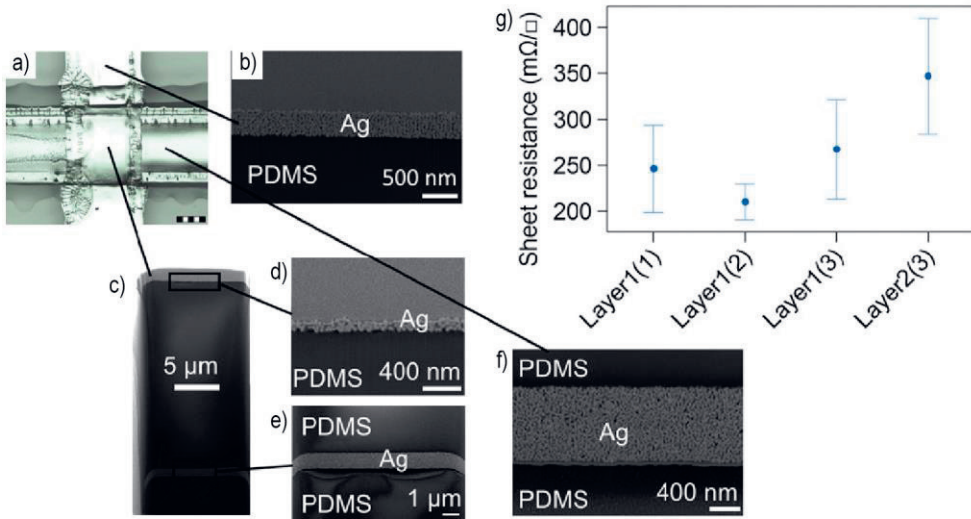
Figure 15. Microscope images of track intersection a) without optimization and b) with optimized patterning strategy. Scale bar 200 μm. Adapted from **Publication III.**

The cross-sectional images of the 2-layer circuits (**Figure 16**b–f) show the bottommost conductive layer being delaminated from the substrate in some pictures. Process issues or FIB could cause this delamination: the images from the line intersections had to be taken using an extremely powerful beam because of the structure thickness. However, as the resistance measurements show (**Figure 16**g), the cracking of the lines does not significantly affect the resistivity of the lines throughout the process. The resistance of the topmost lines was 40 % higher than that of the bottommost lines. The difference is most likely a result of layer thickness: the lines on top of the dielectric are relatively thin (200 nm) compared to the bottommost ones (up to 1 μm).

The dielectric layer appears to be very smooth and uniform in the microscope and SEM images (**Figure 16**). However, the line edges are not entirely straight, indicating that the ink might bulge when high volumes are printed. Bulding could be prevented by increasing the delay between layers or drop spacing. In addition, the surface profile of the 8-layer prints is dome-like, indicating that there is room for further optimization of the dielectric printing parameters.

In **Publication IV**, the pyrolytic silicating (NanoFlame) treatment was used for multilayer fabrication instead of plasma. The results suggest that the formed silica layer may improve the reliability of the conductive lines during the fabrication process because less Ag line cracking and wrinkling was observed. In a sense, this treatment also offers more flexibility and simplicity to the process, as the treatment is done simply by exposing the substrate to the oxidizing flame of this handheld device. However, the control over the process is not as good since it heavily depends on the operator. If the treatment is not even, the printing quality and ink adhesion will suffer due to the hydrophobicity of PDMS. Although the surface energy of the printed

PDMS dielectric was not studied after curing, the Ag ink was observed to bead up instead of forming continuous lines on the pristine, printed PDMS surface. Based on the measured ink surface tension values and the apparent absence of the solvent in the cured structure, the surface energy of the printed PDMS is assumed to be a little lower than the ink surface tension ($\leq$ 21 mN·m^{-1}).

Figure 16. a) Microscope image of the track intersection (scale bar 200 µm), cross-sectional images of b) topmost Ag layer on the substrate (scale bar 500 nm), c) PDMS dielectric (scale bar 5 µm), d) topmost Ag layer on top of the PDMS dielectric (scale bar 400 nm), e) bottommost Ag layer at the intersection (scale bar 1 µm), and f) bottommost Ag layer between PDMS layers (scale bar 400nm); g) sheet resistances of the bottommost layer (Layer1) and the topmost layer (Layer2) after curing of the first layer (1), after curing the dielectric (2), and after curing of the topmost layer (3). Adapted from **Publication III.**

4.4.2   Capacitive pressure sensors

After printing and annealing the Ag NP ink, the electrical properties of the conductive mesh sheets were determined. The sheet resistance of the layers is saturated to around 1–5 Ω·$\square^{-1}$ after printing 2–6 layers of the conductive material. These soft sheets became mechanically stable when more than one Ag NP layer was printed (further details in **Publication V**). To avoid densification of the mesh while maximizing the conductivity of the sensor electrodes. 4-layer prints were used in other trials. 4 layers of PDMS ink were needed to make the dielectric layer uniform. The thickness of both

the conductive and the dielectric layer was approximately 10 µm, and the thickness of the spin-coated reference dielectric was around 10–15 µm.

As seen in **Figure 17**, the integrated PVA mesh layers were effectively used to micro-structure all sensor layers. First, the conductive layer is highly porous, and single nanoparticles are visible on the mesh surface (**Figure 17**a&b). The structure is very different from the tracks fabricated previously in **Publications III** and **IV**. The images indicate that the printed bonding layer made of PDMS ink penetrates the conductive mesh effectively, whereas the pipetted bonding layer seems to leave the conductive layer more porous. However, since the final bond was achieved by pressing the layers together while the device was heated, it is uncertain whether this result is material- or process-dependent. In both cases, the conductive layer is well blended into the PDMS matrix (**Figure 17**c-f), compared to the process used in **Publications III** and **IV**.

Looking at the dielectric layer, one can see a clear difference between the reference sensors and the printed ones. This difference is because the PVA layer in which the PDMS was printed makes the dielectric layer porous (**Figure 17**e&f). Here, instead of using PVA as a sacrificial material that would be removed from the final structure by dissolving, we trapped it (at least in part) inside the PDMS layer. Thus, some unique mechanical and electrical properties were obtained. The first advantage was that even though the printed dielectric is just about 10 µm thick, it could easily be handled with tweezers after curing

Other advantages were observed in the sensor performance tests. The 1 s and 10 s touch test results indicate that the printed sensors are less sensitive to the applied pressure than the reference devices. Moreover, the soft printed sensor with the integrated PVA layer responds remarkably to the low-pressure area. The stiffer printed sensor had a somewhat linear response throughout the load range. Still, unfortunately, its sensitivity was so low that the response could not be separated from background noise in the low-pressure range.

Based on these results, the soft printed sensors were characterized further. In **Figure 18**, a summary of the sensor characteristics (sensitivity, hysteresis, and repeatability) is given. The soft printed sensor seems to have a sublinear response, as the sensitivity decreases at the higher loads (**Figure 18**a). This sublinear tendency might be advantageous in those applications where a vast range of loads should be detected since the slow response saturation may lead to a higher dynamic range. Not surprisingly, our device had a small but not negligible maximum hysteresis of 8.5 % (**Figure 18**b). Still, it could detect pressure reliably even after 2000 cycles with the sinusoidal load of 20 kPa, even though the sensitivity is not as high as in the initial

tests (**Figure 18**c). It is hard to determine the exact cause of this sensitivity degradation. Still, it should be noted that the sensors had been stored for three months in an ambient environment before the cyclic tests were conducted. Therefore, some material degradation may have taken place during that period. However, the dynamic response of the sensor remained stable for the whole cyclic test.
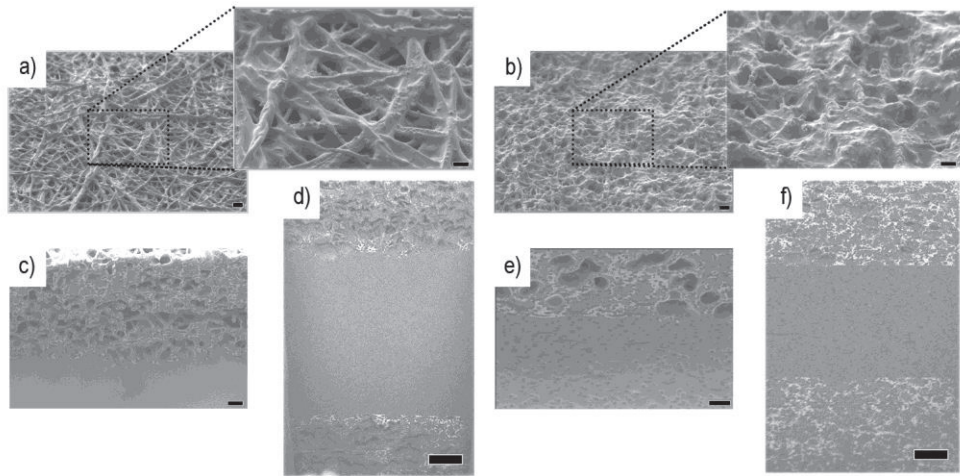
Figure 17. SEM-images of the fabricated sensors showing a) the surface of the reference sensor's mesh electrode, scale bar 1 μm (inset 500 nm), b) surface of the printed sensor's mesh electrode, scale bar 1 μm (inset 500 nm), c) interface between the reference sensor's electrode and the spin-coated dielectric, scale bar 1 μm, d) cross-section of the reference sensor: the spin-coated dielectric is sandwiched between the electrodes, scale bar 3 μm, e) interface between the printed sensor's electrode and the printed PVA-PDMS dielectric, scale bar 1 μm, and f) cross-section of the printed sensor: the printed PVA-PDMS dielectric is sandwiched between the electrodes, scale bar 3 μm. **Publication V**.

Despite these performance limitations, the physical impact on the surroundings and its strength could be detected in real-time, as demonstrated in the supporting video (available online). Thus, even though there is room for device performance in terms of sensitivity, which was only 4 MPa^{-1} at maximum here, this nanomesh-based, digital fabrication approach of PDMS-based electronics applications is promising for soft devices.
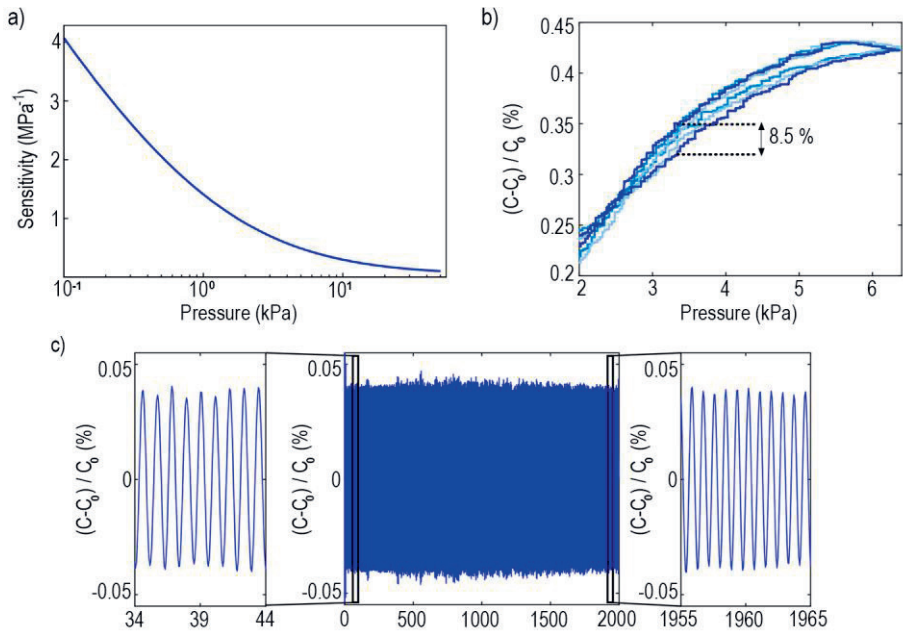
Figure 18. Performance of the soft printed PVA-sensor: a) sensitivity as a function of applied - pressure from 0.1 kPa to 50 kPa, b) the measured response and recovery of the sensor (2–6.4 kPa), maximum hysteresis of 8.5 % shown, and c) sensor performance in a cyclic test, where a loading-unloading cycle was repeated for 2000 cycles at a frequency of 0.5 Hz. Adapted from **Publication V.**

4.4.3 Comparison of the two approaches

Both multilayer fabrication approaches presented here have their advantages and limitations. In general, the method chosen depends on the intended application. The sheet resistance of the nanomesh-based patterns ($3 \, \Omega \cdot \square^{-1}$ at a 10 µm layer thickness) is relatively high compared to the lines deposited directly on PDMS ($< 0.3 \, \Omega \cdot \square^{-1}$ at a 1 µm layer thickness). Therefore, the direct deposition-based approach may be more useful when high conductivity is of the essence. However, as the electrical properties of the structures are based on many factors, such as the curing conditions, layer count, mesh density or thread size, the conductivity of the conductive nanofiber mesh could be improved with further optimization of the mesh structure.

In addition to the electrical properties, the porosity and density of the samples affect the potential uses. As the directly on PDMS-patterned lines are smooth compared to the mesh-like conductors, they could be more useful in high-frequency

applications. As for dielectric printing, the direct deposition could also be tremendously valuable for specific applications like RFID tags' antenna coils, where the overlapping conductive lines need to be separated from each other [219]. However, the surface of the printed dielectric must be treated to enable wetting of the topmost conductive layer. For such as small area, the handheld NanoFlame-tool or something similar could be used to allow selective surface modification without masking the underlying layers.

Another alternative is to use the screen printing method, which is not that sensitive to the substrate properties, and thick, highly conductive lines could be printed in just one pass, as demonstrated in **Publications I and II**. Even though the Ag NP inks are highly conductive, the layer thinness means that the resistance of the lines will be relatively high unless several layers are printed (**Table 2**). Screen-printed Ag flake (or NW) inks would also have intrinsic stretchability. Thus, genuinely stretchable devices could be fabricated without geometrical engineering or pre-stretching of the samples, which is inevitable to make NP patterns stretchable [182], [220]. Other functional materials could also improve the devices' sensitivity or make them optically transparent.

Even though screen printing could be a practical method choice for improving conductivity, especially in further states of the development process, the additive, digital methods are more useful in the first phases of product development where rapid prototyping options are needed. Some adjustments to the PDMS printing process could offer new possibilities for the presented approaches. As the droplet volume and inkjet printing speed are relatively low, another additive method like FDM or DIW could be used instead of inkjet printing. Although the print resolution is likely to suffer, ink formulating could be easier since a broader range of viscosities is within reach. In addition, shaping self-standing silicone elastomer structures by printing could become faster and more straightforward, as the deposited ink volume would be higher.

When the nanomesh PVA substrate was used, both the inkjet-printed PDMS layers and the conductive layers could be made self-standing in a simple manner since the patterns could be deposited directly onto the mesh-like substrate and cured. In addition to the self-standing structure, nanomesh-based layers are breathable, elastic, and transferable. All of these features are attractive for on-skin electronics [221]. Although the general idea of using electrospun materials in electronics fabrication is not entirely new [222]–[224], the method has become quite popular recently. The reasons are, first: suitability for on-skin electronics fabrication [221], [223], [225], [226] and, second: the high porosity together with the large surface area is of interest in triboelectric nanogenerators (TENGs) [227]–[230] and transparent devices [231],

[232]. The presented approach could simplify fabrication significantly because the conductive material can be coated on top of the mesh substrate using a desktop inkjet printer instead of conventional processes like vacuum deposition.

In addition to the conductive layers, the usage of the PVA nanofiber-substrate resulted in exciting properties in the case of PDMS prints. The nanomesh substrate was trapped inside the elastomer matrix. As the printed ink volume was targeted to be high enough to cover the mesh barely, the whole layer became micro-structured. This feature was found to be of significance for the response of the fabricated sensors. It has been shown earlier that PDMS cross-linking density, material choices, and micro-structuring can result in stimulating effects on the dielectric properties and may be used to adjust sensitivity, hysteresis, and linearity of the sensors [44], [189], [233]–[236]. Our work further indicates that a good balance between dielectric softness and microstructural level can improve sensor performance remarkably.

In addition to the effect on sensitivity, the trapped nanofibers offered excellent mechanical support for the thin (10 μm thick) PDMS layers. They enabled effortless handling of the tiny, just 1.5 cm wide samples. It is unclear how the mechanical properties of the PVA-PDMS differ from the cast PDMS, and this should be determined in the future. In addition, to make the dielectric layer more porous, printing on different PVA substrates with variating thicknesses, fiber diameters, and fiber densities should be studied. Alternatively, the electrospun material could be changed to, for example, PU. Electrospun PU-based, PDMS-coated nanomesh has improved mesh conformability in mechanical resilience and thinness [225].

Another limitation of the proposed approach is the obtained sensitivity of less or equal to 4 MPa^{-1}, which is modest compared to more advanced PDMS-based pressure sensors [237]–[241]. Moreover, the ultimate pressure range of the proposed sensors was not determined, although the studied range from 0.1 kPa to 60 kPa should cover most of the skin activities [242]. In the future, the properties of the PVA-PDMS-based dielectrics should be studied more carefully to determine the relationship between the nanofiber structure and the sensor characteristics. In addition to further adjustments of the porous dielectric layer, the options for mimicking the conventional, mold-based micro-structuring approaches like micro-pyramids or domes should be studied since the process could become even more straightforward if the dielectric were shaped additively. The presented technique could thus be applied to, for example, the previously mentioned TENG fabrication.

5 CONCLUSION

Touch panels, smart wearables, intelligent household appliances, and computer-driven automotive equipment are only a few examples of the remarkable advances in electronics so far. However, conventional technologies suffer from limitations such as rigidity, lack of customization, and complexity. The dream of integrating electronics seamlessly into our surroundings and people has led to the pursuit of new technologies, which would enable innovations toward highly customizable, conformable electronics. These alternative technologies, such as printed electronics, have the potential to revolutionize the future electronics market, making new production facilities both less expensive and simpler to set up. Upscaling the production could make new, intelligent, and conformable IoT devices readily available. Ideally, these new applications would be easily affordable and answer individual needs.

This thesis investigated applications of low surface energy polymers for printed electronics. These materials are commonly used as barrier films or sacrificial molds due to their non-sticky, water-repelling surfaces. Still, they can also offer other attractive properties, such as the materials used here: low-loss high-frequency characteristics, which are essential for the rapidly increasing wireless applications, and other valuable properties like various molding options, optical transparency, inertness, biocompatibility, and elasticity. The materials of interest here were, first, a PPE-based polymer blend, and second, a silicone elastomer (PDMS).

The first objective of this thesis was to investigate whether printing of electronics is possible on hydrophobic PPE and PDMS substrates and to what degree the process could be simplified. The definitions for simplicity and straightforwardness are hard to determine explicitly and are highly arguable. Ideally, the printed electronics fabrication process would include only two steps: printing and post-processing. Here, due to the hydrophobic nature of the substrates, surface pre-treatments were also studied for improved printability. Additional topics of interest related to the first question are the mechanical properties of the prints, such as the adhesion of the inks on the substrates and environmental reliability. Since weak bonding increases the likelihood of print delamination and makes the structure more vulnerable to corrosive compounds, the surface treatments may have a significant impact also on device reliability.

Even though the necessity of a prior treatment makes the process more time-consuming and complex, a careful investigation of the suitable methods can be used to reduce both process time and complexity, as shown in this thesis. For example, effective yet simple methods like nitrogen plasma or pyrolytic silicating add just one process step, and the treatment time is only a few minutes. Furthermore, as **Publications I and II** show**,** high-volume printing methods like screen printing and selected material combinations could be used without any additional surface treatments. This simplicity is a significant benefit compared to subtractive processes, where electronics fabrication requires several steps, including sacrificial coatings, photo exposure, and etching, only to pattern the conductive material. Finally, although the print adhesion and material degradation were severe in hot, humid, and salty environments, a proper cover or encapsulation layer would significantly improve the performance. A cover layer is anyhow needed to embed the devices to the surroundings.

As the PPE-based material is readily moldable using injection molding and extrusion, it is thus suitable for 3D molded electronics. In contrast, the silicone elastomer is a liquid, two-component, cross-linkable thermoset material, and options for both additive patterning and shaping are limited. Therefore, this thesis sought to examine the possibilities for additive patterning of PDMS using an electronics printer. The developed PDMS ink could be used with an Ag NP ink to build two types of multilayered structures: stacked conductive circuits and capacitive sensors.

The direct deposition-based approach (**Publications III and IV**) was helpful for its on-demand nature, reducing material consumption and processing time. However, as each layer was cured separately, and the printed PDMS also required plasma treatment to allow Ag NP printing on top of it, the samples needed to be removed from the printer between the printing rounds. In addition, the patterning strategy needed optimization to prevent both ink bleeding and print deformation.

In another multilayer approach that relied on an electrospun, water-soluble mesh template (**Publication V**), self-standing, mechanically robust, conductive, and dielectric films were fabricated. Only the template residues needed to be needed be dissolved in water. Thus, the surface pre-treatment was not required, although one additional step was needed to bond the layers. Pristine PDMS sheets could not be printed here either. Still, the fiber-PDMS composite was advantageous in the capacitance measurements, as the sensor performance improved remarkably compared to that of the reference sensors with the spin-coated dielectric.

The results serve as a reference point for further exploration of fully printed, multifunctional electronics using low surface energy materials. The required number

of process steps is highly dependent on the printing method, selected materials, and patterning strategy. Although the process can be simplified to a great extent by optimizing the fabrication strategy, the chosen approach was always a compromise of process complexity and device performance. The mechanical properties are at least as necessary for developing printed electronics as electrical performance.

As this work was mainly focused on material compatibility and only preliminary studies on device fabrication and performance were conducted, there are several proposals for future work. First, surface treatment impact and aging effects on the PPE substrate's dielectric properties should be studied. These steps are essential to further develop the structures for low-loss high-frequency applications. The encapsulation strategy should be selected accordingly. Further studies on printing parameters should also be conducted, as the semi-manual screen printer's print quality was not optimal. The aim should be to achieve and maintain excellent high-frequency characteristics while improving the mechanical resilience of the samples. Finally, to move from planar PPE applications to 3D structures, the options for extrusion-based fabrication should be studied, and the suitable printing method should be re-evaluated accordingly.

In addition to the previous suggestions, the electrical characteristics of the developed PDMS ink should be explored: features like the relative permittivity, dissipation factor, triboelectricity, or dielectric strength were not studied here. Understanding these parameters will be of the essence when the material is further applied. As the low volume and the limited speed of the inkjet printer prevented pristine PDMS sheet printing here, scaling up to a higher capacity inkjet printer or even changing the printing method should be considered. Additive printing of the substrate and encapsulation layers would enable great freedom of design and simplify the fabrication process. The options for pre-processing and post-processing of the embedded layers without interrupting the production line should also be studied to enhance the process further. A printer with an integrated post-processing unit could be used to solve the latter issue.

Finally, the mechanical properties like flexibility and stretchability of different configurations should be explored. As the results imply, the dielectric softness can be tuned simply by changing the cross-linking ratio of the elastomer or by creating composite layers. Furthermore, the mesh-based structure could withstand the applied stresses during the sensor performance characterization phase without additional engineering. A deeper understanding of the materials' mechanical properties could enable more accurate design and application of structures with controllable stiffness in a purely additive, on-demand manner. Controllable stiffness and the on-demand

shaping capability would also allow micro-structuring of the dielectric. These features would benefit various structures, like triboelectric nanogenerators or E-skin applications.

REFERENCES

[1]   R. Anyoha, "The History of Artificial Intelligence," *Science in the News*, 2017. https://sitn.hms.harvard.edu/flash/2017/history-artificial-intelligence/.

[2]   B. Chertok, M. J. Webber, M. D. Succi, and R. Langer, "Drug Delivery Interfaces in the 21st Century: From Science Fiction Ideas to Viable Technologies," *Mol. Pharm.*, vol. 10, no. 10, pp. 3531–3543, Oct. 2013, doi: 10.1021/mp4003283.

[3]   L. Cavendish, "Welcome to the future: 11 ideas that went from science fiction to reality," *All about Space*, 2020. https://www.space.com/science-fiction-turned-reality.html.

[4]   J. P. Collett, "The History of Electronics - From Vacuum Tubes to Transistors," in *Companion Encyclopedia of Science in the Twentieth Century*, J. Krige and D. Pestre, Eds. Taylor & Francis, 2003, pp. 253–274.

[5]   "ASML opens new state-of-the-art R&D facility in Silicon Valley," 2021. https://www.asml.com/en/news/press-releases/2021/asml-expands-presence-in-silicon-valley-with-new-campus.

[6]   P. F. Moonen, I. Yakimets, and J. Huskens, "Fabrication of Transistors on Flexible Substrates: from Mass-Printing to High-Resolution Alternative Lithography Strategies," *Adv. Mater.*, vol. 24, no. 41, pp. 5526–5541, Nov. 2012, doi: https://doi.org/10.1002/adma.201202949.

[7]   W. Wu, "Inorganic nanomaterials for printed electronics: a review," *Nanoscale*, vol. 9, no. 22, pp. 7342–7372, 2017, doi: 10.1039/C7NR01604B.

[8]   H. Kwon *et al.*, "Overview of recent progress in electrohydrodynamic jet printing in practical printed electronics: focus on the variety of printable materials for each component," *Mater. Adv.*, vol. 2, no. 17, pp. 5593–5615, 2021, doi: 10.1039/D1MA00463H.

[9]   Y. Khan, A. Thielens, S. Muin, J. Ting, C. Baumbauer, and A. C. Arias, "A New Frontier of Printed Electronics: Flexible Hybrid Electronics," *Adv. Mater.*, vol. 32, no. 15, p. 1905279, Apr. 2020, doi: https://doi.org/10.1002/adma.201905279.

[10]   C. Ducas, "Electrical apparatus and method of manufacturing the same," US1563731A, 1925.

[11]   H. Koezuka, A. Tsumura, and T. Ando, "Field-effect transistor with polythiophene thin film," *Synth. Met.*, vol. 18, no. 1, pp. 699–704, 1987, doi: https://doi.org/10.1016/0379-6779(87)90964-7.

[12]   C. W. Tang, "Two-layer organic photovoltaic cell," *Appl. Phys. Lett.*, vol. 48, no. 2, pp. 183–185, Jan. 1986, doi: 10.1063/1.96937.

[13]   J. H. Burroughes *et al.*, "Light-emitting diodes based on conjugated polymers," *Nature*, vol. 347, no. 6293, pp. 539–541, 1990, doi: 10.1038/347539a0.

[14]   J. A. Rogers *et al.*, "Paper-like electronic displays: Large-area rubber-stamped plastic sheets of electronics and microencapsulated electrophoretic inks," *Proc. Natl. Acad. Sci.*, vol. 98, no. 9, pp. 4835–4840, Apr. 2001, doi: 10.1073/pnas.091588098.

[15]   Z. Bao, Y. Feng, A. Dodabalapur, V. R. Raju, and A. J. Lovinger, "High-Performance Plastic Transistors Fabricated by Printing Techniques," *Chem. Mater.*, vol. 9, no. 6, pp. 1299–1301, Jun. 1997, doi: 10.1021/cm9701163.

[16]   D. A. Pardo, G. E. Jabbour, and N. Peyghambarian, "Application of Screen Printing in the

Fabrication of Organic Light-Emitting Devices," *Adv. Mater.*, vol. 12, no. 17, pp. 1249–1252, Sep. 2000, doi: https://doi.org/10.1002/1521-4095(200009)12:17<1249::AID-ADMA1249>3.0.CO;2-Y.

[17]   G. Francis, H. Ryad, Y. Abderrahim, and S. Pratima, "All-Polymer Field-Effect Transistor Realized by Printing Techniques," *Science (80-.).*, vol. 265, no. 5179, pp. 1684–1686, Sep. 1994, doi: 10.1126/science.265.5179.1684.

[18]   R. B. A., N. Babak, and J. J. M., "All-Inorganic Field Effect Transistors Fabricated by Printing," *Science (80-.).*, vol. 286, no. 5440, pp. 746–749, Oct. 1999, doi: 10.1126/science.286.5440.746.

[19]   S. B. Fuller, E. J. Wilhelm, and J. M. Jacobson, "Ink-jet printed nanoparticle microelectromechanical systems," *J. Microelectromechanical Syst.*, vol. 11, no. 1, pp. 54–60, 2002, doi: 10.1109/84.982863.

[20]   A. Kamyshny, M. Ben-Moshe, S. Aviezer, and S. Magdassi, "Ink-Jet Printing of Metallic Nanoparticles and Microemulsions," *Macromol. Rapid Commun.*, vol. 26, no. 4, pp. 281–288, Feb. 2005, doi: https://doi.org/10.1002/marc.200400522.

[21]   Y. Noguchi, T. Sekitani, and T. Someya, "Organic-transistor-based flexible pressure sensors using ink-jet-printed electrodes and gate dielectric layers," *Appl. Phys. Lett.*, vol. 89, no. 25, p. 253507, Dec. 2006, doi: 10.1063/1.2416001.

[22]   S. H. Ko, J. Chung, H. Pan, C. P. Grigoropoulos, and D. Poulikakos, "Fabrication of multilayer passive and active electric components on polymer using inkjet printing and low temperature laser processing," *Sensors Actuators A Phys.*, vol. 134, no. 1, pp. 161–168, 2007, doi: https://doi.org/10.1016/j.sna.2006.04.036.

[23]   D. R. Hines, V. W. Ballarotto, E. D. Williams, Y. Shao, and S. A. Solin, "Transfer printing methods for the fabrication of flexible organic electronics," *J. Appl. Phys.*, vol. 101, no. 2, p. 24503, Jan. 2007, doi: 10.1063/1.2403836.

[24]   H. Kang, R. Kitsomboonloha, J. Jang, and V. Subramanian, "High-Performance Printed Transistors Realized Using Femtoliter Gravure-Printed Sub-10 µm Metallic Nanoparticle Patterns and Highly Uniform Polymer Dielectric and Semiconductor Layers," *Adv. Mater.*, vol. 24, no. 22, pp. 3065–3069, Jun. 2012, doi: https://doi.org/10.1002/adma.201200924.

[25]   Y. Bonnassieux *et al.*, "The 2021 flexible and printed electronics roadmap," *Flex. Print. Electron.*, vol. 6, no. 2, p. 23001, 2021, doi: 10.1088/2058-8585/abf986.

[26]   K. Parida *et al.*, "Extremely stretchable and self-healing conductor based on thermoplastic elastomer for all-three-dimensional printed triboelectric nanogenerator," *Nat. Commun.*, vol. 10, no. 1, p. 2158, 2019, doi: 10.1038/s41467-019-10061-y.

[27]   X. Zhou *et al.*, "All 3D-printed stretchable piezoelectric nanogenerator with non-protruding kirigami structure," *Nano Energy*, vol. 72, p. 104676, 2020, doi: https://doi.org/10.1016/j.nanoen.2020.104676.

[28]   K. Sim *et al.*, "An epicardial bioelectronic patch made from soft rubbery materials and capable of spatiotemporal mapping of electrophysiological activity," *Nat. Electron.*, vol. 3, no. 12, pp. 775–784, 2020, doi: 10.1038/s41928-020-00493-6.

[29]   V. Subramanian *et al.*, "High-Speed Printing of Transistors: From Inks to Devices," *Proc. IEEE*, vol. 103, no. 4, pp. 567–582, 2015, doi: 10.1109/JPROC.2015.2408321.

[30]   N. Karim, S. Afroj, S. Tan, K. S. Novoselov, and S. G. Yeates, "All Inkjet-printed Graphene-Silver Composite Ink on Textiles for Highly Conductive Wearable Electronics Applications," *Sci. Rep.*, vol. 9, no. 1, p. 8035, 2019, doi: 10.1038/s41598-019-44420-y.

[31]   M. Kerndl and P. Šteffan, "Usage of offset printing technology for printed electronics and smart labels," in *2020 43rd International Conference on Telecommunications and Signal Processing (TSP)*, 2020, pp. 637–639, doi: 10.1109/TSP49548.2020.9163543.

[32]   Y. Kusaka, N. Fukuda, and H. Ushijima, "Recent advances in reverse offset printing: An emerging process for high-resolution printed electronics," *Jpn. J. Appl. Phys.*, vol. 59, no.

SG, 2020, doi: 10.7567/1347-4065/ab6462.

[33] S. Emamian, B. B. Narakathu, A. A. Chlaihawi, B. J. Bazuin, and M. Z. Atashbar, "Screen printing of flexible piezoelectric based device on polyethylene terephthalate (PET) and paper for touch and force sensing applications," *Sensors Actuators A Phys.*, vol. 263, pp. 639–647, 2017, doi: https://doi.org/10.1016/j.sna.2017.07.045.

[34] S. Cai, Y. Sun, Z. Wang, W. Yang, X. Li, and H. Yu, "Mechanisms, influencing factors, and applications of electrohydrodynamic jet printing," *Nanotechnol. Rev.*, vol. 10, no. 1, pp. 1046–1078, 2021, doi: doi:10.1515/ntrev-2021-0073.

[35] D. F. Fernandes, C. Majidi, and M. Tavakoli, "Digitally printed stretchable electronics: a review," *J. Mater. Chem. C*, vol. 7, no. 45, pp. 14035–14068, 2019, doi: 10.1039/C9TC04246F.

[36] A. H. Espera, J. R. C. Dizon, Q. Chen, and R. C. Advincula, "3D-printing and advanced manufacturing for electronics," *Prog. Addit. Manuf.*, vol. 4, no. 3, pp. 245–267, 2019, doi: 10.1007/s40964-019-00077-7.

[37] J. Lee, H.-C. Kim, J.-W. Choi, and I. H. Lee, "A review on 3D printed smart devices for 4D printing," *Int. J. Precis. Eng. Manuf. Technol.*, vol. 4, no. 3, pp. 373–383, 2017, doi: 10.1007/s40684-017-0042-x.

[38] O. Rusanen, T. Simula, P. Niskala, V. Lindholm, and M. Heikkinen, "Injection Molded Structural Electronics Brings Surfaces to Life," in *2019 22nd European Microelectronics and Packaging Conference & Exhibition (EMPC)*, Sep. 2019, pp. 1–7, doi: 10.23919/EMPC44848.2019.8951795.

[39] J. Kim, R. Kumar, A. J. Bandodkar, and J. Wang, "Advanced Materials for Printed Wearable Electrochemical Devices: A Review," *Adv. Electron. Mater.*, vol. 3, no. 1, p. 1600260, Jan. 2017, doi: https://doi.org/10.1002/aelm.201600260.

[40] K. Fukuda and T. Someya, "Recent Progress in the Development of Printed Thin-Film Transistors and Circuits with High-Resolution Printing Technology," *Adv. Mater.*, vol. 29, no. 25, p. 1602736, Jul. 2017, doi: https://doi.org/10.1002/adma.201602736.

[41] T. D. Ngo, A. Kashani, G. Imbalzano, K. T. Q. Nguyen, and D. Hui, "Additive manufacturing (3D printing): A review of materials, methods, applications and challenges," *Compos. Part B Eng.*, vol. 143, pp. 172–196, 2018, doi: https://doi.org/10.1016/j.compositesb.2018.02.012.

[42] Q. Huang and Y. Zhu, "Printing Conductive Nanomaterials for Flexible and Stretchable Electronics: A Review of Materials, Processes, and Applications," *Adv. Mater. Technol.*, vol. 4, no. 5, p. 1800546, May 2019, doi: https://doi.org/10.1002/admt.201800546.

[43] Y. Liao, R. Zhang, and J. Qian, "Printed electronics based on inorganic conductive nanomaterials and their applications in intelligent food packaging," *RSC Adv.*, vol. 9, no. 50, pp. 29154–29172, 2019, doi: 10.1039/C9RA05954G.

[44] J. Shi *et al.*, "Multiscale Hierarchical Design of a Flexible Piezoresistive Pressure Sensor with High Sensitivity and Wide Linearity Range," *Small*, vol. 14, no. 27, p. 1800819, Jul. 2018, doi: https://doi.org/10.1002/smll.201800819.

[45] Y. Wang, T. Yokota, and T. Someya, "Electrospun nanofiber-based soft electronics," *NPG Asia Mater.*, vol. 13, no. 1, p. 22, 2021, doi: 10.1038/s41427-020-00267-8.

[46] W.-T. Park and Y.-Y. Noh, "A self-aligned high resolution patterning process for large area printed electronics," *J. Mater. Chem. C*, vol. 5, no. 26, pp. 6467–6470, 2017, doi: 10.1039/C7TC01590A.

[47] A. Hanif, T. Q. Trung, S. Siddiqui, P. T. Toi, and N.-E. Lee, "Stretchable, Transparent, Tough, Ultrathin, and Self-limiting Skin-like Substrate for Stretchable Electronics," *ACS Appl. Mater. Interfaces*, vol. 10, no. 32, pp. 27297–27307, Aug. 2018, doi: 10.1021/acsami.8b08283.

[48] S.-J. Potts, C. Phillips, E. Jewell, B. Clifford, Y. C. Lau, and T. Claypole, "High-speed

imaging the effect of snap-off distance and squeegee speed on the ink transfer mechanism of screen-printed carbon pastes," *J. Coatings Technol. Res.*, vol. 17, no. 2, pp. 447–459, 2020, doi: 10.1007/s11998-019-00291-6.

[49]   N. Kapur, S. J. Abbott, E. D. Dolden, and P. H. Gaskell, "Predicting the Behavior of Screen Printing," *IEEE Trans. Components, Packag. Manuf. Technol.*, vol. 3, no. 3, pp. 508–515, 2013, doi: 10.1109/TCPMT.2012.2228743.

[50]   K. Cao, K. Cheng, and Z. Wang, "Optimization of Screen Printing Process," in *2006 7th International Conference on Electronic Packaging Technology*, 2006, pp. 1–4, doi: 10.1109/ICEPT.2006.359881.

[51]   K. Suganuma, "Printing Technology BT - Introduction to Printed Electronics," K. Suganuma, Ed. New York, NY: Springer New York, 2014, pp. 23–48.

[52]   B. N. Altay *et al.*, "Impact of Substrate and Process on the Electrical Performance of Screen-Printed Nickel Electrodes: Fundamental Mechanism of Ink Film Roughness," *ACS Appl. Energy Mater.*, vol. 1, no. 12, pp. 7164–7173, Dec. 2018, doi: 10.1021/acsaem.8b01618.

[53]   D.-Y. Shin, Y. Lee, and C. H. Kim, "Performance characterization of screen printed radio frequency identification antennas with silver nanopaste," *Thin Solid Films*, vol. 517, no. 21, pp. 6112–6118, 2009, doi: https://doi.org/10.1016/j.tsf.2009.05.019.

[54]   B. Fasolt, M. Hodgins, G. Rizzello, and S. Seelecke, "Effect of screen printing parameters on sensor and actuator performance of dielectric elastomer (DE) membranes," *Sensors Actuators A Phys.*, vol. 265, pp. 10–19, 2017, doi: https://doi.org/10.1016/j.sna.2017.08.028.

[55]   N. Komoda, M. Nogi, K. Suganuma, K. Kohno, Y. Akiyama, and K. Otsuka, "Printed silver nanowire antennas with low signal loss at high-frequency radio," *Nanoscale*, vol. 4, no. 10, pp. 3148–3153, 2012, doi: 10.1039/C2NR30485F.

[56]   A. Hudd, "Inkjet printing technologies," in *The Chemistry of Inkjet Inks*, S. Magdassi, Ed. New Jersey-London-Singapore: World Scientific, 2010, pp. 3–18.

[57]   C. Ning, Z. Zhou, G. Tan, Y. Zhu, and C. Mao, "Electroactive polymers for tissue regeneration: Developments and perspectives," *Prog. Polym. Sci.*, vol. 81, pp. 144–162, 2018, doi: https://doi.org/10.1016/j.progpolymsci.2018.01.001.

[58]   M. Bashir and P. Rajendran, "A review on electroactive polymers development for aerospace applications," *J. Intell. Mater. Syst. Struct.*, vol. 29, no. 19, pp. 3681–3695, Sep. 2018, doi: 10.1177/1045389X18798951.

[59]   J. Jiang *et al.*, "Fabrication of Transparent Multilayer Circuits by Inkjet Printing," *Adv. Mater.*, vol. 28, no. 7, pp. 1420–1426, Feb. 2016, doi: https://doi.org/10.1002/adma.201503682.

[60]   P. Leleux *et al.*, "Ionic Liquid Gel-Assisted Electrodes for Long-Term Cutaneous Recordings," *Adv. Healthc. Mater.*, vol. 3, no. 9, pp. 1377–1380, Sep. 2014, doi: https://doi.org/10.1002/adhm.201300614.

[61]   M. S. Chavali and M. P. Nikolova, "Metal oxide nanoparticles and their applications in nanotechnology," *SN Appl. Sci.*, vol. 1, no. 6, p. 607, 2019, doi: 10.1007/s42452-019-0592-3.

[62]   Z. Zhu *et al.*, "Functional Metal Oxide Ink Systems for Drop-on-Demand Printed Thin-Film Transistors," *Langmuir*, vol. 36, no. 30, pp. 8655–8667, Aug. 2020, doi: 10.1021/acs.langmuir.0c00835.

[63]   Q. Lei, J. He, B. Zhang, J. Chang, and D. Li, "Microscale electrohydrodynamic printing of conductive silver features based on in situ reactive inks," *J. Mater. Chem. C*, vol. 6, no. 2, pp. 213–218, 2018, doi: 10.1039/C7TC04114D.

[64]   J.-J. Chen, G.-Q. Lin, Y. Wang, E. Sowade, R. R. Baumann, and Z.-S. Feng, "Fabrication of conductive copper patterns using reactive inkjet printing followed by two-step

electroless plating," *Appl. Surf. Sci.*, vol. 396, pp. 202–207, 2017, doi: https://doi.org/10.1016/j.apsusc.2016.09.152.

[65] D. Li, D. Sutton, A. Burgess, D. Graham, and P. D. Calvert, "Conductive copper and nickel lines via reactive inkjet printing," *J. Mater. Chem.*, vol. 19, no. 22, pp. 3719–3724, 2009, doi: 10.1039/B820459D.

[66] Y. Choi, K. Seong, and Y. Piao, "Metal−Organic Decomposition Ink for Printed Electronics," *Adv. Mater. Interfaces*, vol. 6, no. 20, p. 1901002, Oct. 2019, doi: https://doi.org/10.1002/admi.201901002.

[67] S. P. Douglas, S. Mrig, and C. E. Knapp, "MODs vs. NPs: Vying for the Future of Printed Electronics," *Chem. – A Eur. J.*, vol. 27, no. 31, pp. 8062–8081, Jun. 2021, doi: https://doi.org/10.1002/chem.202004860.

[68] W. Dong, C. Zhu, D. Ye, and Y. Huang, "Optimal design of self-similar serpentine interconnects embedded in stretchable electronics," *Appl. Phys. A*, vol. 123, no. 6, p. 428, 2017, doi: 10.1007/s00339-017-0985-3.

[69] Y. Su *et al.*, "In-Plane Deformation Mechanics for Highly Stretchable Electronics," *Adv. Mater.*, vol. 29, no. 8, p. 1604989, Feb. 2017, doi: https://doi.org/10.1002/adma.201604989.

[70] N. Alcheikh, S. F. Shaikh, and M. M. Hussain, "Ultra-stretchable Archimedean interconnects for stretchable electronics," *Extrem. Mech. Lett.*, vol. 24, pp. 6–13, 2018, doi: https://doi.org/10.1016/j.eml.2018.08.005.

[71] J. Bian, Y. Ding, Y. Duan, X. Wan, and Y. Huang, "Buckling-driven self-assembly of self-similar inspired micro/nanofibers for ultra-stretchable electronics," *Soft Matter*, vol. 13, no. 40, pp. 7244–7254, 2017, doi: 10.1039/C7SM01686G.

[72] S.-H. Ke *et al.*, "Printing the Ultra-Long Ag Nanowires Inks onto the Flexible Textile Substrate for Stretchable Electronics," *Nanomaterials* , vol. 9, no. 5. 2019, doi: 10.3390/nano9050686.

[73] N. Matsuhisa *et al.*, "Printable elastic conductors with a high conductivity for electronic textile applications," *Nat. Commun.*, vol. 6, no. 1, p. 7461, 2015, doi: 10.1038/ncomms8461.

[74] S. Choi *et al.*, "Stretchable Heater Using Ligand-Exchanged Silver Nanowire Nanocomposite for Wearable Articular Thermotherapy," *ACS Nano*, vol. 9, no. 6, pp. 6626–6633, Jun. 2015, doi: 10.1021/acsnano.5b02790.

[75] F. Spina, A. Pouryazdan, J. Costa, L. Ponce Cuspinera, and N. Münzenrieder, "Directly 3D-printed monolithic soft robotic gripper with liquid metal microchannels for tactile sensing," *Flex. Print. Electron.*, vol. 4, Jul. 2019, doi: 10.1088/2058-8585/ab3384.

[76] Y. Mao, Y. Wu, P. Zhang, Y. Yu, Z. He, and Q. Wang, "Nanocellulose-based reusable liquid metal printed electronics fabricated by evaporation-induced transfer printing," *J. Mater. Sci. Technol.*, vol. 61, pp. 132–137, 2021, doi: https://doi.org/10.1016/j.jmst.2020.05.040.

[77] S.-H. Min, G.-Y. Lee, and S.-H. Ahn, "Direct printing of highly sensitive, stretchable, and durable strain sensor based on silver nanoparticles/multi-walled carbon nanotubes composites," *Compos. Part B Eng.*, vol. 161, pp. 395–401, 2019, doi: https://doi.org/10.1016/j.compositesb.2018.12.107.

[78] Y. Wang, A. Liu, Y. Han, and T. Li, "Sensors based on conductive polymers and their composites: a review," *Polym. Int.*, vol. 69, no. 1, pp. 7–17, Jan. 2020, doi: https://doi.org/10.1002/pi.5907.

[79] A. Falco, F. C. Loghin, M. Becherer, P. Lugli, J. F. Salmerón, and A. Rivadeneyra, "Low-Cost Gas Sensing: Dynamic Self-Compensation of Humidity in CNT-Based Devices," *ACS Sensors*, vol. 4, no. 12, pp. 3141–3146, Dec. 2019, doi: 10.1021/acssensors.9b01095.

[80] Y. Liao *et al.*, "Highly conductive carbon-based aqueous inks toward electroluminescent devices, printed capacitive sensors and flexible wearable electronics," *RSC Adv.*, vol. 9, no.

27, pp. 15184–15189, 2019, doi: 10.1039/C9RA01721F.

[81] S. Mekhmouken *et al.*, "Gold nanoparticle-based eco-friendly ink for electrode patterning on flexible substrates," *Electrochem. commun.*, vol. 123, p. 106918, 2021, doi: https://doi.org/10.1016/j.elecom.2021.106918.

[82] K. Izumi, Y. Ochiai, D. Shiokawa, Y. Yoshida, D. Kumaki, and S. Tokito, "Effects of silver nanowire concentration on resistivity and flexibility in hybrid conducting films," *Jpn. J. Appl. Phys.*, vol. 56, no. 5S2, p. 05EB02, 2017, doi: 10.7567/jjap.56.05eb02.

[83] L.-C. Jia, C.-G. Zhou, W.-J. Sun, L. Xu, D.-X. Yan, and Z.-M. Li, "Water-based conductive ink for highly efficient electromagnetic interference shielding coating," *Chem. Eng. J.*, vol. 384, p. 123368, 2020, doi: https://doi.org/10.1016/j.cej.2019.123368.

[84] M. Kanzaki, Y. Kawaguchi, and H. Kawasaki, "Fabrication of Conductive Copper Films on Flexible Polymer Substrates by Low-Temperature Sintering of Composite Cu Ink in Air," *ACS Appl. Mater. Interfaces*, vol. 9, no. 24, pp. 20852–20858, Jun. 2017, doi: 10.1021/acsami.7b04641.

[85] A. Corletto and J. G. Shapter, "High-resolution and scalable printing of highly conductive PEDOT:PSS for printable electronics," *J. Mater. Chem. C*, vol. 9, no. 40, pp. 14161–14174, 2021, doi: 10.1039/D1TC03761G.

[86] M. Y. Teo, L. Stuart, H. Devaraj, C. Y. Liu, K. C. Aw, and J. Stringer, "The in situ synthesis of conductive polyaniline patterns using micro-reactive inkjet printing," *J. Mater. Chem. C*, vol. 7, no. 8, pp. 2219–2224, 2019, doi: 10.1039/C8TC06485G.

[87] A. Aziz, M. B. Bazbouz, and M. E. Welland, "Double-Walled Carbon Nanotubes Ink for High-Conductivity Flexible Electrodes," *ACS Appl. Nano Mater.*, vol. 3, no. 9, pp. 9385–9392, Sep. 2020, doi: 10.1021/acsanm.0c02013.

[88] J. Zhang, X. Li, M. Zhang, Q. Zhu, and X. Sun, "Flexible and ultra-thin silver films with superior electromagnetic interference shielding performance via spin-coating silver metal–organic decomposition inks," *Mater. Adv.*, vol. 3, no. 1, pp. 647–657, 2022, doi: 10.1039/D1MA00918D.

[89] J. Li *et al.*, "Solution-processable organic and hybrid gate dielectrics for printed electronics," *Mater. Sci. Eng. R Reports*, vol. 127, pp. 1–36, 2018, doi: https://doi.org/10.1016/j.mser.2018.02.004.

[90] S. K. Garlapati, M. Divya, B. Breitung, R. Kruk, H. Hahn, and S. Dasgupta, "Printed Electronics Based on Inorganic Semiconductors: From Processes and Materials to Devices," *Adv. Mater.*, vol. 30, no. 40, p. 1707600, Oct. 2018, doi: https://doi.org/10.1002/adma.201707600.

[91] A. Chortos, E. Hajiesmaili, J. Morales, D. R. Clarke, and J. A. Lewis, "3D Printing of Interdigitated Dielectric Elastomer Actuators," *Adv. Funct. Mater.*, vol. 30, no. 1, p. 1907375, Jan. 2020, doi: https://doi.org/10.1002/adfm.201907375.

[92] M. G. Mohammed and R. Kramer, "All-Printed Flexible and Stretchable Electronics," *Adv. Mater.*, vol. 29, no. 19, p. 1604965, May 2017, doi: 10.1002/adma.201604965.

[93] S. Magdassi, "Ink Requirements and Formulation Guidelines," in *The Chemistry of Inkjet Inks*, S. Magdassi, Ed. New Jersey-London-Singapore: World Scientific, 2010, pp. 19–42.

[94] J. Law and R. Rennie, "viscosity." Oxford University Press, 2020, doi: 10.1093/acref/9780198841227.013.4281.

[95] Z. Żolek-Tryznowska, "6 - Rheology of Printing Inks," J. Izdebska and S. B. T.-P. on P. Thomas, Eds. William Andrew Publishing, 2016, pp. 87–99.

[96] J. Law and R. Rennie, "Newtonian fluid." Oxford University Press, 2020, doi: 10.1093/acref/9780198841227.013.2849.

[97] C. Xu and N. Willenbacher, "How rheological properties affect fine-line screen printing of pastes: a combined rheological and high-speed video imaging study," *J. Coatings Technol. Res.*, vol. 15, no. 6, pp. 1401–1412, 2018, doi: 10.1007/s11998-018-0091-2.

[98]   P.-G. de Gennes, F. Brochard-Wyart, and D. Quéré, "Capillarity: Deformable Interfaces," in *Capillarity and Wetting Phenomena*, New York, NY: Springer New York, 2004, pp. 1–31.

[99]   B. He, S. Yang, Z. Qin, B. Wen, and C. Zhang, "The roles of wettability and surface tension in droplet formation during inkjet printing," *Sci. Rep.*, vol. 7, no. 1, p. 11841, 2017, doi: 10.1038/s41598-017-12189-7.

[100]   V. Bergeron, D. Bonn, J. Y. Martin, and L. Vovelle, "Controlling droplet deposition with polymer additives," *Nature*, vol. 405, no. 6788, pp. 772–775, 2000, doi: 10.1038/35015525.

[101]   D. Jang, D. Kim, and J. Moon, "Influence of Fluid Physical Properties on Ink-Jet Printability," *Langmuir*, vol. 25, no. 5, pp. 2629–2635, Mar. 2009, doi: 10.1021/la900059m.

[102]   N. Reis, C. Ainsley, and B. Derby, "Ink-jet delivery of particle suspensions by piezoelectric droplet ejectors," *J. Appl. Phys.*, vol. 97, no. 9, p. 94903, Apr. 2005, doi: 10.1063/1.1888026.

[103]   B.-J. de Gans, P. C. Duineveld, and U. S. Schubert, "Inkjet Printing of Polymers: State of the Art and Future Developments," *Adv. Mater.*, vol. 16, no. 3, pp. 203–213, Feb. 2004, doi: 10.1002/adma.200300385.

[104]   E. Tekin, P. J. Smith, and U. S. Schubert, "Inkjet printing as a deposition and patterning tool for polymers and inorganic particles," *Soft Matter*, vol. 4, no. 4, pp. 703–713, 2008, doi: 10.1039/B711984D.

[105]   J. Samuel and P. Edwards, "Solvent-Based Inkjet Inks," in *The Chemistry of Inkjet Inks*, S. Magdassi, Ed. New Jersey-London-Singapore: World Scientific, 2010, pp. 141–160.

[106]   D. Soltman and V. Subramanian, "Inkjet-printed Line Morphologies and Temperature Control of the Coffee Ring Effect," *Langmuir*, vol. 24, no. 5, pp. 2224–2231, Mar. 2008, doi: 10.1021/la7026847.

[107]   S.-J. Potts, C. Phillips, T. Claypole, and E. Jewell, "The Effect of Carbon Ink Rheology on Ink Separation Mechanisms in Screen-Printing," *Coatings*, vol. 10, no. 10. 2020, doi: 10.3390/coatings10101008.

[108]   C. Yüce, K. Okamoto, L. Karpowich, A. Adrian, and N. Willenbacher, "Non-volatile free silver paste formulation for front-side metallization of silicon solar cells," *Sol. Energy Mater. Sol. Cells*, vol. 200, p. 110040, 2019, doi: https://doi.org/10.1016/j.solmat.2019.110040.

[109]   K. Abdel Aal and N. Willenbacher, "Front side metallization of silicon solar cells – A high-speed video imaging analysis of the screen printing process," *Sol. Energy Mater. Sol. Cells*, vol. 217, p. 110721, 2020, doi: https://doi.org/10.1016/j.solmat.2020.110721.

[110]   Y. Son *et al.*, "Application of the specific thermal properties of Ag nanoparticles to high-resolution metal patterning," *Thermochim. Acta*, vol. 542, pp. 52–56, 2012, doi: https://doi.org/10.1016/j.tca.2012.03.004.

[111]   J. Simon and A. Langenscheidt, "Curing behavior of a UV-curable inkjet ink: Distinction between surface-cure and deep-cure performance," *J. Appl. Polym. Sci.*, vol. 137, no. 40, p. 49218, Oct. 2020, doi: https://doi.org/10.1002/app.49218.

[112]   M. Abulikemu, E. H. Da'as, H. Haverinen, D. Cha, M. A. Malik, and G. E. Jabbour, "In Situ Synthesis of Self-Assembled Gold Nanoparticles on Glass or Silicon Substrates through Reactive Inkjet Printing," *Angew. Chemie Int. Ed.*, vol. 53, no. 2, pp. 420–423, Jan. 2014, doi: https://doi.org/10.1002/anie.201308429.

[113]   C. Sturgess, C. J. Tuck, I. A. Ashcroft, and R. D. Wildman, "3D reactive inkjet printing of polydimethylsiloxane," *J. Mater. Chem. C*, vol. 5, no. 37, pp. 9733–9745, 2017, doi: 10.1039/c7tc02412f.

[114]   L. Sun *et al.*, "Flexible high-frequency microwave inductors and capacitors integrated on a polyethylene terephthalate substrate," *Appl. Phys. Lett.*, vol. 96, no. 1, p. 13509, Jan. 2010, doi: 10.1063/1.3280040.

[115]   W. Shen, X. Zhang, Q. Huang, Q. Xu, and W. Song, "Preparation of solid silver nanoparticles for inkjet printed flexible electronics with high conductivity," *Nanoscale*, vol. 6, no. 3, pp. 1622–1628, 2014, doi: 10.1039/C3NR05479A.

[116] A. Capasso, A. E. Del Rio Castillo, H. Sun, A. Ansaldo, V. Pellegrini, and F. Bonaccorso, "Ink-jet printing of graphene for flexible electronics: An environmentally-friendly approach," *Solid State Commun.*, vol. 224, pp. 53–63, 2015, doi: https://doi.org/10.1016/j.ssc.2015.08.011.

[117] K. Alzoubi, S. Lu, B. Sammakia, and M. Poliks, "Experimental and Analytical Studies on the High Cycle Fatigue of Thin Film Metal on PET Substrate for Flexible Electronics Applications," *IEEE Trans. Components, Packag. Manuf. Technol.*, vol. 1, no. 1, pp. 43–51, 2011, doi: 10.1109/TCPMT.2010.2100911.

[118] R. D. Rodriguez *et al.*, "Ultra-Robust Flexible Electronics by Laser-Driven Polymer-Nanomaterials Integration," *Adv. Funct. Mater.*, vol. 31, no. 17, p. 2008818, Apr. 2021, doi: https://doi.org/10.1002/adfm.202008818.

[119] R. F. de Oliveira *et al.*, "Water-gated organic transistors on polyethylene naphthalate films," *Flex. Print. Electron.*, vol. 1, no. 2, p. 25005, 2016, doi: 10.1088/2058-8585/1/2/025005.

[120] T. N. Ng *et al.*, "Scalable printed electronics: an organic decoder addressing ferroelectric non-volatile memory," *Sci. Rep.*, vol. 2, no. 1, p. 585, 2012, doi: 10.1038/srep00585.

[121] R. O. F. Verkuijlen, M. H. A. van Dongen, A. A. E. Stevens, J. van Geldrop, and J. P. C. Bernards, "Surface modification of polycarbonate and polyethylene naphtalate foils by UV-ozone treatment and µPlasma printing," *Appl. Surf. Sci.*, vol. 290, pp. 381–387, 2014, doi: https://doi.org/10.1016/j.apsusc.2013.11.089.

[122] S. Park, H.-Y. Chang, S. Rahimi, A. L. Lee, L. Tao, and D. Akinwande, "Transparent Nanoscale Polyimide Gate Dielectric for Highly Flexible Electronics," *Adv. Electron. Mater.*, vol. 4, no. 2, p. 1700043, Feb. 2018, doi: https://doi.org/10.1002/aelm.201700043.

[123] W.-Y. Chang, T.-H. Fang, S.-H. Yeh, and Y.-C. Lin, "Flexible Electronics Sensors for Tactile Multi-Touching," *Sensors* , vol. 9, no. 2. 2009, doi: 10.3390/s9021188.

[124] M. Matsumura and R. P. Camata, "Pulsed laser deposition and photoluminescence measurements of ZnO thin films on flexible polyimide substrates," *Thin Solid Films*, vol. 476, no. 2, pp. 317–321, 2005, doi: https://doi.org/10.1016/j.tsf.2004.10.019.

[125] W. J. Hyun, E. B. Secor, M. C. Hersam, C. D. Frisbie, and L. F. Francis, "High-Resolution Patterning of Graphene by Screen Printing with a Silicon Stencil for Highly Flexible Printed Electronics," *Adv. Mater.*, vol. 27, no. 1, pp. 109–115, Jan. 2015, doi: https://doi.org/10.1002/adma.201404133.

[126] H.-P. Phan *et al.*, "High temperature silicon-carbide-based flexible electronics for monitoring hazardous environments," *J. Hazard. Mater.*, vol. 394, p. 122486, 2020, doi: https://doi.org/10.1016/j.jhazmat.2020.122486.

[127] R. Liu *et al.*, "In Situ Growth of Silver Film on Polyimide with Tuned Morphologies for Flexible Electronics," *Langmuir*, vol. 37, no. 31, pp. 9540–9546, Jul. 2021, doi: 10.1021/acs.langmuir.1c01392.

[128] H. R. Khaleel, H. M. Al-Rizzo, D. G. Rucker, and S. Mohan, "A Compact Polyimide-Based UWB Antenna for Flexible Electronics," *IEEE Antennas Wirel. Propag. Lett.*, vol. 11, pp. 564–567, 2012, doi: 10.1109/LAWP.2012.2199956.

[129] V. Zardetto, T. M. Brown, A. Reale, and A. Di Carlo, "Substrates for flexible electronics: A practical investigation on the electrical, film flexibility, optical, temperature, and solvent resistance properties," *J. Polym. Sci. Part B Polym. Phys.*, vol. 49, no. 9, pp. 638–648, May 2011, doi: https://doi.org/10.1002/polb.22227.

[130] W. A. MacDonald *et al.*, "Latest advances in substrates for flexible electronics," *J. Soc. Inf. Disp.*, vol. 15, no. 12, pp. 1075–1083, Dec. 2007, doi: https://doi.org/10.1889/1.2825093.

[131] K. Suganuma, "Substrate and Barrier Film," in *Introduction to printed electronics*, New York: Springer, 2014, pp. 87–94.

[132] W. Dang, V. Vinciguerra, L. Lorenzelli, and R. Dahiya, "Printable stretchable interconnects," *Flex. Print. Electron.*, vol. 2, no. 1, p. 13003, 2017, doi: 10.1088/2058-

8585/aa5ab2.

[133] Y. Liu, M. Pharr, and G. Antonio Salvatore, "Lab-on-Skin: A Review of Flexible and Stretchable Electronics for Wearable Health Monitoring," *ACS Nano*, vol. 11, no. 10, pp. 9614–9635, Sep. 2017, doi: 10.1021/acsnano.7b04898.

[134] R. A. Shanks and I. Kong, "General Purpose Elastomers: Structure, Chemistry, Physics and Performance BT - Advances in Elastomers I: Blends and Interpenetrating Networks," P. M. Visakh, S. Thomas, A. K. Chandra, and A. P. Mathew, Eds. Berlin, Heidelberg: Springer Berlin Heidelberg, 2013, pp. 11–45.

[135] Y. Wang *et al.*, "A durable nanomesh on-skin strain gauge for natural skin motion monitoring with minimum mechanical constraints," *Sci. Adv.*, vol. 6, no. 33, p. eabb7043, Aug. 2020, doi: 10.1126/sciadv.abb7043.

[136] S. Lee *et al.*, "Nanomesh pressure sensor for monitoring finger manipulation without sensory interference," *Science (80-.).*, vol. 370, no. 6519, pp. 966 LP – 970, Nov. 2020, doi: 10.1126/science.abc9735.

[137] Z. Gozutok, O. Kinj, I. Torun, A. T. Ozdemir, and M. S. Onses, "One-step deposition of hydrophobic coatings on paper for printed-electronics applications," *Cellulose*, vol. 26, no. 5, pp. 3503–3512, 2019, doi: 10.1007/s10570-019-02326-y.

[138] T.-H. Joubert, P. H. Bezuidenhout, H. Chen, S. Smith, and K. J. Land, "Inkjet-printed Silver Tracks on Different Paper Substrates," *Mater. Today Proc.*, vol. 2, no. 7, pp. 3891–3900, 2015, doi: https://doi.org/10.1016/j.matpr.2015.08.018.

[139] A. Colas and J. Curtis, "7 - Silicones," in *Plastics Design Library*, K. Modjarrad and S. B. T.-H. of P. A. in M. and M. D. Ebnesajjad, Eds. Oxford: William Andrew Publishing, 2013, pp. 131–143.

[140] P. Król and B. Król, "Surface free energy of polyurethane coatings with improved hydrophobicity," *Colloid Polym. Sci.*, vol. 290, no. 10, pp. 879–893, 2012, doi: 10.1007/s00396-012-2598-x.

[141] J. Pippola, T. Marttila, and L. Frisk, "Protective coatings of electronics under harsh thermal shock," *Microelectron. Reliab.*, vol. 54, no. 9, pp. 2048–2052, 2014, doi: https://doi.org/10.1016/j.microrel.2014.07.106.

[142] D. Maddipatla, B. B. Narakathu, and M. Atashbar, "Recent Progress in Manufacturing Techniques of Printed and Flexible Sensors: A Review," *Biosensors* , vol. 10, no. 12. 2020, doi: 10.3390/bios10120199.

[143] "PREPERM® L260." Premix Group, p. 2, 2015.

[144] H. Li, Y. Ma, and Y. Huang, "Material innovation and mechanics design for substrates and encapsulation of flexible electronics: a review," *Mater. Horizons*, vol. 8, no. 2, pp. 383–400, 2021, doi: 10.1039/D0MH00483A.

[145] T. H. J. van Osch, J. Perelaer, A. W. M. de Laat, and U. S. Schubert, "Inkjet Printing of Narrow Conductive Tracks on Untreated Polymeric Substrates," *Adv. Mater.*, vol. 20, no. 2, pp. 343–345, Jan. 2008, doi: https://doi.org/10.1002/adma.200701876.

[146] K. Dogome, T. Enomae, and A. Isogai, "Method for controlling surface energies of paper substrates to create paper-based printed electronics," *Chem. Eng. Process. Process Intensif.*, vol. 68, pp. 21–25, 2013, doi: https://doi.org/10.1016/j.cep.2013.01.003.

[147] P. Zheng *et al.*, "Surface modification of polyimide (PI) film using water cathode atmospheric pressure glow discharge plasma," *Appl. Surf. Sci.*, vol. 259, pp. 494–500, 2012, doi: https://doi.org/10.1016/j.apsusc.2012.07.073.

[148] S. Park *et al.*, "Silicones for Stretchable and Durable Soft Devices: Beyond Sylgard-184," *ACS Appl. Mater. & Interfaces*, vol. 10, no. 13, pp. 11261–11268, Mar. 2018, doi: 10.1021/acsami.7b18394.

[149] E. Gonzalez, M. D. Barankin, P. C. Guschl, and R. F. Hicks, "Remote Atmospheric-Pressure Plasma Activation of the Surfaces of Polyethylene Terephthalate and

Polyethylene Naphthalate," *Langmuir*, vol. 24, no. 21, pp. 12636–12643, Nov. 2008, doi: 10.1021/la802296c.

[150] A. Frohn and N. Roth, "Theory BT - Dynamics of Droplets," A. Frohn and N. Roth, Eds. Berlin, Heidelberg: Springer Berlin Heidelberg, 2000, pp. 1–61.

[151] S. Ebnesajjad, "Chapter 5 - Theories of Adhesion," S. B. T.-S. T. of M. for A. B. (Second E. Ebnesajjad, Ed. Oxford: William Andrew Publishing, 2014, pp. 77–91.

[152] B. Parbhoo, L.-A. O'Hare, and S. R. Leadley, "Chapter 14 - Fundamental aspects of adhesion technology in silicones," D. A. Dillard, A. V Pocius, and M. B. T.-A. S. and E. Chaudhury, Eds. Amsterdam: Elsevier Science B.V., 2002, pp. 677–709.

[153] I. Reinhold, "Inkjet Printing of Functional Materials and Post-Processing," *Nanomaterials for 2D and 3D Printing.* pp. 27–49, Apr. 10, 2017, doi: https://doi.org/10.1002/9783527685790.ch2.

[154] J. Schirmer, J. Roudenko, M. Reichenberger, S. Neermann, and J. Franke, "Adhesion Measurements for Printed Electronics: A Novel Approach to Cross Cut Testing," in *2018 41st International Spring Seminar on Electronics Technology (ISSE)*, 2018, pp. 1–5, doi: 10.1109/ISSE.2018.8443665.

[155] A. Ryspayeva *et al.*, "A rapid technique for the direct metallization of PDMS substrates for flexible and stretchable electronics applications," *Microelectron. Eng.*, vol. 209, pp. 35–40, Mar. 2019, doi: 10.1016/J.MEE.2019.03.001.

[156] S. Ebnesajjad, "Chapter 9 - Plasma Treatment of Polymeric Materials," S. B. T.-S. T. of M. for A. B. (Second E. Ebnesajjad, Ed. Oxford: William Andrew Publishing, 2014, pp. 227–269.

[157] I. Mathieson and R. H. Bradley, "Improved adhesion to polymers by UV/ozone surface oxidation," *Int. J. Adhes. Adhes.*, vol. 16, no. 1, pp. 29–31, 1996, doi: https://doi.org/10.1016/0143-7496(96)88482-X.

[158] T. Laine-Ma, P. Ruuskanen, S. Kortet, and M. Karttunen, "Electroless copper plating and surface characterization of thermoplastic PPO based printed circuit boards," *Circuit World*, vol. 35, no. 4, pp. 22–30, Jan. 2009, doi: 10.1108/03056120911002389.

[159] S. S. Yoon *et al.*, "Direct metallization of gold patterns on polyimide substrate by microcontact printing and selective surface modification," *Microelectron. Eng.*, vol. 85, no. 1, pp. 136–142, 2008, doi: https://doi.org/10.1016/j.mee.2007.04.142.

[160] K. Dae-Hyeong *et al.*, "Epidermal Electronics," *Science (80-.).*, vol. 333, no. 6044, pp. 838–843, Aug. 2011, doi: 10.1126/science.1206157.

[161] E. V Agina *et al.*, "Polymer Surface Engineering for Efficient Printing of Highly Conductive Metal Nanoparticle Inks," *ACS Appl. Mater. Interfaces*, vol. 7, no. 22, pp. 11755–11764, Jun. 2015, doi: 10.1021/am508905t.

[162] S. H. Jeong, S. Zhang, K. Hjort, J. Hilborn, and Z. Wu, "PDMS-Based Elastomer Tuned Soft, Stretchable, and Sticky for Epidermal Electronics," *Adv. Mater.*, vol. 28, no. 28, pp. 5830–5836, 2016, doi: 10.1002/adma.201505372.

[163] S. Xiao, X. Hao, Y. Yang, L. Li, N. He, and H. Li, "Feasible fabrication of a wear-resistant hydrophobic surface," *Appl. Surf. Sci.*, vol. 463, pp. 923–930, 2019, doi: https://doi.org/10.1016/j.apsusc.2018.09.030.

[164] J. Wang *et al.*, "Fabrication of hydrophobic surface with hierarchical structure on Mg alloy and its corrosion resistance," *Electrochim. Acta*, vol. 55, no. 22, pp. 6897–6906, 2010, doi: https://doi.org/10.1016/j.electacta.2010.05.070.

[165] Y. Y. Yao, Y. J. Ding, H. P. Li, S. Chen, R. Guo, and J. Liu, "Multi-Substrate Liquid Metal Circuits Printing via Superhydrophobic Coating and Adhesive Patterning," *Adv. Eng. Mater.*, vol. 21, no. 7, p. 1801363, Jul. 2019, doi: https://doi.org/10.1002/adem.201801363.

[166] R. N. Shimizu and N. R. Demarquette, "Evaluation of surface energy of solid polymers

using different models," *J. Appl. Polym. Sci.*, vol. 76, no. 12, pp. 1831–1845, Jun. 2000, doi: https://doi.org/10.1002/(SICI)1097-4628(20000620)76:12<1831::AID-APP14>3.0.CO;2-Q.

[167]   R. M. Thurston, J. D. Clay, and M. D. Schulte, "Effect of Atmospheric Plasma Treatment On Polymer Surface Energy and Adhesion," *J. Plast. Film Sheeting*, vol. 23, no. 1, pp. 63–78, Jan. 2007, doi: 10.1177/8756087907078698.

[168]   P. F. Rios, H. Dodiuk, S. Kenig, S. McCarthy, and A. Dotan, "The effect of polymer surface on the wetting and adhesion of liquid systems," *J. Adhes. Sci. Technol.*, vol. 21, no. 3–4, pp. 227–241, Jan. 2007, doi: 10.1163/156856107780684567.

[169]   H. Drnovská, L. Lapčík, V. Buršíková, J. Zemek, and A. M. Barros-Timmons, "Surface properties of polyethylene after low-temperature plasma treatment," *Colloid Polym. Sci.*, vol. 281, no. 11, pp. 1025–1033, 2003, doi: 10.1007/s00396-003-0871-8.

[170]   S. P. Lacour, "Stretchable Thin-Film Electronics," *Stretchable Electronics*. pp. 81–109, Dec. 28, 2012, doi: https://doi.org/10.1002/9783527646982.ch4.

[171]   M. Wang *et al.*, "Single-electrode triboelectric nanogenerators based on sponge-like porous PTFE thin films for mechanical energy harvesting and self-powered electronics," *J. Mater. Chem. A*, vol. 5, no. 24, pp. 12252–12257, 2017, doi: 10.1039/C7TA02680C.

[172]   H. Zou *et al.*, "Quantifying the triboelectric series," *Nat. Commun.*, vol. 10, no. 1, p. 1427, 2019, doi: 10.1038/s41467-019-09461-x.

[173]   M. Kuang *et al.*, "Inkjet Printing Patterned Photonic Crystal Domes for Wide Viewing-Angle Displays by Controlling the Sliding Three Phase Contact Line," *Adv. Opt. Mater.*, vol. 2, no. 1, pp. 34–38, Jan. 2014, doi: https://doi.org/10.1002/adom.201300369.

[174]   D.-Y. Khang, J. A. Rogers, and H. H. Lee, "Mechanical Buckling: Mechanics, Metrology, and Stretchable Electronics," *Adv. Funct. Mater.*, vol. 19, no. 10, pp. 1526–1536, May 2009, doi: https://doi.org/10.1002/adfm.200801065.

[175]   V. Correia *et al.*, "Design and fabrication of multilayer inkjet-printed passive components for printed electronics circuit development," *J. Manuf. Process.*, vol. 31, pp. 364–371, 2018, doi: https://doi.org/10.1016/j.jmapro.2017.11.016.

[176]   P. Gokhale *et al.*, "Controlling the crack formation in inkjet-printed silver nanoparticle thin-films for high resolution patterning using intense pulsed light treatment," *Nanotechnology*, vol. 28, no. 49, p. 495301, 2017, doi: 10.1088/1361-6528/aa9238.

[177]   P. F. Flowers, C. Reyes, S. Ye, M. J. Kim, and B. J. Wiley, "3D printing electronic components and circuits with conductive thermoplastic filament," *Addit. Manuf.*, vol. 18, pp. 156–163, 2017, doi: https://doi.org/10.1016/j.addma.2017.10.002.

[178]   J. Zimmermann *et al.*, "Ultrathin Fully Printed Light-Emitting Electrochemical Cells with Arbitrary Designs on Biocompatible Substrates," *Adv. Mater. Technol.*, vol. 4, no. 3, p. 1800641, Mar. 2019, doi: https://doi.org/10.1002/admt.201800641.

[179]   L.-W. Lo, J. Zhao, H. Wan, Y. Wang, S. Chakrabartty, and C. Wang, "An Inkjet-printed PEDOT:PSS-Based Stretchable Conductor for Wearable Health Monitoring Device Applications," *ACS Appl. Mater. Interfaces*, vol. 13, no. 18, pp. 21693–21702, May 2021, doi: 10.1021/acsami.1c00537.

[180]   J. Abu-Khalaf *et al.*, "Optimization of Geometry Parameters of Inkjet-printed Silver Nanoparticle Traces on PDMS Substrates Using Response Surface Methodology," *Materials* , vol. 12, no. 20. 2019, doi: 10.3390/ma12203329.

[181]   Y. Y. Lim, Y. M. Goh, and C. Liu, "Surface Treatments for Inkjet Printing onto a PTFE-Based Substrate for High Frequency Applications," *Ind. Eng. Chem. Res.*, vol. 52, no. 33, pp. 11564–11574, Aug. 2013, doi: 10.1021/ie4006639.

[182]   L.-W. Lo, H. Shi, H. Wan, Z. Xu, X. Tan, and C. Wang, "Inkjet-printed Soft Resistive Pressure Sensor Patch for Wearable Electronics Applications," *Adv. Mater. Technol.*, vol. 5, no. 1, p. 1900717, Jan. 2020, doi: 10.1002/admt.201900717.

[183]   M. Amjadi, A. Pichitpajongkit, S. Lee, S. Ryu, and I. Park, "Highly Stretchable and Sensitive Strain Sensor Based on Silver Nanowire–Elastomer Nanocomposite," *ACS Nano*, vol. 8, no. 5, pp. 5154–5163, May 2014, doi: 10.1021/nn501204t.

[184]   P. Ren and J. Dong, "Direct Fabrication of VIA Interconnects by Electrohydrodynamic Printing for Multi-Layer 3D Flexible and Stretchable Electronics," *Adv. Mater. Technol.*, vol. 6, no. 9, p. 2100280, Sep. 2021, doi: https://doi.org/10.1002/admt.202100280.

[185]   E. Stucchi, G. Dell'Erba, P. Colpani, Y.-H. Kim, and M. Caironi, "Low-Voltage, Printed, All-Polymer Integrated Circuits Employing a Low-Leakage and High-Yield Polymer Dielectric," *Adv. Electron. Mater.*, vol. 4, no. 12, p. 1800340, Dec. 2018, doi: https://doi.org/10.1002/aelm.201800340.

[186]   L. Tang, J. Zhang, Y. Tang, J. Kong, T. Liu, and J. Gu, "Polymer matrix wave-transparent composites: A review," *J. Mater. Sci. Technol.*, vol. 75, pp. 225–251, 2021, doi: https://doi.org/10.1016/j.jmst.2020.09.017.

[187]   T. J. Wallin, J. Pikul, and R. F. Shepherd, "3D printing of soft robotic systems," *Nat. Rev. Mater.*, vol. 3, no. 6, pp. 84–100, 2018, doi: 10.1038/s41578-018-0002-2.

[188]   I. D. Johnston, D. K. McCluskey, C. K. L. Tan, and M. C. Tracey, "Mechanical characterization of bulk Sylgard 184 for microfluidics and microengineering," *J. Micromechanics Microengineering*, vol. 24, no. 3, p. 35017, 2014, doi: 10.1088/0960-1317/24/3/035017.

[189]   J. Hwang, S. Goo Lee, S. Kim, J. Sung Kim, D. Hwan Kim, and W. Hyoung Lee, "Unveiling Viscoelastic Response of Capacitive-type Pressure Sensor by Controlling Cross-Linking Density and Surface Structure of Elastomer," *ACS Appl. Polym. Mater.*, vol. 2, no. 6, pp. 2190–2198, May 2020, doi: 10.1021/acsapm.0c00193.

[190]   J. Kim *et al.*, "Wearable smart sensor systems integrated on soft contact lenses for wireless ocular diagnostics," *Nat. Commun.*, vol. 8, no. 1, p. 14997, 2017, doi: 10.1038/ncomms14997.

[191]   V. Pekkanen *et al.*, "Utilizing inkjet printing to fabricate electrical interconnections in a system-in-package," *Microelectron. Eng.*, vol. 87, no. 11, pp. 2382–2390, 2010, doi: https://doi.org/10.1016/j.mee.2010.04.013.

[192]   ASTM, "Standard Test Methods for Rating Adhesion by Tape Test. D3359-17." 2017.

[193]   JEDEC solid state technology association, "Steady State Temperature Humidity Bias Life Test. JESD22-A101C." 2009.

[194]   International Electrotechnical Commission, "Environmental testing - Part 2-52: Tests - Test Kb: Salt mist, cyclic (sodium chloride solution).IEC 60068-2-52:2017." 2017.

[195]   I. Byun, A. W. Coleman, and B. Kim, "SAM meets MEMS: Reliable fabrication of stable Au-patterns embedded in PDMS using dry peel-off process," *Microsyst. Technol.*, vol. 20, no. 10–11, pp. 1783–1789, 2014, doi: 10.1007/s00542-013-1923-8.

[196]   V. Jokinen, P. Suvanto, and S. Franssila, "Oxygen and nitrogen plasma hydrophilization and hydrophobic recovery of polymers," *Biomicrofluidics*, vol. 6, no. 1, 2012, doi: 10.1063/1.3673251.

[197]   C.-Y. Li and Y.-C. Liao, "Adhesive Stretchable Printed Conductive Thin Film Patterns on PDMS Surface with an Atmospheric Plasma Treatment," *ACS Appl. Mater. Interfaces*, vol. 8, no. 18, pp. 11868–11874, May 2016, doi: 10.1021/acsami.6b02844.

[198]   M. N. Kirikova *et al.*, "Direct-write printing of reactive oligomeric alkoxysilanes as an affordable and highly efficient route for promoting local adhesion of silver inks on polymer substrates," *J. Mater. Chem. C*, vol. 4, no. 11, pp. 2211–2218, 2016, doi: 10.1039/c5tc03497c.

[199]   J. Wu *et al.*, "Inkjet-printed microelectrodes on PDMS as biosensors for functionalized microfluidic systems," *Lab Chip*, vol. 15, no. 3, pp. 690–695, 2015, doi: 10.1039/c4lc01121j.

[200]   N. Adly *et al.*, "Printed microelectrode arrays on soft materials: from PDMS to hydrogels,"

npj Flex. Electron., vol. 2, no. 1, p. 15, 2018, doi: 10.1038/s41528-018-0027-z.

[201] S. Khan, S. Ali, A. Khan, M. Ahmed, B. Wang, and A. Bermak, "Inkjet printing of multi-stripes based deflection monitoring sensor on flexible substrate," *Sensors Actuators A Phys.*, vol. 323, p. 112638, 2021, doi: https://doi.org/10.1016/j.sna.2021.112638.

[202] H. Cho, Y. Lee, B. Lee, J. Byun, S. Chung, and Y. Hong, "Stretchable strain-tolerant soft printed circuit board: a systematic approach for the design rules of stretchable interconnects," *J. Inf. Disp.*, vol. 21, no. 1, pp. 41–47, Jan. 2020, doi: 10.1080/15980316.2019.1680451.

[203] J. M. Abu-Khalaf, L. Al-Ghussain, and A. Al-Halhouli, "Fabrication of Stretchable Circuits on Polydimethylsiloxane (PDMS) Pre-Stretched Substrates by Inkjet Printing Silver Nanoparticles," *Materials* , vol. 11, no. 12. 2018, doi: 10.3390/ma11122377.

[204] A. Mamidanna, C. Lefky, and O. Hildreth, "Drop-on-demand printed microfluidics device with sensing electrodes using silver and PDMS reactive inks," *Microfluid. Nanofluidics*, vol. 21, no. 11, pp. 1–9, 2017, doi: 10.1007/s10404-017-2010-8.

[205] Y. Peng *et al.*, "The elastic microstructures of inkjet printed polydimethylsiloxane as the patterned dielectric layer for pressure sensors," *Appl. Phys. Lett.*, vol. 110, no. 26, p. 261904, Jun. 2017, doi: 10.1063/1.4990528.

[206] D. McCoul, S. Rosset, S. Schlatter, and H. Shea, "Inkjet 3D printing of UV and thermal cure silicone elastomers for dielectric elastomer actuators," *Smart Materials and Structures*, vol. 26, no. 12. 2017, doi: 10.1088/1361-665X/aa9695.

[207] Y.-I. Lee and Y.-H. Choa, "Adhesion enhancement of ink-jet printed conductive copper patterns on a flexible substrate," *J. Mater. Chem.*, vol. 22, no. 25, pp. 12517–12522, 2012, doi: 10.1039/C2JM31381B.

[208] S. Bin Lee and Y.-K. Kim, "Adhesion Improvement of Polyimide/Metal Interface by He/O2/NF3 Atmospheric Pressure Plasma," *Plasma Process. Polym.*, vol. 6, no. S1, pp. S525–S529, Jun. 2009, doi: https://doi.org/10.1002/ppap.200931111.

[209] Y. Yoon, J. D. Angel, and D. C. Hansen, "Atmospheric Corrosion of Silver in Outdoor Environments and Modified Accelerated Corrosion Chambers," *Corrosion*, vol. 72, no. 11, pp. 1424–1432, Aug. 2016, doi: 10.5006/2079.

[210] D. Liang *et al.*, "Effects of Sodium Chloride Particles, Ozone, UV, and Relative Humidity on Atmospheric Corrosion of Silver," *J. Electrochem. Soc.*, vol. 157, no. 4, p. C146, 2010, doi: 10.1149/1.3310812.

[211] H. Lin, G. S. Frankel, and W. H. Abbott, "Analysis of Ag Corrosion Products," *J. Electrochem. Soc.*, vol. 160, no. 8, pp. C345–C355, 2013, doi: 10.1149/2.055308jes.

[212] K. Kokko, A. Parviainen, and L. Frisk, "Corrosion protection of anisotropically conductive adhesive joined flip chips," *Microelectron. Reliab.*, vol. 50, no. 8, pp. 1152–1158, 2010, doi: https://doi.org/10.1016/j.microrel.2010.04.010.

[213] N. Kim, W. J. Potscavage, A. Sundaramoothi, C. Henderson, B. Kippelen, and S. Graham, "A correlation study between barrier film performance and shelf lifetime of encapsulated organic solar cells," *Sol. Energy Mater. Sol. Cells*, vol. 101, pp. 140–146, 2012, doi: https://doi.org/10.1016/j.solmat.2012.02.002.

[214] L. Li, Y. Bai, L. Li, S. Wang, and T. Zhang, "A Superhydrophobic Smart Coating for Flexible and Wearable Sensing Electronics," *Adv. Mater.*, vol. 29, no. 43, p. 1702517, Nov. 2017, doi: https://doi.org/10.1002/adma.201702517.

[215] M. Rohaim, J. J. J. Kangas, R. Mikkonen, and M. Mäntysalo, "Design of Thin, High Permittivity, Multiband, Monopole-Like Antennas," in *2020 IEEE 19th Biennial Conference on Electromagnetic Field Computation (CEFC)*, 2020, pp. 1–4, doi: 10.1109/CEFC46938.2020.9451492.

[216] V. Ozbolat, M. Dey, B. Ayan, A. Povilianskas, M. C. Demirel, and I. T. Ozbolat, "3D Printing of PDMS Improves Its Mechanical and Cell Adhesion Properties," *ACS Biomater.*

Sci. & Eng., vol. 4, no. 2, pp. 682–693, Jan. 2018, doi: 10.1021/acsbiomaterials.7b00646.

[217] K. Du *et al.*, "Digital Light Processing 3D Printing of PDMS-Based Soft and Elastic Materials with Tunable Mechanical Properties," *ACS Appl. Polym. Mater.*, vol. 3, no. 6, pp. 3049–3059, Jun. 2021, doi: 10.1021/acsapm.1c00260.

[218] M. Śliwiak, R. Bui, M. A. Brook, and P. R. Selvaganapathy, "3D printing of highly reactive silicones using inkjet type droplet ejection and free space droplet merging and reaction," *Addit. Manuf.*, vol. 46, p. 102099, 2021, doi: https://doi.org/10.1016/j.addma.2021.102099.

[219] M. H. Behfar *et al.*, "Failure Mechanisms in Flip-Chip Bonding on Stretchable Printed Electronics," *Adv. Eng. Mater.*, vol. n/a, no. n/a, p. 2100264, Sep. 2021, doi: https://doi.org/10.1002/adem.202100264.

[220] S. Ding *et al.*, "Highly stretchable conductors comprising composites of silver nanowires and silver flakes," *J. Nanoparticle Res.*, vol. 23, no. 4, p. 111, 2021, doi: 10.1007/s11051-021-05219-z.

[221] A. Miyamoto *et al.*, "Inflammation-free, gas-permeable, lightweight, stretchable on-skin electronics with nanomeshes," *Nat. Nanotechnol.*, vol. 12, no. 9, pp. 907–913, 2017, doi: 10.1038/nnano.2017.125.

[222] C. Kim, K.-S. Yang, and W.-J. Lee, "The Use of Carbon Nanofiber Electrodes Prepared by Electrospinning for Electrochemical Supercapacitors," *Electrochem. Solid-State Lett.*, vol. 7, no. 11, p. A397, 2004, doi: 10.1149/1.1801631.

[223] S. Marx, M. V Jose, J. D. Andersen, and A. J. Russell, "Electrospun gold nanofiber electrodes for biosensors," *Biosens. Bioelectron.*, vol. 26, no. 6, pp. 2981–2986, 2011, doi: https://doi.org/10.1016/j.bios.2010.11.050.

[224] D. Li, G. Ouyang, J. T. McCann, and Y. Xia, "Collecting Electrospun Nanofibers with Patterned Electrodes," *Nano Lett.*, vol. 5, no. 5, pp. 913–916, May 2005, doi: 10.1021/nl0504235.

[225] W. Yan *et al.*, "A durable nanomesh on-skin strain gauge for natural skin motion monitoring with minimum mechanical constraints," *Sci. Adv.*, vol. 6, no. 33, p. eabb7043, Nov. 2021, doi: 10.1126/sciadv.abb7043.

[226] F.-C. Liang *et al.*, "An intrinsically stretchable and ultrasensitive nanofiber-based resistive pressure sensor for wearable electronics," *J. Mater. Chem. C*, vol. 8, no. 16, pp. 5361–5369, 2020, doi: 10.1039/D0TC00593B.

[227] S. Zhao *et al.*, "All-Nanofiber-Based Ultralight Stretchable Triboelectric Nanogenerator for Self-Powered Wearable Electronics," *ACS Appl. Energy Mater.*, vol. 1, no. 5, pp. 2326–2332, May 2018, doi: 10.1021/acsaem.8b00439.

[228] N. Sun *et al.*, "Waterproof, breathable and washable triboelectric nanogenerator based on electrospun nanofiber films for wearable electronics," *Nano Energy*, vol. 90, p. 106639, 2021, doi: https://doi.org/10.1016/j.nanoen.2021.106639.

[229] P. Xiao *et al.*, "A breathable, biodegradable, antibacterial, and self-powered electronic skin based on all-nanofiber triboelectric nanogenerators," *Sci. Adv.*, vol. 6, no. 26, p. eaba9624, Oct. 2021, doi: 10.1126/sciadv.aba9624.

[230] X. Wang *et al.*, "A Highly Stretchable Transparent Self-Powered Triboelectric Tactile Sensor with Metallized Nanofibers for Wearable Electronics," *Adv. Mater.*, vol. 30, no. 12, p. 1706738, Mar. 2018, doi: https://doi.org/10.1002/adma.201706738.

[231] G. H. Kim, H. Woo, S. Kim, T. An, and G. Lim, "Highly-robust, solution-processed flexible transparent electrodes with a junction-free electrospun nanofiber network," *RSC Adv.*, vol. 10, no. 17, pp. 9940–9948, 2020, doi: 10.1039/C9RA10278G.

[232] Y.-K. Fuh and L.-C. Lien, "Pattern transfer of aligned metal nano/microwires as flexible transparent electrodes using an electrospun nanofiber template," *Nanotechnology*, vol. 24,

no. 5, p. 55301, 2013, doi: 10.1088/0957-4484/24/5/055301.

[233]   Y. Kumaresan, O. Ozioko, and R. Dahiya, "Effect of Dielectric and Stiffness of Soft Material between the Electrodes of a Capacitive Pressure Sensor on its Performance," in *2020 IEEE International Conference on Flexible and Printable Sensors and Systems (FLEPS)*, 2020, pp. 1–4, doi: 10.1109/FLEPS49123.2020.9239583.

[234]   M. Li, J. Liang, X. Wang, and M. Zhang, "Ultra-Sensitive Flexible Pressure Sensor Based on Microstructured Electrode," *Sensors* , vol. 20, no. 2. 2020, doi: 10.3390/s20020371.

[235]   X. Zeng *et al.*, "Tunable, Ultrasensitive, and Flexible Pressure Sensors Based on Wrinkled Microstructures for Electronic Skins," *ACS Appl. Mater. Interfaces*, vol. 11, no. 23, pp. 21218–21226, Jun. 2019, doi: 10.1021/acsami.9b02518.

[236]   Y. Pang *et al.*, "Epidermis Microstructure Inspired Graphene Pressure Sensor with Random Distributed Spinosum for High Sensitivity and Large Linearity," *ACS Nano*, vol. 12, no. 3, pp. 2346–2354, Mar. 2018, doi: 10.1021/acsnano.7b07613.

[237]   J. Wu *et al.*, "Rational design of flexible capacitive sensors with highly linear response over a broad pressure sensing range," *Nanoscale*, vol. 12, no. 41, pp. 21198–21206, 2020, doi: 10.1039/D0NR06386J.

[238]   L. Ma *et al.*, "Highly sensitive flexible capacitive pressure sensor with a broad linear response range and finite element analysis of micro-array electrode," *J. Mater.*, vol. 6, no. 2, pp. 321–329, 2020, doi: https://doi.org/10.1016/j.jmat.2019.12.008.

[239]   Z. Guo *et al.*, "Printed and Flexible Capacitive Pressure Sensor with Carbon Nanotubes based Composite Dielectric Layer," *Micromachines* , vol. 10, no. 11. 2019, doi: 10.3390/mi10110715.

[240]   Y. Xiong *et al.*, "A flexible, ultra-highly sensitive and stable capacitive pressure sensor with convex microarrays for motion and health monitoring," *Nano Energy*, vol. 70, p. 104436, 2020, doi: https://doi.org/10.1016/j.nanoen.2019.104436.

[241]   X. Shuai *et al.*, "Highly Sensitive Flexible Pressure Sensor Based on Silver Nanowires-Embedded Polydimethylsiloxane Electrode with Microarray Structure," *ACS Appl. Mater. Interfaces*, vol. 9, no. 31, pp. 26314–26324, Aug. 2017, doi: 10.1021/acsami.7b05753.

[242]   Y. Zang, F. Zhang, C. Di, and D. Zhu, "Advances of flexible pressure sensors toward artificial intelligence and health care applications," *Mater. Horizons*, vol. 2, no. 2, pp. 140–156, 2015, doi: 10.1039/C4MH00147H.

PUBLICATIONS

PUBLICATION
I

Benchmark Study of Screen Printable Silver Inks on a PPE Based Substrate

R. Mikkonen, M. Mäntysalo

Benchmark Study of Screen Printable Silver Inks on a PPE Based Substrate

Riikka Mikkonen and Matti Mäntysalo

Laboratory of Electronics and Communications Engineering Tampere University of Technology
P.O. Box 692, FI 33101, Tampere, Finland
riikka.mikkonen@tut.fi

Abstract— In this study, two silver inks are screen printed and their performance on a PPE polymer compound is evaluated. Both physical and chemical surface pre-treatments are used to modify substrate surface roughness and energy. Electrical performance of printed structures is evaluated by sheet resistance measurements. In addition, a crosscut adhesion test is used to evaluate mechanical performance of printed patterns. Low sheet resistances can be obtained with used materials. However, there is a significant difference in adhesion level. By substrate surface pre-treatments, adhesion level can be improved, and tape test ink removal can be decreased even from 15% to 0%. These results indicate that PPE substrate may be utilized in production of high quality printed electronics applications.

Keywords— *PPE; printed electronics; screen printing; surface treatment*

I. INTRODUCTION

Printed Electronics (PE) enable fabrication of cost-effective, large-area wireless applications, which may be integrated into novel electronics substrates, such as stretchable thermoplastic polyurethane [1,2] or 3D molded interconnect device (MID). These applications can be utilized in various industry fields, such as automotive industry or health care, where integration of electrical devices directly into supportive structures can provide significant benefits, as devices do not require additional space and no external wiring is required. Significant benefits of PE technology lie in cost-effective wireless sensor applications, such as radiofrequency identification (RFID) and Internet-of-Everything (IoE), since sensors and antenna structures may be integrated in everyday environment, thus enabling efficient device functionality without need for user control [3].

Fabrication of sufficient high frequency (HF) structures sets specific requirements for the used materials. First, conductor materials with low resistivity are required, since low DC sheet resistance is essential to ensure proper HF functionality. In addition, several requirements are set for the substrate material. Substrate materials used in HF applications include for example polyethylene terephthalate (PTFE; Teflon) and polyphenylene oxide (PPO). Low relative permittivity and dissipation factor make these materials attractive for HF applications, since signal will not be attenuated by the substrate [4].

In this study, a novel polyphenylene ether (PPE) polymer compound, is studied in PE applications. This substrate has been developed for especially HF applications. In addition, substrates may be fabricated by injection molding, which enables manufacturing of innovative 3D substrate shapes, i.e. 3D antennas [5]. Therefore, this polymer is an attractive alternative for substrate material in printed HF structures.

From printing point of view, the main challenge of PPE substrate material is its hydrophobic nature. Hydrophobic substrate may not be wetted properly, which is likely to cause issues with print quality and possibly with mechanical performance of printed structures. Therefore, surface modification may be necessary to improve substrate wettability and to ensure good adhesion between ink and substrate.

In this study, highly conductive commercial silver inks are used to print conductive structures on PPE substrate. High metal contents enable high DC conductivity, which is essential for low-loss HF signals. In addition, the effect of substrate surface pre-treatments (oxygen plasma, sulfuric acid, and potassium hydroxide) on substrate parameters and ink-substrate interactions are inspected.

II. EXPERIMENTS

A. Materials

Square-shaped (10 cm x 10 cm) PPE substrates Preperm® L260 (3 mm thickness) from Premix were used in this study. Key parameters of this substrate material include low relative permeability ($\varepsilon r = 2.6$) and low dissipation factor (DF = 0.0006) [6].

For printing of test patterns, two screen printable silver inks were selected: CRSN2442 from SunChemical and DuPont 5064H. Ink parameters used as selection criteria are listed in Table I. Both inks are solvent-based and their viscosities are suitable for screen printing. Metal content of both inks is higher than 60 wt%, which should provide sufficient electrical performance. In literature, these inks have been compared to each other for example by Muck [7] and Kavcic [8], where ink properties were studied in RFID applications printed on paper

substrates. Sheet resistances below 100 mΩ/□ were obtained even on extremely porous paper substrates.

Ink	Ink parameters			
	Ag (%)	Solvent	Viscosity (cP)	sheet resistance (mΩ/□@25 µm)
CRSN2442	69 - 71	Propylene di-acetate	2,000 – 3,000	10
5064H	63 - 66	C11-ketone	10,000-20,000	<14

B. Substrate pre-treatment methods

Due to the hydrophobic nature of PPE substrates, surface energy increasing pre-treatments were selected to enhance substrate wetting. Both physical and chemical treatments were used to inspect the effects of different treatment types.

Oxygen plasma was used as a physical treatment, since this treatment is widely known for its surface energy increasing abilities. Furthermore, this treatment is widely used as an adhesion promoter [11-13]. In this study, an Oxford Plasma Technology RIE System 100 plasma printer was used for plasma treatments. Used treatment parameters are presented in Table II.

TABLE II. PLASMA TREATMENT PARAMETERS

Treatment	Time (min.)	Exposure power (W)	Chamber pressure (mTr)	Gas (O₂) amount (sccm)
1	1	25	56.0	30.0
2	1	50	56.0	30.0
3	1	75	56.0	30.0

Three chemical treatments were used to modify substrate surface 1) Sulfuric acid (H2SO4) with 98 % concentration, 2) Potassium hydroxide (KOH) with 1.0 M concentration, and 3) KOH with 30 % concentration [11; 14]. Substrates were dipped in chemical containers for etching. Afterwards, chemical remnants were wiped off with deionized (DI) water. Treatment parameters used in these treatments are presented in Table III.

TABLE III. CHEMICAL ETCHING PARAMETERS

Sulfuric acid etching				
1 min.	2 min.	5 min.	10 min.	15 min.
KOH 1.0M				
1 min.	2 min.	5 min.	10 min.	15 min.
KOH 30%				
-	-	5 min.	10 min.	-

C. Printing and post-treatment

Test patterns were printed in cleanroom conditions using a manual single-sheet TIC SCF300 screen printer. A screen with NBC UX79-45 polyester mesh (opening 81µm, theoretical wet thickness 27.7µm) was used in printing.

After the printing phase, samples were cured in oven according to datasheet recommendations. 5064H was cured at 130 °C for 20 minutes, and CRSN2442 was cured in 150 °C for 30 minutes.

D. Characterization

To inspect the effects of the used surface treatments, several characterization methods were utilized. Dyne pens with a range from 30 mN/m to 60 mN/m were used for measurement of substrate surface energies before and after treatments. In addition, an optical profilometer Veeco Wyko NT1100 was used to measure the surface profiles of different substrates.

After printing, conductivity and adhesion of fabricated samples were analyzed. Two different test patterns were designed, one for conductivity measurements and other for adhesion measurements. In Fig. 1 are demonstrated the test patterns used in this survey. Pattern Fig. 1A) includes 10 basic conductor structures used in four point probe (4PP) measurements to determine sheet resistances. A Keithley 2425 sourcemeter was used in these tests. Sheet resistance Rs was then determined based on obtained results and conductor dimensions:

$$R_S = R\frac{w}{l}, \qquad (1)$$

where R is measured conductor resistance, l is theoretical conductor length (32 mm) and w is theoretical conductor width (1.3 mm) (Fig. 1A)).
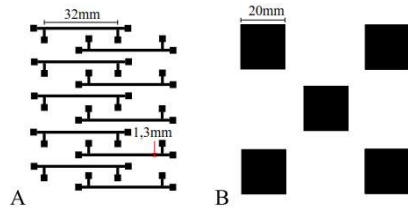

Fig. 1. Designed test patterns for A) sheet resistance measurements B) adhesion evaluation.

In addition to sheet resistance measurements, adhesion of different substrate-ink combinations was evaluated to compare mechanical strength of used inks, and also to inspect used surface treatments' effect on adhesion of ink-substrate interface. Adhesion test pattern (Fig. 1B)) was designed for these experiments. A crosscut test was used for adhesion evaluation, according to ASTM D3359 standard [15].

III. RESULTS AND DISCUSSION

A. Substrate surface

In Table IV, measured surface energies of fabricated test samples are presented. It was observed that initial surface energy of the used substrate material is rather low, approximately 30 mN/m, but may be more than doubled, depending on the used surface treatment. Both oxygen plasma and H2SO4 seemed to increase surface energy significantly, whereas KOH treatment seemed to have no effect on the wetting abilities of PPE substrate, regardless of the base concentration. Explanation may lie in the solvent resistance of the substrate material, since the strongest KOH concentration was only 30 %.

Furthermore, it was observed that increment of surface energy by H2SO4 was saturated after 5-minute etching, a 5-minute treatment was used in further experiments. With KOH, 5-minute treatment was also used, since surface energy was not changed by any treatments.

TABLE IV. MEASURED SURFACE ENERGIES

Reference (PPE)				
mN/m	30-32			
Oxygen plasma treatment				
mN/m	≥ 60			
H$_2$SO$_4$ etching				
	1 min.	2 min.	5 min.	10 min.	15 min.
mN/m	38	46	56-58	58-60	58-60
KOH 1.0M etching				
	1 min.	2 min.	5 min.	10 min.	15 min.
mN/m	32-34	32-34	32-34	32-34	32-34
KOH 30 % etching				
	-	-	5 min.	10 min.	-
mN/m	-	-	32-34	32-34	-

In addition, plasma treatment increased surface energy beyond the Dyne pen range already with exposure power of 25 W, and therefore analysis of surface profile was necessary to find differences between plasma treatments. It was observed that increment of exposure power led to more effective etching. This phenomenon is demonstrated in Fig. 2. Since 75 W exposure power seemed to lead to highest average roughness of the substrate, it was used in further experiments.
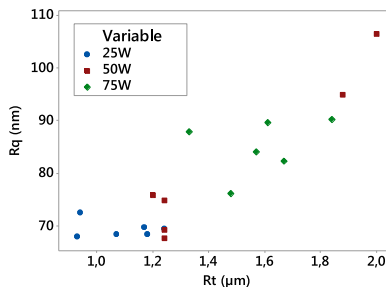
Fig. 2. Measured R$_q$/R$_t$ with different plasma exposure powers.

After the initial surface characterization, new samples were fabricated with the chosen substrate surface pre-treatments. Surface profiles were measured again with optical profilometer and differences between each treatment were compared. Results of this measurement are presented in Fig. 3. Plasma treatment would appear to have most significant effect on the surface profile of the substrates, whereas no significant change was observed with chemical treatments.
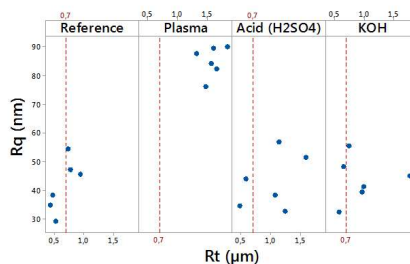
B. Print quality

Fig.3. Measured R$_q$/R$_t$ with surface pre-treatments.

Print quality was evaluated by line thickness inspection with the optical profilometer. Variation in line thickness depending on the used ink is demonstrated in Table V. It may be observed that thicker lines were obtained with SunChemical CRSN2442 ink than with DuPont 5064H ink. This is most likely due to the higher silver content of CRSN2442 ink. At the same time, lines are rougher. Surface treatments did not have any effect on line thickness or roughness.

Furthermore, it was observed that increment of line thickness led to rougher conductor surface in each inks data. This phenomenon is presented in Fig. 4 results. It seems that especially with CRSN2442 ink, increasing line thickness causes more surface roughness, whereas roughness of 5064H ink does not increase significantly. The importance of conductor surface roughness is emphasized especially at high frequencies due to

skin effect [16]. In order to provide good quality HF conductors, process should be optimized.

TABLE V. Measured Line Thickness And Roughness For Both Inks

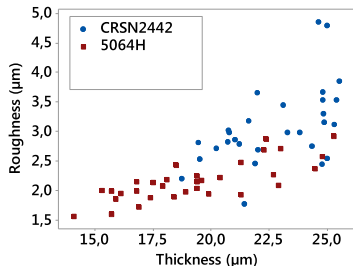| Ink	Thickness (μm)	Roughness (μm)	Samples
CRSN2442	22,81±2,13	3,08±0,67	29
5064H	19,33±3,01	2,15±0,33	32

Fig. 4. Measured conductor line roughness per line thickness.

C. Sheet resistance

Calculated sheet resistances of printed patterns (Fig. 1A)) using (1) are presented in Fig. 5. It was observed that surface treatments seem to lower sheet resistance mean values, excluding H_2SO_4, which seems to have negative impact on the sheet resistance. On the other hand, there is more deviation in CRSN2442 results on treated substrates, whereas 5064H results include less deviation on treated surfaces. Due to the higher silver content, CRSN2442 values should be a bit lower than 5064H values. However, as measured sheet resistance values of Table VI indicate, CRSN2442 sheet resistance was similar or even higher than that of 5064H. This difference may have been caused by annealing parameters, since datasheet conditions were used.

Still, most of the measured values are between 10 mΩ/□ - 20 mΩ/□, and therefore both inks are likely to perform well at high frequencies, as stated in [17]. However, as observed in [17], low DC sheet resistance alone cannot guarantee required HF performance, since substrate surface roughness as well as the conductor uniformity and roughness affect HF attenuation.

D. Adhesion

On the contrary to the conductivity measurements, crosscut adhesion test revealed significant differences between used inks. Results are demonstrated in Fig. 6.

TABLE VI. Measured Sheet Resistances

Ink/Substrate	Sheet resistance (mΩ/□)		
	Mean	*St.Dev.*	*Samples*
CRSN2442/PPE	17,28	1,13	20
5064H/PPE	18,86	3,21	20
CRSN2442/Plasma	15,47	2,71	20
5064H/Plasma	15,17	1,17	20
CRSN2442/H$_2$SO$_4$	23,78	3,17	20
5064H/H$_2$SO$_4$	39,36	10,34	16
CRSN2442/KOH	16,14	3,25	20
5064H/KOH	13,90	1,70	18

5064H adhesion was excellent even on the bare PPE substrate, whereas CRSN2442 adhesion is significantly worse. Comparison of treated samples indicates that plasma treatment is an excellent adhesion promoter for this substrate material, CRSN2442 adhesion was improved from levels 3B-4B (tape removal 5-15 %) to level 5B (tape removal 0%).

On the other hand, chemical treatments do not have any effect on the adhesion level. Reason may be found in the surface characterization results: chemical etching does not alter surface profile of the substrate. Therefore, it may be concluded that surface must be roughened to obtain better adhesion.

It may be observed that all of the ten fabricated samples of each ink-substrate pair are not included in the graph. This is due to the substrate imperfections, which cause ink removal from the substrate, and thus cannot be compared to other results. Therefore it may be concluded that molding process has a significant effect on mechanical performance of inks.

On the other hand, another adhesion test would be required to measure adhesion strength between inks and substrates, since the crosscut test is only aimed at quick evaluation of initial coating adhesion. In addition, number of fabricated samples is rather small, and therefore more samples would be needed for a more accurate adhesion classification. Furthermore, reliability tests are needed to inspect the aging tendency of the material interfaces. However, this test has provided a directional estimation of ink adhesion and surface treatment effects.
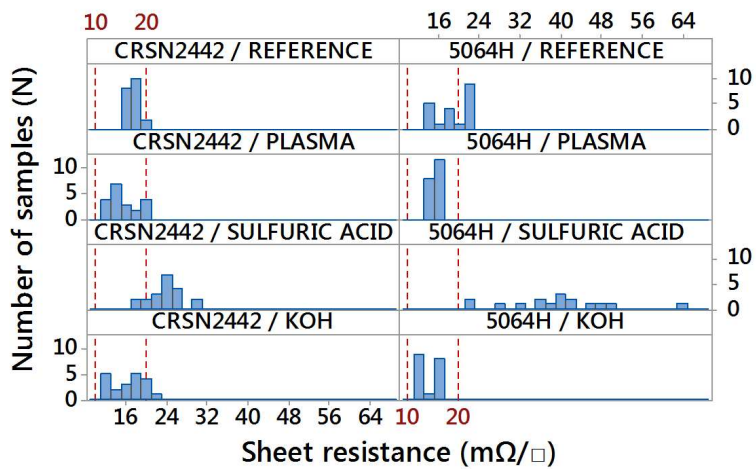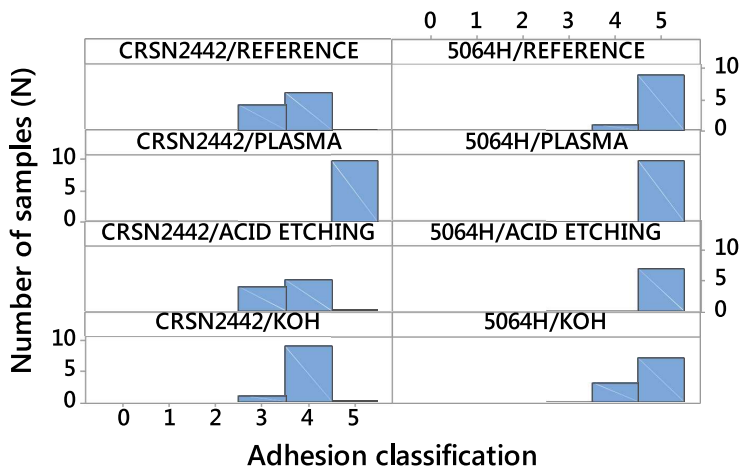
Fig.5. Measured sheet resistances.

Fig. 6. Adhesion classification rates.

IV. CONCLUSIONS

In this paper, printability and performance of two commercial silver inks were evaluated on a PPE based polymer substrate. The purpose was to inspect surface treatment effects and to compare ink performance. This substrate is aimed at HF applications and therefore it is essential to find such conductive materials, which provide low sheet resistance and therefore enable sufficient HF performance in printed electronics applications.

In this study, obtained sheet resistances were between 10-20 mΩ/$\square$, which indicates good conductivity. However, printed lines were rather rough, and therefore process optimization is needed to obtain good quality conductors. In addition, further characterization of HF properties is required. Even though suitable conductive material and surface treatment was found, more surface treatments and materials should be studied to find alternative ink-substrate combinations for wide variety of HF applications. In addition, long-term reliability of substrate-ink interfaces should be studied.

REFERENCES

[1] T. Vuorinen, et al., " Printed, Skin-Mounted Hybrid System for ECG Measurements", In Proc. of Electronic System and Technology Conference (ESTC), Grenoble, France, September 2016.

[2] T. Vuorinen, et al., "Inkjet-Printed Graphene/PEDOT:PSS Temperature Sensors on a Skin-Conformable Polyurethane Substrate", Sci Rep. 6:35289, 2016. doi: 10.1038/srep35289.

[3] W. Clemens, D. Lupo, S. Kirchmeyer, K. Hecker, C. Ranfeld, OE-A Roadmap for Organic and Printed Electronics, 7th Edition, OE-A, Frankfurt, (2017).

[4] J. A. Paulsen, M. Renn, K. Christenson, and R. Plourde, "Printing conformal electronics on 3D structures with Aerosol Jet technology," IEEE Future of Instrumentation International Workshop (FIIW), pp. 1-4, December 2012.

[5] J. Coonrod, "Understanding When To Use FR-4 Or High Frequency Laminates," OnBoarg Technology, 2011, pp. 26-30.

[6] Preperm®L260 Technical Datasheet, Premix Oy.

[7] T. Muck, "Printed UHF RFID antenna on coated cardboard," Advances in Printing and Media Technology, IARIGAI, Darmstadt, Germany, pp. 83-90, September 2012.

[8] U. Kavcic, "UHF RFID Tags with Printed Antennas on Recycled Papers and Cardboards," Materials and Technology, Vol. 48, No. 2, 2014, pp. 261-267.

[9] CRSN2442 Conductive Silver Ink, Technical Data Sheet, SunChemical.

[10] DuPont 5064H, Technical Data Sheet, DuPont.

[11] T. Laine-Ma, P. Ruuskanen, S. Kortet, M. Karttunen, "Electroless copper plating and surface characterization of thermoplastic PPO based printed circuit boards," Circuit World, Vol. 35, No. 4, 2009, pp. 22-30.

[12] A. Vesel, M. Mozetič, "7 - Low-Pressure Plasma-Assisted Polymer Surface Modifications," in: J. Izdebska, S. Thomas (ed.), Printing on Polymers, William Andrew Publishing, 2016, pp. 101-121.

[13] A. Vesel, I. Junkar, U. Cvelbar, J. Kovac, M. Mozetic, "Surface modification of polyester by oxygen- and nitrogen-plasma treatment, Surface and Interface Analysis," Vol. 40, No. 11, 2008, pp. 1444-1453.

[14] E. Ranucci, Ã Sandgren, N. Andronova, A. Albertsson, "Improved polyimide/metal adhesion by chemical modification approaches," Journal of Applied Polymer Science, Vol. 82, No. 8, 2001, pp. 1971-1985.

[15] ASTM D3359-09e2, Standard Test Methods for Measuring Adhesion by Tape Test, ASTM International, Pennsylvania, 2009.

[16] T. Björninen, S. Merilampi, L. Ukkonen, L. Sydänheimo, P. Ruuskanen, "The Effect of Fabrication Method on Passive UHF RFID Tag Performance," International Journal of Antennas and Propagation, Vol. 2009, 2009, pp. 8.

[17] E. Halonen et al., "Environmental protection of inkjet-printed Ag conductors," Microelectronic Engineering, Vol. 88, No. 9, 2011, pp. 2970-2976.

PUBLICATION
II

Evaluation of screen printed silver trace performance and long-term reliability against environmental stress on a low surface energy substrate

R. Mikkonen, M. Mäntysalo

ELSEVIER
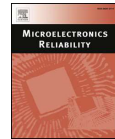
Evaluation of screen printed silver trace performance and long-term reliability against environmental stress on a low surface energy substrate

Riikka Mikkonen*, Matti Mäntysalo

Tampere University of Technology, Laboratory of Electronics and Communications Engineering, Korkeakoulunkatu 3, 33720 Tampere, Finland

A R T I C L E I N F O	A B S T R A C T
Keywords: Printed electronics PPE Surface modification Adhesion Environmental stress Reliability	Otherwise attractive substrate materials for printed electronics may have such surface characteristics that make patterning challenging. This article focuses on the printability and performance characterization of conductive patterns on a low surface energy substrate. Surface characteristics of a hydrophobic polyphenylene ether (PPE) substrate and the effects of surface modification using chemical and physical pre-treatments were studied. In addition, silver ink performance and its reliability on this substrate were evaluated. The surface was characterized by surface energy measurements and surface profile analysis. Screen-printed test patterns were characterized to evaluate print quality and electrical and mechanical performance. A further inspection of substrate-ink interactions was conducted using environmental reliability tests. It was observed that ink adhesion could be significantly promoted by choosing a suitable surface pre-treatment method. Low sheet resistances were obtained, and thus, suitable inks for further characterization were found. In addition, it was observed that environmental stress has a significant impact on ink-substrate interactions.

1. Introduction

Printed electronics (PE) make it possible to fabricate intelligent applications with the potential to revolutionize the future electronics market. The importance of printed electronics is emphasized in various sensing and monitoring applications, where thin and wireless devices on flexible and stretchable platforms enable device integration into an everyday environment, and are thus one of the key applications on the path towards the Internet of Everything (IoE) [1–6].

Since many sensing applications operate at high frequencies, it is necessary to find materials enabling sufficient functionality in this area. Proper functionality of printed high frequency (HF) structures places requirements on both the coating and substrate materials. For example, conductive material should be selected so that DC sheet resistance is as low as possible. In addition, printed conductors should be smooth to enable fast signal transmission. On the other hand, basic substrate requirements include low relative permittivity and dissipation factor to prevent signal attenuation via the substrate material [1,7,8].

Furthermore, materials should be selected so that ink-substrate interface interactions enable proper wetting of the substrate and sufficient ink adhesion on the used substrate material. These properties may be enhanced by, for example, surface modification prior to printing. Thus, the substrate surface is altered by modifying the chemical compound and surface profile [9,10]. In addition to the initial performance

characterization of the printed structures, a reliability study is necessary in the development of printed electronics. For example, relatively thin and soft printed lines can easily be scratched. Additionally, structures have to endure plenty of stress during product lifetime. By using accelerated reliability tests, the long-term reliability of the applications may be inspected efficiently, without the need to wait until the end of product lifetime during normal usage [11]. With these tests, such material interfaces can be found that make printed structures better able to endure environmental stress and remain reliable, even in harsh environments [12].

In this study, the authors continue their earlier benchmark study of silver ink performance on a PPE-based HF substrate material [13]. This polymer compound is designed for GHz applications, with a dissipation factor below 0.001 and a dielectric constant of 2.60 [14]. Therefore, it is an attractive substrate material for applications operating in the GHz range and could be used as a platform for printed large-area antennas and other wireless applications, such as molded interconnect devices. The variety of studied silver inks has been broadened and the effects of new surface pre-treatments on substrate material are studied. Environmental stress tests (85% relative humidity (RH)/85 °C test, cyclic salt mist test) are used to evaluate the effect of elevated temperature and salt exposure in humid conditions on long-term reliability.

* Corresponding author
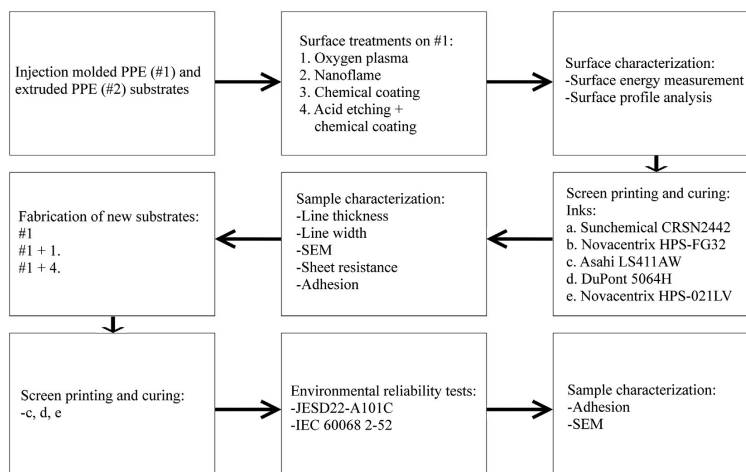*E-mail address:* riikka.mikkonen@tut.fi (R. Mikkonen).

Fig. 1. Test matrix including all variables and process steps.

2. Experimental section

Fig. 1 introduces the reader to the process steps and test variables included in this survey. A detailed discussion of both materials and methods is included in the following sections.

2.1. Materials

The purpose of this study was to continue the authors' benchmark study of silver ink printability on PPE, and therefore, an injection-molded PPE substrate (10 cm × 10 cm) with 3 mm thickness was used. In addition, an extruded PPE substrate (10 cm × 10 cm) with 1 mm thickness was studied to compare the effects of the molding process and substrate thickness on the surface parameters and final performance. These substrates are relatively thick for conventional printed electronics applications. However, since our purpose is to find HF applicable materials, which are suitable for fabrication of three-dimensional (3D) objects, like molded interconnect devices, or large area devices, substrate dimensions are considered sufficient for our purposes.

In our earlier study [13], SunChemical CRSN2442 and DuPont 5064H screen printing inks were used. Since low sheet resistances were obtained, research was continued to inspect the effects of substrate surface pre-treatments further. In addition, three other silver inks were selected for further comparison of the conductive materials. The most critical ink parameters obtained from the datasheets are listed in Table 1.

All of the selected inks have high silver contents, which helps decrease the sheet resistance of the printed structures. In addition, inks with different viscosities were selected to inspect their effect on print quality, and thus, on conductor performance. Furthermore, inks with different solvents were selected to compare their properties. HPS-021LV differs from other inks because it is aqueous. This aqueous ink is more environmentally friendly than other inks, and is therefore an attractive choice. In the extant literature, this ink has been studied, for example, in works by Sipilä [15] and Björninen [16], where it was successfully used to print HF structures on challenging substrates, such as plywood and textiles.

Other studies on the selected inks include, for example, a work by Happonen [17], where 5064H was compared to LS411AW via sheet

Table 1
Material parameters of the used conductive inks [20–24].

Ink	Ag [%]	Solvent	Viscosity [cP]	Sheet resistance
Manufacturer				[mΩsq^{-1}@ thickness]
CRSN2442 SunChemical	69–71	Propylene diacetate	2000–3000	10@25 µm
5064H DuPont	63–66	C11-ketone	10,000–20,000	< 14@25 µm
LS411AW Asahi	65–75	Butyl cellosolve acetate, isophorone	20,000–30,000	< 40@10 µm
HPS-FG32 Novacentrix	75	Butyl carbitol	8000	25@25 µm
HPS-021LV Novacentrix	75	Water	2600	≤14@25 µm

resistance and bending abilities. The results indicated that excellent electrical performance could be obtained with both inks, but they were not successful with the cyclic bending tests. LS411AW was also included in studies by Jansson [18] and Voutilainen [19], where it was used to fabricate more complex structures, such as moisture sensors [18] as well as inductors and capacitors [19]. The results indicated that low sheet resistances could be obtained and that the structures can endure environmental stress well.

2.2. Methods

2.2.1. Surface pre-treatment methods

The authors observed previously that oxygen plasma treatment is a sufficient surface treatment for enhancing the adhesion of a substrate-ink interface [13]. Therefore, it was used in this survey to see if it would also work with other inks. However, etching with sulfuric acid (H_2SO_4) or potassium hydroxide (KOH) did not improve the performance results.

Since sulfuric acid had an increasing effect on the substrate surface energy, though, it was nevertheless used in this survey as a base for chemical coating with ethyltriglycol. To inspect the effect of prior acid

Table 2
Chemical coating parameters.

Substrate	Coating layers	Curing conditions
Native PPE	3	100 °C/15 min
PPE with 5 min. H₂SO₄ etching	1	100 °C/15 min

etching on coating behavior, ethyltriglycol was also applied to the native PPE. Since the native PPE was not wetted as well as the pretreated substrate, three layers of coating were applied. All coated samples were cured in an oven at 100 °C for 15 min after each coating layer had been applied. A summary of the chemical treatment parameters that were used is provided in Table 2.

In addition, physical flame-pyrolytic silicating via a Nanoflame pistol [25] was used. With this technique, surface is modified via formation of silicon dioxide layer on the treated surface. This surface treatment has been used successfully in prior studies to modify substrates and as an adhesion promoter, for example in a study by Pekkanen [26]. A Polytec Nanoflame pistol was used to heat the substrate surface and, at the same time, the heated pistol gas formed silica oxides on the substrate surface. Due to the large surface area and rapid heating of the substrate, substrates were first treated from one direction, after which the substrate was rotated 90° and the treatment was repeated to ensure an even treating of surface. The extruded, 1 mm thick PPE substrate was used without any additional surface pre-treatment.

2.2.2. Screen printing and post-treatment

When all substrates had been prepared, test patterns were printed in cleanroom conditions with a semimanual single sheet screen printer SCF300. An aluminum screen with NBC UX79-45 polyester mesh (opening 81 μm, theoretical wet thickness 27.7 μm) [27] was used. After printing, the samples were cured in an oven according to datasheet recommendations: HPS-021LV was cured at 150 °C for 30 min, HPS-FG32 at 140 °C for 10 min, CRSN2442 at 150 °C for 30 min, LS411AW at 150 °C for 20 min, and 5064H at 130 °C for 20 min.

2.3. Environmental reliability tests

In addition to the initial performance evaluation, accelerated reliability tests were executed to assess the effects of environmental stress on mechanical performance. First, a JEDEC JESD22-A101C 500 h storage test (85 °C temperature and 85% relative humidity (RH)) was used [28]. This test is widely used to evaluate product aging in normal storing conditions. Samples were placed into a Weiss C340 chamber.

In addition, an IEC 60068 2-52 salt mist test was used to inspect the aging effect of high relative humidity in a salty environment [29]. This test is important for structures aimed at outdoor applications and especially in a marine environment. For this test, the samples were first exposed to sodium chloride (NaCl) mist for 2 h, after which time they were kept in 93% RH for 168 h. This cycle was then repeated. The samples were placed in an Ascott S450XP chamber during this test. To minimize the effect of uneven salt spray in the chamber, the samples were placed in random order into the chamber. After the test, the samples were rinsed with deionized (DI) water to remove the excess salt and, thus, to suspend any corrosive reactions.

2.4. Characterization

For comparison of the surface pre-treatment effects, an optical profilometer Veeco Wyko NT1100 was used to measure the surface profiles of the fabricated substrates. Roughness data was collected from the measured profile range R_t. Range is determined as the difference between the highest peak and lowest valley of the surface profile as follows:

$$R_t = R_p - R_v, \tag{1}$$

where R_p is the highest peak and R_v is the lowest valley of the substrate. In addition, RMS roughness R_q was used for roughness data collection. R_q is calculated as follows:

$$R_q = \frac{1}{n} \sum_{i=1}^{n} y_i^2, \tag{2}$$

where y is the deviation over the roughness mean and n is the number of samples [30]. Since this parameter is greatly affected by deviations from the surface mean line, it is a good data parameter for rough surfaces.

In addition, a set of Dyne pens with a surface tension range of 30–60 mNm⁻¹ were used to measure the surface energies of all substrates. With this method, surface energy is determined by drawing a line on the substrate with a test pen. Ink either forms a continuous line on the surface or withdraws back into droplets, depending on the surface tension of the ink.

Printed line thicknesses were measured with an optical profilometer using the roughness parameters R_t and R_q. A scanning electron microscope (SEM) was used to inspect the surface topology of the cured ink structures. In addition, an optical microscope was used to measure the conductor line widths.

The electrical performance of the printed samples was evaluated using a four-point probe (4PP) sheet resistance measurement and a crosscut adhesion test. First, supply current I (10 mA) was fed to the printed conductor pattern and the resulting voltage difference U was measured with a Keithley 2425 sourcemeter. The obtained values and conductor dimensions (width $w = 1.3$ mm, length $l = 32$ mm) were then used to calculate sheet resistance R_s:

$$R_s = \frac{U}{I} \frac{w}{l}. \tag{3}$$

The electrical performance of the samples was not measured after the reliability tests, since prior studies by, for example, Caglar [31], Halonen [32] and Xie [2] have stated that the sheet resistance of silver conductors is not altered significantly in similar environmental stress tests, in comparison to the drastic adhesion degradation that was reported after these tests. Therefore, only interface adhesion was evaluated here, and electrical performance characterization was left to further stages of research, where possible effects on, for example, HF performance will be studied.

Additionally, a square pattern (2 cm × 2 cm) was used to evaluate the initial mechanical performance of the substrate-ink interface after curing and to inspect the effects of environmental stress. For this evaluation, a crosscut adhesion test was executed according to the ASTM-D3359 standard [33]. This standard is widely used for adhesion rating in the field of printed electronics, and it was therefore considered a suitable test method for this study [34–38].

3. Results

3.1. Substrate surface characteristics

3.1.1. Surface energy

Table 3 shows the measured surface energies for each test substrate type. The surface energies of the extruded PPE and injection-molded PPE matched due to the similar chemical compound. We observed that original surface energy value of the PPE substrate could be at least doubled with oxygen plasma and Nanoflame surface treatments. These results suggest that new functional groups were formed on substrate surface. On the other hand, ethyltriglycol coating sprayed on the native PPE did increase the surface energy partially. This result was mainly due to the uneven wetting of the chemical-substrate interface. We observed that ethyltriglycol could not wet native PPE even when multiple coating layers were applied, whereas the acid-etched substrate was

Table 3
Measured surface energies for each test substrate type.

Substrate	Surface energy [mNm^{-1}]
Native PPE (injection-molded)	30–32
O$_2$ plasma treatment	≥ 60
Nanoflame treatment	≥ 60
Ethyltriglycol coating	33–39
H$_2$SO$_4$ coating & ethyltriglycol coating	58–60
Extruded PPE	30–32

wetted extremely well even with one coating layer. We had observed earlier in [13] that etching with sulfuric acid increased the surface energy of PPE significantly (56–58 mN/m). Therefore, it is likely that ethyltriglycol wetting is improved on acid-etched substrate, because chemical surface tension and substrate surface energy are better matched.

On the other hand, the ethyltriglycol coating did not seem to affect the surface energy of the acid-etched PPE significantly, only an increment of 2–4 mN/m was observed in Dyne test pen measurements. However, since the test accuracy was limited to 2 mN/m, it was hard to confirm whether the surface energy had been changed.

3.1.2. Surface profile

Fig. 2 presents the surface profile measurement results. Plasma treatment results, which the authors obtained earlier [13], are used here as a reference for comparison with the other treatments. We observed that all of the chosen surface treatments alter the substrate surface profile. Applying chemical coating to the native PPE increased the surface roughness, and chemical coating of the acid-etched substrate led to significant alteration of the surface profile. In addition, a rather rough surface was obtained with the Nanoflame treatment, although modification was not as significant as with the plasma treatment. The results obtained from the extruded PPE are presented in a separate graph, since the roughness parameters of the extruded substrate are an order of magnitude higher when compared to the other results.
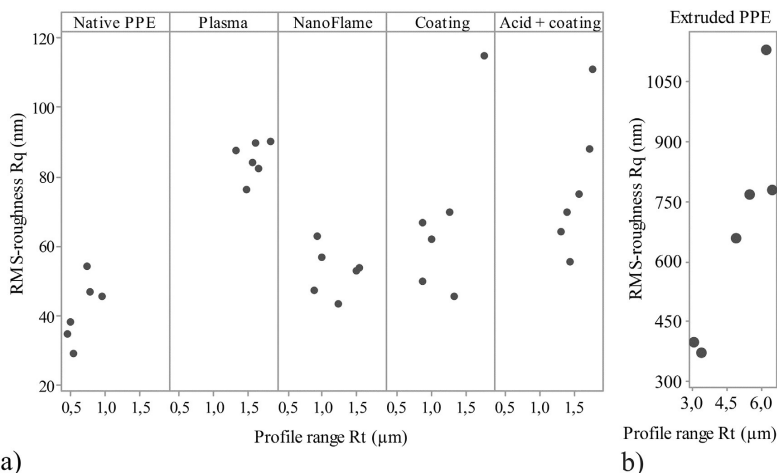
3.2. Print quality

Fig. 3 shows the measured line widths of the printed traces. A comparison was made between the traces printed with all the inks on native PPE samples and the traces printed on significantly altered substrates: plasma treated, acid etched + ethyltrigycol coated, and extruded PPE. Here, the line widths 1300 μm and 1400 μm were used as reference lines to improve the readability.

We observed differences between the inks that were used. We also observed significant spreading from the target width of 1300 μm with almost all ink-substrate combinations; best control over line width was obtained with aqueous HPS-021LV ink, whereas other inks spread significantly on similar substrates. Water surface tension (approximately 72 mN/m) [39] is high compared to the measured PPE surface energy, 30–32 mN/m, and wetting was thus more controlled. According to manufacturer information, the surface tension of other solvents is similar or even lower than PPE substrate surface energy, and thus they are more likely to spread.

Furthermore, we noted that the substrate surface parameters affect the line spreading of the inks. The measurement data in Fig. 3 indicates that both increased surface energy (plasma and combined chemical treatment) and increased surface roughness (extruded PPE) enhanced line spreading compared to results measured on native PPE substrates. Since the measured lines were even 100 μm wider than the targeted values, it might be necessary to consider alternative surface modification methods whenever finer features of printed patterns are required. It has been demonstrated earlier that these pastes can be used to fabrifcate relatively fine features by screen printing: Kujala showed in [40] that both DuPont 5064H and Asahi LS411AW inks can be used to print 50 μm wide vias, and conductive traces with line width below 500 μm. Additionally, SunChemical CRSN2442 and Novacentrix HPS-021LV inks have been succesfully used to fabricate narrow lines with screen printing [41,42]. Above-mentioned features are close to the limits of screen printing processing, even though they are still coarse in comparison to, for example, laser-shaped LTCC conductors [43]. However, our aim is for large area electronics, and therefore, screen printing is considered a sufficient fabrication method for our purposes.
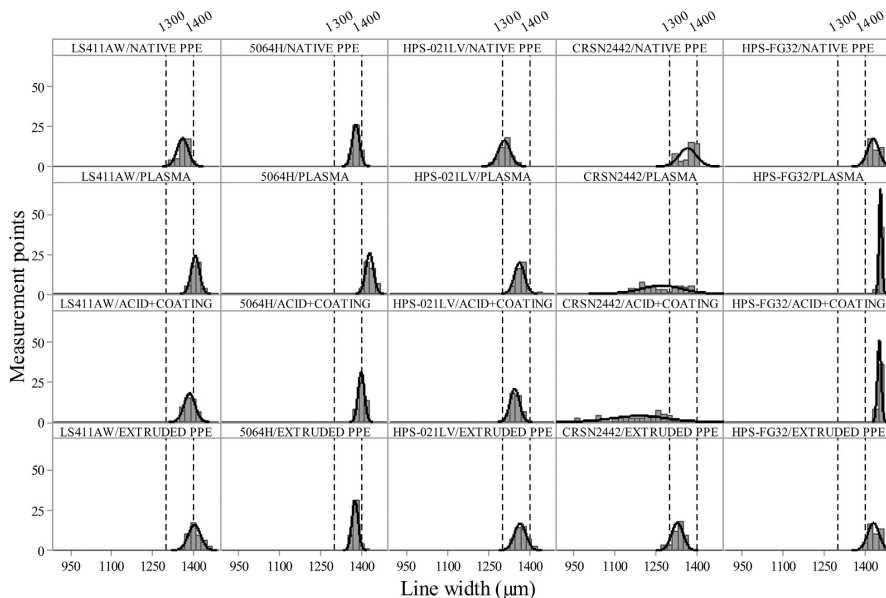
We observed abnormally narrow lines and deviation in the

Fig. 2. Measured surface profiles of the native, injection-molded PPE and of the substrates with surface pre-treatments. Extruded substrate results are included in a separate graph. Measured RMS roughness R_q is presented as a function of the profile range R_t.

Fig. 3. Measured line widths for all inks on native PPE, plasma treated PPE, acid-etched and coated PPE, and extruded PPE.

measured widths in the CRSN2442 data on plasma-treated substrates and on ethyltriglycol-coated, acid-etched substrates. This behavior was most likely caused by variation in the ink volume on the screen during printing and simultaneous screen clogging. Therefore, no conclusions can be made regarding CRSN2442 ink spreading abilities on those substrates.

In addition to variations in line spreading, we noted differences in both line thickness and roughness between the inks that were used. The measured line thicknesses and conductor surface roughnesses are presented in Fig. 4a, where the line thickness was obtained from the measured profile range value R_t, and the conductor surface roughness was obtained from the measured RMS roughness R_q.

We obtained approximately 25% thinner lines with the HPS-FG32 than with other inks. On the other hand, this ink tended to spread more.

Significant deviation in the measured thickness data of the HPS-021LV and Asahi LS411AW inks was observed. All of the inks were printed using the same screen, and it is likely that the parameters of those inks caused the variations. Asahi LS411AW viscosity is significantly higher than the viscosities of other inks (Table 1), which may have a negative effect on process control. In contrast, HPS-021LV viscosity is the lowest of the used inks (Table 1), and the ink tends to try rapidly during printing due to water evaporation. Therefore, the ink volume is harder to control.

We observed differences between the used inks in the roughness data. Normalized surface roughness by line thickness is presented in Fig. 4b. The line roughness of HPS-FG32 can be partially explained by flake composition: the SEM image (Fig. 5b) indicates that ink flakes form a rather loose structure, increasing surface roughness. On the
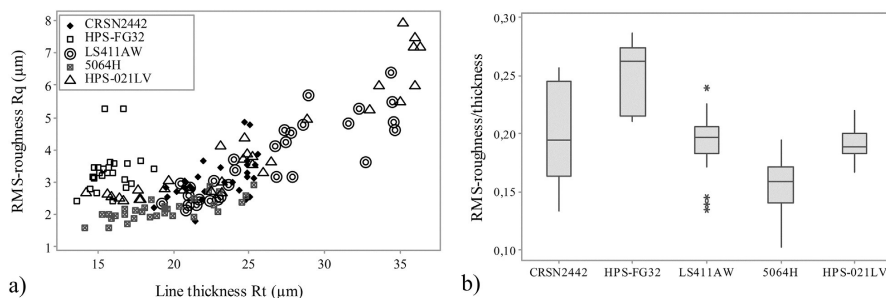
Fig. 4. a) Measured conductor RMS roughness R_q as a function of measured conductor line thickness R_t with the used silver inks; b) RMS roughness R_q, normalized by measured conductor line thickness R_t.
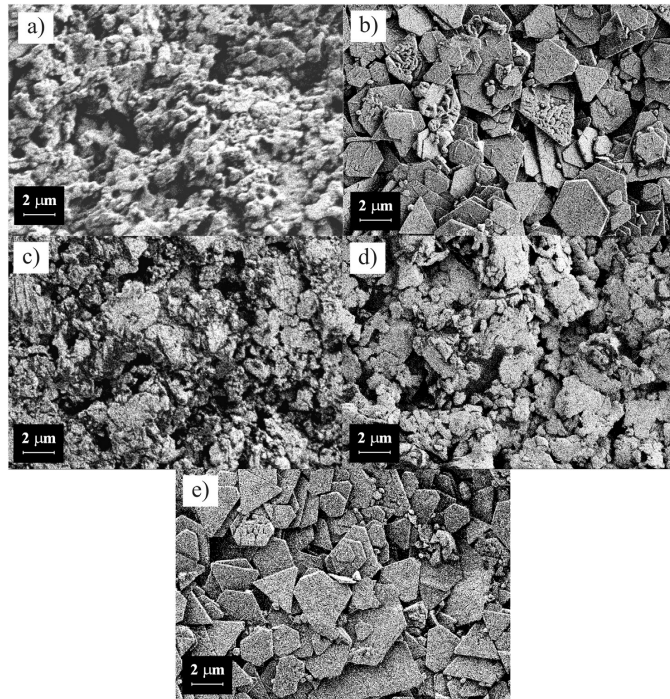
Fig. 5. SEM images of the conductor surface of a) CRSN2442 ink, b) HPS-FG32 ink, c) LS411AW ink, d) 5064H ink, and e) HPS-021LV ink. Magnification 15 k, EHT voltage 1.00 kV.

other hand, the formed lines are widely spread and thin, which may have a negative effect on the surface roughness.

On the contrary, LS411AW flake size varied (Fig. 5c), thus enabling a relatively smooth conductor surface compared to the obtained thickness values. Furthermore, comparison of the HPS021LV roughness data (Fig. 4b) and flake composition (Fig. 5e) indicates that the compact flake structure of cured ink enables a relatively smooth conductor surface. The lowest relative roughness was obtained with 5064H ink, with the conductor surfaces being rather smooth compared to the other inks, even though more variation in the results could be observed.

We observed significant variation in CRSN2442 line roughness in relation to the obtained thickness, with the mean value being close to the overall average roughness obtained with the used inks. The cured structure appears to consist of spherical particles and flakes (Fig. 5a), and variations in the roughness were most likely related to printing parameters, such as screen pressure. It is also possible that ink rheology affected the results. In total, measured roughness values are rather convenient, considering that the particle size of these inks is on the micrometer scale, and particles are overlapping in the cured structure.

3.3. Electrical performance

Sheet resistances calculated by (3) from the measured currents and voltages are presented in Fig. 6. In Fig. 6, 10 mΩ/sq and 20 mΩ/sq are used as reference lines, since the lowest measured values were approximately 10 mΩ/sq and a sheet resistance of 20 mΩ/sq was still

sufficient, when considering future research.

The measured HPS-FG32 sheet resistances were more than two times higher than the measured values of the other inks, indicating poor conductivity. After analyzing the first sample set, we fabricated new HPS-FG32 samples on a few selected test substrates with doubled curing time. These experiments were conducted in order to investigate the effect of curing conditions on sheet resistance. The test parameter and result summary are given in Table 4. We observed that a longer curing time provided better electrical performance, but the sheet resistance values were still high in comparison to other inks. Even though narrow lines with higher thickness could be produced, resistance would still be high, according to manufacturer information. Therefore, it may be concluded that this material is not competitive with other inks.

Comparison of other inks indicated that the lowest sheet resistances, between 10 and 20 mΩ/sq, are obtained with HPS-021LV, 5064H, and CRSN2442, whereas LS411AW sheet resistances are a little higher, approximately 15–25 mΩ/sq. However, these values are still sufficient for our purposes. In general, the obtained sheet resistance values match the datasheet information when the measured line thickness values are considered. However, we did observe significant deviation in the measured values. To improve sheet resistance stability, decreasing variation in both the line thickness and roughness through better process control would be necessary. In addition, better control over variations in line spreading would be required.

Furthermore, process optimization would provide benefits at high frequencies. Even though the measured sheet resistances are suitable
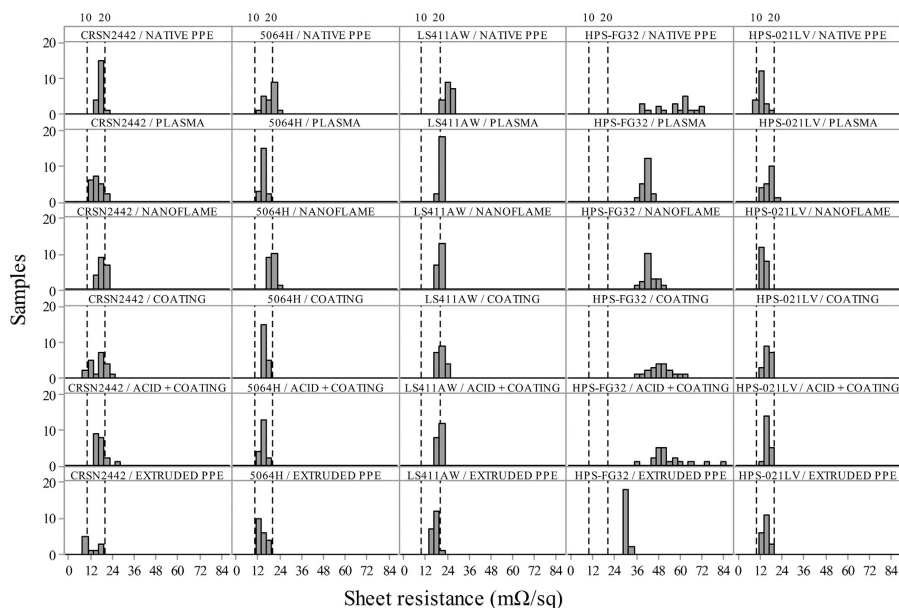
Fig. 6. Measured sheet resistances with each ink/substrate combination.

Table 4

Measured HPS-FG32 sheet resistances with different curing conditions.

Substrate	Sheet resistance: Curing 140 °C/10 min	Sheet resistance: Curing 140 °C/20 min
Native PPE	56.53 ± 11.08 mΩ/sq	43.54 ± 2.52 mΩ/sq
O₂ plasma treated PPE	41.31 ± 2.21 mΩ/sq	40.63 ± 1.62 mΩ/sq
acid etched and coated PPE	53.47 ± 11.11 mΩ/sq	54.95 ± 5.52 mΩ/sq

for HF applications, as stated earlier by, for example, Halonen [32], it has been observed [7,32,44] that many other parameters, such as substrate surface and conductor roughness, affect HF performance greatly. Therefore, process optimization is required in order to produce high-quality HF conductors. For example, the current density is packed to the conductor surface due to the skin effect at high frequencies, and thus a rough conductor surface lengthens the signal path, increasing signal losses [7,44,45].

3.4. Mechanical performance

3.4.1. Adhesion after curing

The results of the ASTM-D3359 crosscut adhesion test are presented in Fig. 7. A few samples had to be discarded from the analysis since ink adhesion failed due to imperfections in the substrate surface caused by the injection-molding process. Therefore, those results are not comparable to results obtained on a smooth substrate surface.

These results indicate that the adhesion of LS411AW, 5064H, and HPS-021LV inks was excellent, even on the native PPE substrates. On the other hand, as observed already in [13], CRSN2442 adhesion was poorer (ink removal 5–15%) on the native PPE substrates. However, the surface treatments that were used seem to have improved the adhesion of this ink, and ink removal could be reduced to 0–5%. Therefore, it is

likely that new functional groups have been formed on PPE surface, enhancing ink adhesion. Furthermore, effect on adhesion has been most significant with those treatments that caused both increment in surface energy and in surface roughness.

On the other hand, chemical coating on native PPE had no effect on ink adhesion. Even though ink removal seems to have increased with few inks using this treatment, more experiments would be needed to confirm if this treatment has any effect on adhesion level. It is also possible that poor wetting on native PPE prevents this chemical from adhering well to substrate, and thus, this coating layer might be removed with ink in the crosscut test. Additionally, it should be noted that since chemical coating was first cured at 100 °C, and inks printed on top of this coating were annealed at higher temperatures, it is possible that interaction of chemical coating with printed pastes is excessively enhanced. Therefore, it would be beneficial to determine, whether different results would be obtained using ink annealing temperatures not exceeding chemical curing temperature.

In addition, we observed that printing on the extruded substrate led to significant variation in the adhesion level. LS411AW and HPS-021LV adhesion was excellent even on this substrate, whereas significant adhesion failures were observed with the 5064H and CRSN2442 inks. This difference was most likely caused by the extremely rough surface, which prevented the interlocking of the latter inks. These results emphasize the importance of balance between the substrate surface chemistry and roughness: surface roughness may have a positive effect on ink bonding on a hydrophilic substrate, but a rough surface of a hydrophobic compound may weaken the bonds between the ink and substrate, consequently weakening the adhesion [46].

The HPS-FG32 results were not included in this analysis, since we noted that the first sample batch of HPS-FG32 ink had not dried properly: ink cohesion of all the samples failed in the crosscut test. Further inspection revealed that the remaining ink layer on the
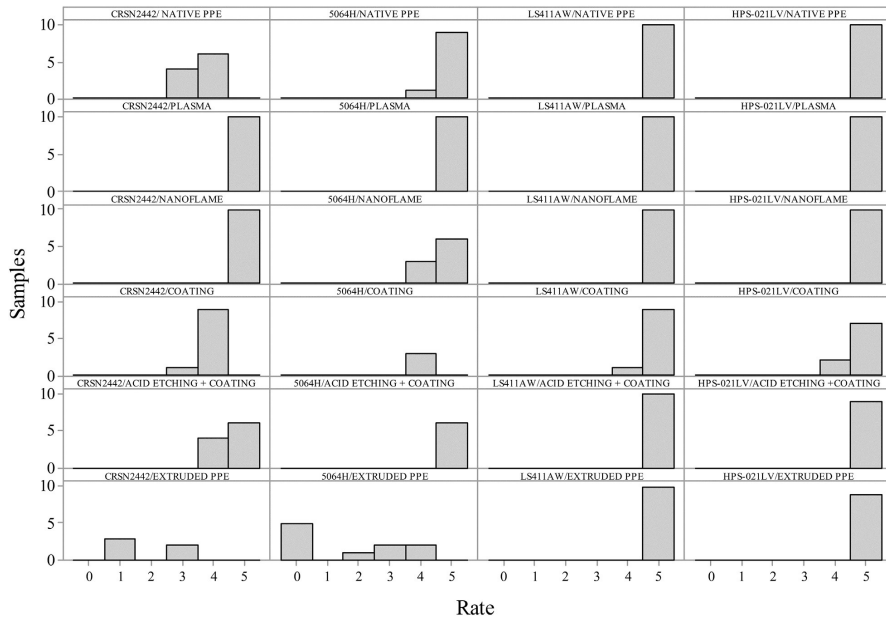
Fig. 7. ASTM-D3359 test results for each ink/substrate combination.

substrate was conductive, whereas the removed ink layer was not. Furthermore, since the sheet resistance of the second batch was still insufficient for further research, the ink was discarded from further analysis, and thus ink adhesion was not evaluated.

3.4.2. Effect of environmental stress

Based on both the sheet resistance measurements and the initial adhesion evaluation, we chose the best material combinations for the environmental reliability tests. Since both the electrical and mechanical performance of the LS411AW, 5064H, and HPS-021LV inks were excellent, they were selected for further experiments. We selected an oxygen plasma treatment and the combined treatment of acid etching and chemical coating as substrate treatment methods. These treatments had the most significant effect on surface roughness and energy, and their effect on ink adhesion was positive. A native, injection-molded PPE was used as a reference substrate for evaluating these pre-treated substrates. The fabricated sample sets are presented in Table 5.

Fig. 8 shows the effects of environmental stress on the ink-substrate interface behavior. Further discussion of different failure types is provided as supplementary information. Adhesion of the samples remained excellent in high relative humidity and elevated temperature of the 85% RH/85 °C test, since the adhesion of only three samples printed with DuPont 5064H ink failed, and therefore, no degradation of the adhesion level could be observed. These results are in line with work done by Putaala et al. [3], where RFID tags printed on different polymer compounds and reliability in the 85% RH/85 °C test was evaluated. Their samples did not fail until over 1000 h exposure to these conditions.

We observed several cohesion failures with HPS-021LV ink. The removed ink layer was extremely thin, indicating that moisture had penetrated the outer surface of the samples during the test, but that the corrosive effect was not severe. Additionally, the substrate cohesion of a few samples failed, indicating that the PPE-based compound was affected by the test conditions. The least number of failures occurred with the native PPE samples, where a 0–5% failure rate was observed.

On the other hand, more substrate failures occurred with the surface pre-treated samples, where we observed substrate cohesion failures even in 20% of the samples. Therefore, it is possible that these surface pretreatments decrease the moisture resistance of the PPE compound. Still, these results are promising considering the fact that common PE substrate materials, such as polyimide (PI) and polyethylene terephtalate (PET), typically have severe issues related to moisture absorbance, and are thus susceptible to environmental stress [47,48].

In contrast to results from the 85% RH/85 °C test, exposure to NaCl mist in a humid environment lowered the adhesion level significantly. In addition to adhesion failures, a significant number of ink cohesion failures occurred with all inks, and substrate surface cohesion failed as well.

After conducting the salt mist test, we observed areas with color alterations in the silver surface of the samples fabricated with LS411AW and 5064H inks. The 5064H alteration was more significant and its

Table 5
Fabricated sample sets for reliability tests with chosen inks and substrates.

Set	Ink	Substrate	85% RH/85 °C	Salt mist
1	LS-411AW	Native PPE	x	x
2	LS-411AW	Plasma treated	x	x
3	LS-411AW	Acid etched & coated	x	x
4	5064H	Native PPE	x	x
5	5064H	Plasma treated	x	x
6	5064H	Acid etched & coated	x	x
7	HPS-021LV	Native PPE	x	x
8	HPS-021LV	Plasma treated	x	x
9	HPS-021LV	Acid etched & coated	x	x
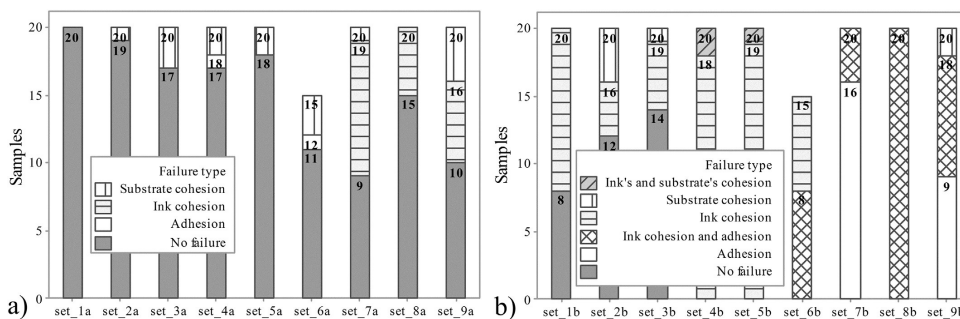
Fig. 8. Ink-substrate interface: adhesion and cohesion failures after a) 85% RH/85 °C test and b) salt mist test. Sets 1–3 were printed with Asahi LS411AW ink, sets 4–6 were printed with DuPont 5064H ink, and sets 7–9 were printed with Novacentrix HPS-021LV ink. Sets 1, 4, and 7 were printed on a native PPE substrate, sets 2, 5, and 8 on a plasma treated PPE substrate, and sets 3, 6, and 9 on an acid-etched and chemically-coated PPE substrate.
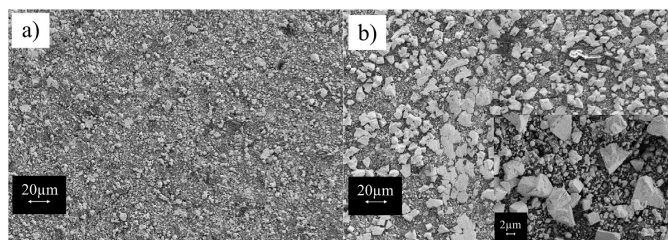
Fig. 9. SEM images obtained from a) the middle of the 5064H ink surface b) the edge of the 5064H ink surface. Magnification 917; EHT voltage 3.00 kV.

effect on ink cohesion was more severe. The SEM images obtained from our samples with dark areas indicate that new crystal particles formed on top of the silver layer. These results are presented in Fig. 9. Prior studies have found that in highly humid conditions, silver tends to react with NaCl, creating silver chloride (AgCl) crystals on a silver surface [49–51]. Therefore, it is possible that the crystal particles observed in this study consisted of AgCl. On the other hand, it has been observed that in a salt spray chamber, it is possible that the AgCl that forms dissolves in NaCl, and that new, big Ag particles may form [49–51]. Additionally, other corrosion products, such as oxides and other chlorides, have been observed. In our study, the size of the detected particles varies from tens of nanometers to several micrometers, suggesting that several corrosion products may have formed on the samples.

We also observed that these particles had formed particularly at the edges of the silver-coated area, whereas the center of the samples was not significantly corroded. Since we also observed that the flake structure is more compact in the middle of the samples, it can be concluded that reactions causing silver surface darkening could not take place in the middle due to the surface composition. It is also possible that the printing process made the sample edges rougher.

During the crosscut test, we observed that only the thin, darkened silver layer was removed from the top of the LS411AW and 5064H samples, whereas the rest of the silver coating remained intact, indicating that corrosive reactions affected only the surface area of the silver layer. However, we could not classify the adhesion of these samples since cohesion failures have not been included in the ASTM-D3359 standard.

In contrast, we could not observe visual alterations in the HPS-021LV samples. This difference was most likely caused by the flake

topologies (Fig. 5e): HPS-021LV flakes seem to form a more compact structure than other ink flakes, possibly because there are less solvent residues left after curing in low temperatures, since the water boiling point is reached below those temperatures. Therefore, the sprayed NaCl cannot interact with printed silver that easily. It is also possible that the corrosion products later dissolved into the NaCl solution in the salt spray chamber, but Ag corrosion still took place [49].

The classification results for the remaining samples without cohesion failures are presented in Fig. 10 for the 85% RH/85 °C test and the salt mist test, respectively. Since the 85% RH/85 °C test did not affect the ink-substrate interface properties, adhesion remained excellent. LS411AW survived both tests extremely well, even the salt mist test did not degrade its adhesion on any substrate. In addition, 5064H adhesion degradation was not significant, since ink removal was still 5% or less, even after the salt mist test.

In contrast, HPS-021LV adhesion degraded even from 0% ink removal to > 65% removal after the salt mist test. Additionally, we observed both ink cohesion and adhesion failures in several samples, and no samples survived this test without any failures. Therefore, it may be concluded that this test was extremely severe for this ink type, even though no visual signs of corrosion could be observed. Therefore, it is possible that even though HPS-021LV composition after curing seems more compact than the composition of other inks, residues of the solvents and binders in other inks provide better protection against environmental corrosion.

Additionally, we noted that the effect of the substrate surface pre-treatment on adhesion was significant in this test, since ink removal on acid-etched and coated samples was only 5%, compared to 65% removal on native PPE. Adhesion on plasma-treated samples also seemed to remain tolerable, but since ink cohesion failed on all samples, the
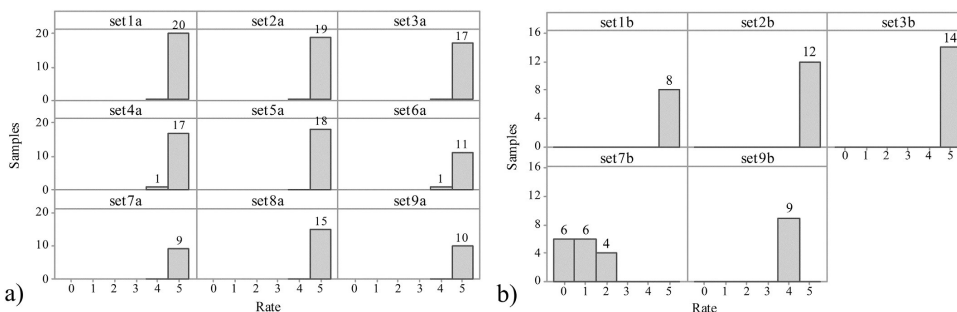
Fig. 10. Ink-substrate interface: adhesion and cohesion failures after a) 85% RH/85 °C test and b) salt mist test. Sets 1–3 were printed with Asahi LS411AW ink, sets 4–6 were printed with DuPont 5064H ink, and sets 7–9 were printed with Novacentrix HPS-021LV ink. Sets 1, 4, and 7 were printed on a native PPE substrate, sets 2, 5, and 8 on a plasma-treated PPE substrate, and sets 3, 6, and 9 on an acid-etched and chemically-coated PPE substrate.

adhesion could not be classified. This result indicates that strong chemical bonds are necessary for reliable printed structures, and it likewise suggests that organic components would be beneficial for this ink composition, too.

Again, an effect on the substrate cohesion after exposure to environmental stress was observed, with a failure rate of 5–20% occurring in several sample sets. Even though the exposure time in this test was rather short compared to the 85% RH/85 °C test, we still observed almost as many substrate failures. These results emphasize the harshness of this kind of environment. However, as concluded in, for example [49–51], in a standard salt chamber environment there are less reactive species, like sulfides or ozone, in the air, and therefore, the corrosion in a salt chamber is negligible in comparison to a real marine environment. Therefore, intense protection of the printed structures is required in marine applications.

Here, we observed that environmental stress can cause drastic adhesion degradation of printed silver on a polymer substrate. These findings are similar to those of Xie, Caglar and Halonen [2,31,32]. As mentioned earlier, we did not measure in-situ sheet resistance of the samples during the reliability tests or the sheet resistance after reliability tests, because it has been stated before for example in [2,31,32] that effect on silver resistance is not significant even after the salt fog test, in comparison to adhesion degradation. Even though resistance increment up to 6–21% may occur [2,31,32], this change is considered negligible in comparison to the observed adhesion degradation. Additionally, severe demalination of conductive traces eventually leads to system failure, independent on electrical performance. Therefore, electrical performance optimization will be beneficial only after adhesion issues have first been solved, as emphasized in [32], where a protective layer was applied, and no change in sheet resistance occurred in any conditions. Still, adhesion degradation was significant, even though similar protective coating was used. Of course, maintaining sufficient conductivity level is important, and in further stages, it would be beneficial to confirm electrical performance after exposure to environmental stress, especially to investigate both the possible effect of protective coatings, and the impact of environmental stress on HF performance [32]. Sheet resistance determination can be made both in situ and consequently, as demonstrated for example in [43].

3.5. Discussion

A comparison of the line widths measured with an optical microscope revealed that surface treatments tend to increase the conductor line width. Based on these results, it may be concluded that both increased surface energy and a roughened substrate surface clearly promote ink spreading on this low-surface energy substrate.

In addition, we found differences between the inks that were used. Inks with organic solvents resulted in wider lines than originally designed, whereas the spreading of lines printed with aqueous HPS-021LV was more controlled.

Significant line spreading is often problematic in such applications, where the downscaling of printed features is necessary. Additionally, in some other application consider areas, narrower structures would be crucial and alternative methods should be considered. However, the aim of our work was to find solutions for such antennas and base station structures, where the miniaturizing of electronics is not essentially required. Therefore, wide lines and line spreading are not a significant issue for future work, especially when taken into account in feature design.

Several of the inks chosen seem suitable for HF applications based on the obtained low sheet resistance values. Still, further investigation is required in order to confirm the effects of conductor surface roughness on the final performance.

In addition, we observed that the surface treatments that were used could improve adhesion significantly. In particular, the Nanoflame treatment and chemical coating on the acid-etched substrate improved the results and ink removal was reduced to 0%, even when the removal was originally 15%. The authors also observed that the oxygen plasma treatment had a similar promoting effect on adhesion, which is in line with previous findings [13]. These results indicate that both an increment of surface energy and surface roughening are needed to promote ink adhesion on this substrate material.

In addition to the initial adhesion strength, the surface treatments had a positive effect on the sample reliability. However, as observed after the salt mist test, sufficient protection of the printed structures is necessary in harsh conditions to prevent both adhesion and cohesion failures in the used materials. Second, such protection would help maintain electrical performance at the required level.

The significance of the ink composition in regards to reliability was emphasized in these tests. Furthermore, the results indicate that surface pre-treatments might damage the substrate by, for example, increasing moisture absorption. Additionally, the possible effects of the surface treatments on high frequency characteristics of the used PPE substrate are still unknown, and they require further investigation before these treatments can be utilized in printed HF applications on this substrate.

4. Conclusion

In this study, we studied the performance of five commercially available silver inks on a PPE-based substrate. We inspected the effect

of surface pre-treatments on test substrates by analyzing both the surface properties and final performance of the printed structures. In addition, we used environmental stress tests to evaluate the long-term reliability of the printed structures.

The results indicate that such commercial inks are able to provide both low sheet resistance and excellent adhesion on the test substrates. On the other hand, by choosing a suitable surface treatment, the substrate-ink interface performance may be improved significantly, and thus the variety of suitable inks may be widened.

The environmental reliability test results indicate that the test structures were able to withstand even rather harsh conditions. However, in extremely harsh conditions, such as a marine environment, it is important to provide sufficient environmental protection, such as barrier layers, to ensure the long-term reliability of applications.

Our results indicate that PPE is a sufficient substrate material for large area printed electronics. In this study, we concluded that both the materials and process parameters affect the final print quality, and thus, also the conductor performance. Therefore, further research is needed to optimize both the material parameters and fabrication process. Other recommendations for future work include HF characterization for both the test substrates and inks. In addition, protection methods against environmental stress should be studied.

Acknowledgements

Appendix A. Supplementary data

Supplementary data to this article can be found online at https://doi.org/10.1016/j.microrel.2018.05.010.

References

[1] H. Sillanpää, (Ph.D. Thesis), Tampere University of Technology, (June, 2014).
[2] L. Xie, M. Mäntysalo, A.L. Cabezas, Y. Feng, F. Jonsson, L. Zheng, Electrical performance and reliability evaluation of inkjet-printed Ag interconnections on paper substrates, Mater. Lett. 88((2012) 68–72, http://dx.doi.org/10.1016/j.matlet.2012.08.030.
[3] J. Putaala, J. Niittynen, J. Hannu, S. Myllymäki, E. Kunnari, M. Mäntysalo, J. Hagberg, Capability assessment of inkjet printing for reliable RFID applications, IEEE Trans. Device Mater. Reliab. 17 (2017) 281–290, http://dx.doi.org/10.1109/TDMR.2016.2636342.
[4] Y.S. Rim, S.-H. Bae, H. Chen, N. De Marco, Y. Yang, Recent progress in materials and devices toward printable and flexible sensors, Adv. Mater. 28 (2016) 4415–4440, http://dx.doi.org/10.1002/adma.201505118.
[5] Z. Bao, X. Chen, Flexible and stretchable devices, Adv. Mater. 28 (2016) 4177–4179, http://dx.doi.org/10.1002/adma.201601422.
[6] S. Khan, L. Lorenzelli, R.S. Dahiya, Technologies for printing sensors and electronics over large flexible substrates: a review, IEEE Sensors J. 15 (2015) 3164–3185, http://dx.doi.org/10.1109/JSEN.2014.2375203.
[7] N. Komoda, M. Nogi, K. Suganuma, K. Kohno, Y. Akiyama, K. Otsuka, Printed silver nanowire antennas with low signal loss at high-frequency radio, Nano 4 (2012) 3148–3153, http://dx.doi.org/10.1039/C2NR30485F.
[8] A.B. Menicanin, L.D. Zivanov, M.S. Damnjanovic, A.M. Maric, Low-cost CPW meander inductors utilizing ink-jet printing on flexible substrate for high-frequency applications, IEEE Trans. Electron Devices 60 (2013) 827–832, http://dx.doi.org/10.1109/TED.2012.2234461.
[9] U. Zorll, A.A. Tracton (Ed.), Coatings Technology: Fundamentals, Testing and

Processing Techniques, CRC Press, 2006(Ch. 6).
[10] P. De Gennes, F. Brochard-Wyart, D. Quéré, Capillarity and Wetting Phenomena; Drops, Bubbles, Pearls, Waves, Springer Science and Business Media, Inc., NY, USA, 2004.
[11] R.K. Ulrich, R.K. Ulrich, W.D. Brown (Eds.), Advanced Electronic Packaging, Wiley, 2006, pp. 651–690.
[12] J. Lilja, V. Pynttäri, T. Kaija, R. Mäkinen, E. Halonen, H. Sillanpää, J. Heikkinen, M. Mäntysalo, P. Salonen, P. De Maagt, Body-worn antennas making a splash: lifejacket-integrated antennas for global search and rescue satellite system, IEEE Trans. Antennas Propag. 55 (2013) 324–341, http://dx.doi.org/10.1109/MAP.2013.6529385.
[13] R. Mikkonen, M. Mäntysalo, Benchmark study of screen printable silver inks on a PPE based substrate, Proc. of 21st EMPC 2017, Warsaw, Poland, 11th–13th September, 2017, (2018) (in press).
[14] Preperm®L260, TDS, Premix Oy.
[15] E. Sipilä, J. Virkki, L. Sydänheimo, L. Ukkonen, Experimental study on brush-painted passive RFID-based humidity sensors embedded into plywood structures, Int. J. Antennas Propag. 2016 (2016), http://dx.doi.org/10.1155/2016/1203673.
[16] T. Björninen, J. Virkki, L. Sydänheimo, L. Ukkonen, Manufacturing of antennas for passive UHF RFID tags by direct write dispensing of copper and silver inks on textiles, Proc. of ICEAA 2015, IEEE, 2015, pp. 589–592, , http://dx.doi.org/10.1109/ICEAA.2015.7297183.
[17] T. Happonen, T. Ritvonen, P. Korhonen, J. Häkkinen, T. Fabritius, Bending reliability of printed conductors deposited on plastic foil with various silver pastes, Int. J. Adv. Manuf. Technol. 82 (2016) 1633–1673, http://dx.doi.org/10.1007/s00170-015-7403-9.
[18] E. Jansson, J. Hast, J. Petäjä, J. Honkala, J. Häkkinen, O. Huttunen, Improving conductivity of rotary screen printed microparticle silver conductors using a roll-to-roll calendering process, J. Print Media Technol. Res. 4 (2015) 19–26, http://dx.doi.org/10.14622/JPMTR-1442.
[19] J.V. Voutilainen, T. Happonen, J. Häkkinen, Reliability of silkscreen printed planar capacitors and inductors under accelerated thermal cycling and humidity bias life testing, Proc. of 4th ESTC, 2012, pp. 1–6, , http://dx.doi.org/10.1109/ESTC.2012.6542201.
[20] CRSN2442 Conductive Silver Ink, TDS, SunChemical.
[21] 5064H, TDS, DuPont.
[22] Metalon HPS-FG32 silver screen ink, TDS, Novacentrix, 2016 Available https://www.novacentrix.com/sites/default/files/pdf/Metalon%20HPS-FG32.pdf , Accessed date: 27 October 2017.
[23] LS411AW Silver conductive paste, TDS, Asahi Chemical Research Laboratory CO., LTD.
[24] Metalon HPS-021LV silver screen ink, TDS, Novacentrix, 2012 Available https://store.novacentrix.com/v/vspfiles/assets/images/metalon%20hps-021lv_2230.1.pdf , Accessed date: 27 October 2017.
[25] P.T. Polytec, NanoFlame surface pre-treatment, https://www.intertronics.co.uk/product/nanoflame-nf02-surface-pretreatment-device/, (2016) , Accessed date: 4 April 2018.
[26] V. Pekkanen, M. Mäntysalo, K. Kaija, P. Mansikkamäki, E. Kunnari, K. Laine, J. Niittynen, S. Koskinen, E. halonen, U. Caglar, Utilizing inkjet printing to fabricate electrical interconnections in a system-in-package, Microelectron. Eng. 87 (2010) 2382–2390, http://dx.doi.org/10.1016/j.mee.2010.04.013.
[27] High modulud polyester monofilament mesh for technical screen printing applications, NBC Meshtec, Inc, http://www.nbc-jp.com/eng/product/2016Alpha_l_ux_ex_spec.pdf , Accessed date: 4 April 2018.
[28] JEDEC Standard, JESD22-A101C Steady State Temperature Humidity Bias Life Test, JEDEC Solid State Technology Association, USA, 2009.
[29] IEC 60068 2-52, International Electrotechnical Commission, (1996).
[30] E.S. Gadelmawla, M.M. Koura, T.M.A. Maksoud, I.M. Elewa, H.H. Soliman, Roughness parameters, J. Mater. Process. Technol. 123 (2002) 133–145, http://dx.doi.org/10.1016/S0924-0136(02)00060-2.
[31] U. Caglar, P. Mansikkamäki, Temperature-dependent reliability of inkjet-printed silver structure in constant humidity environment, Proc. of NIP 24, 2008, pp. 387–390.
[32] E. Halonen, V. Pynttäri, J. Lilja, H. Sillanpää, M. Mäntysalo, J. Heikkinen, R. Mäkinen, T. Kaija, P. Salonen, Environmental protection of inkjet-printed Ag conductors, Microelectron. Eng. 88 (2011) 2970–2976, http://dx.doi.org/10.1016/j.mee.2011.04.038.
[33] ASTM-D3359-09e2, Standard Test Methods for Measuring Adhesion by Tape Test, ASTM International, USA, 2009.
[34] Y.-I. Lee, Y.-H. Choa, Adhesion enhancement of ink-jet printed conductive copper patterns on a flexible substrate, J. Mater. Chem. 22 (2012) 12517–12522, http://dx.doi.org/10.1039/C2JM31381B.
[35] Y. Chang, D.-Y. Wang, Y.-L. Tai, Z.-G. Yang, Preparation, characterization and reaction mechanism of a novel silver-organic conductive ink, J. Mater. Chem. 22 (2012) 25296–25301, http://dx.doi.org/10.1039/C2JM34569B.
[36] J. Park, H. Nguyen, S. Park, J. Lee, B. Kim, D. Lee, Roll-to-roll gravure printed silver patterns to guarantee printability and functionality for mass production, Curr. Appl. Phys. 15 (2015) 367–376, http://dx.doi.org/10.1016/j.cap.2015.01.007.
[37] Y.-S. Hsiao, W.-T. WHang, S.-C. Wu, K.-R. Chuang, Chemical formation of palladium-free surface-nickelized polyimide film for flexible electronics, Thin Solid Films 516 (2008) 4258–4266, http://dx.doi.org/10.1016/j.tsf.2007.12.166.
[38] T. Zhang, E. Asher, J. Young, A new printed electronics approach eliminating redundant fabrication process of vertical interconnect accesses: building multilayered circuits in porous materials, Adv. Funct. Mater. (2018), http://dx.doi.org/10.1002/admt.201700346.
[39] J. Kalová, R. Mareš, Reference values of surface tension of water, Int. J.

Thermophys. 36 (2015) 1396–1404, http://dx.doi.org/10.1007/s10765-015-1907-2.

[40] M. Kujala, (M.Sc. Thesis), Tampere University of Technology, (April 2018).

[41] P. Escobedo, M.A. Carvajal, L.F. Capitán-Vallvey, J. Fernández-Salmerón, A. Martínez-Olmos, A.J. Palma, Passive UHF RFID tag for multispectral assessment, Sensors 16 (2016), http://dx.doi.org/10.3390/s16071085.

[42] W. Zhou, F.A. List, C.E. Duty, S. Babu, Fabrication of conductive paths on a fused deposition modeling substrate using inkjet deposition, Rapid Prototyp. J. 22 (2016) 77–86, http://dx.doi.org/10.1108/RPJ-05-2014-0070.

[43] D. Nowak, A. Dziedzic, Reliability of Fine-Line Thick-Film and LTCC Conductors at High-Temperature Operation, Proc. 37th Int, Spring Seminar on Electronics Technology, ISSE, 2014, pp. 176–179.

[44] T. Björninen, S. Merilampi, L. Ukkonen, L. Sydänheimo, P. Ruuskanen, The effect of fabrication method on passive UHF RFID tag performance, Int. J. Antennas Propag. 2009 (2009), http://dx.doi.org/10.1155/2009/920947.

[45] H. Yang, K.W. Chen (Ed.), The Electrical Engineering Handbook, Academic Press, 2004, p. 518.

[46] P. De Gennes, F. Brochard-Wyart, D. Quéré, Capillarity and Wetting Phenomena: Drops, Bubbles, Pearls, Waves, Springer Science and Business Media, Inc., New York, USA, 2004, p. 221.

[47] S. Lahokallio, K. Saarinen, L. Frisk, Effect of high-humidity testing on material parameters of flexible printed circuit board materials, J. Electron. Mater. 42 (2013) 2822–2834, http://dx.doi.org/10.1007/s11664-013-2652-6.

[48] B.-H. Bae, M.-S. Yeong, B.R. Lee, J.-H. Choo, E.-K. Choi, J.-S. Yoon, J.-B. Park, Effects of various environmental conditions on the electrical properties and interfacial reliability of printed Ag/polyimide system, Proc. of IEE. Electron. Compon. Technol. Conf. (ECTC) 64th, 2014, pp. 1735–1739, , http://dx.doi.org/10.1109/ECTC.2014.6897531.

[49] H. Lin, G.S. Frankel, W.H. Abbott, Analysis of Ag corrosion products, J. Electrochem. Soc. 160 (2013) C345–C355, http://dx.doi.org/10.1149/2.055308jes.

[50] D. Liang, H.C. Allen, G.S. Frankel, Z.Y. Chen, R.G. Kelly, Y. Wu, B.E. Wyslouzil, Effects of sodium chloride particles, ozone, UV, and relative humidity on atmospheric corrosion of silver, J. Electrochem. Soc. 157 (2010) C146–C156, http://dx.doi.org/10.1149/1.3310812.

[51] Y. Yoon, J.D. Angel, D.C. Hansen, Atmospheric corrosion of silver in outdoor environments and modified accelerated corrosion chambers, Corrosion 72 (2016) 1424–1432, http://dx.doi.org/10.5006/2079.

PUBLICATION
III

Inkjet printable polydimethylsiloxane for all-inkjet-printed multilayered soft electrical applications

R. Mikkonen, P. Puistola, I. Jönkkäri, M. Mäntysalo

ACS APPLIED MATERIALS & INTERFACES

Inkjet Printable Polydimethylsiloxane for All-Inkjet-Printed Multilayered Soft Electrical Applications

Riikka Mikkonen,* Paula Puistola, Ilari Jönkkäri, and Matti Mäntysalo

Cite This: ACS Appl. Mater. Interfaces 2020, 12, 11990−11997   Read Online

| ACCESS | Metrics & More | Article Recommendations | Supporting Information |

ABSTRACT: In recent years, additive manufacturing of polydimethylsiloxane (PDMS) has gained interest for the development of soft electronics. To build complex electrical devices, fabrication of multilayered structures is required. We propose here a straightforward digital printing fabrication process of silicone rubber-based, multilayered electronics. An inkjet-printable PDMS solution was developed for the digital patterning of elastomeric structures. The silicone ink was used together with a highly conductive silver nanoparticle (Ag NP) ink for the fabrication of all-inkjet-printed multilayered electrical devices. The application of the multilayered circuit board was successful. The sheet resistances were below 0.3 Ω/□, and the conductive layer thickness was less than 1 μm. The electrical insulation between the conductive layers was done by printing a 20−25 μm-thick dielectric PDMS layer selectively on top of the bottommost conductive layer.

KEYWORDS: polydimethylsiloxane, elastomer, dielectric, inkjet printing, multilayer, printed electronics
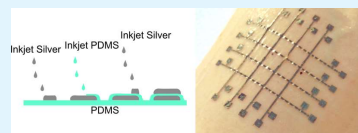
INTRODUCTION

Polydimethylsiloxane (PDMS) is a widely used silicone elastomer because of its biocompatibility, low cost, and optical transparency. Properties such as nontoxicity, chemical inertness, and high elasticity make it suitable for both in vitro and in vivo applications, including, for example, tissue mimicking, electronic skin (e-skin) applications, and microfluidics.[1−4]

In order to fabricate 3D-shaped PDMS structures conventionally by means of lithography or mold casting, several process steps and tools, such as mask aligners, evaporation or sputter deposition tools, and etching equipment, are required. In addition, the fabrication process may require using hazardous chemicals.[5,6] To address the inconvenience of these PDMS fabrication processes, several approaches of additive manufacturing have been presented in recent years, including 3D printing of PDMS using supportive baths and gels,[7,8] and curing with either heat or UV light.[9−11] Additive manufacturing enables more rapid prototyping and iteration rounds at a low cost, and even complex shapes imitating human hands or blood vessels can be fabricated.[10]

Digital drop-on-demand (DOD) printing is a great example of additive manufacturing techniques. These digital printing techniques, such as inkjet printing, can be used both in laboratory prototyping and on an industrial scale.[12,13] The main benefits of these techniques include low material consumption and contactless printing. Sturgess et al. presented an approach[14] where PDMS was DOD inkjet-printed to produce ziggurat-shaped 3D objects. They used the two components of Sylgard 184 silicone as inks, and these components were printed sequentially. Thus, the elastomer was cross-linked in the process.

In addition to the abovementioned benefits, the inkjet printing technology is also compatible with large or irregularly shaped substrate materials. Therefore, DOD printing is a promising technology for the manufacturing of soft, large area, flexible, and stretchable electronics. Examples of inkjet-printed, wearable devices include tattoo-like devices,[15] piezoelectric devices,[16,17] and other skin-conformable systems.[18,19] To apply the inkjet printing of PDMS in electronic fabrication, McCoul 3D inkjet-printed commercial silicone elastomer foils were used for dielectric elastomer actuators.[20] In the approach of Peng et al., an inkjet printable PDMS was used to make microlens arrays for pressure sensors.[21] In order to fabricate printed functional systems from passive components to the final devices, deposition of more than one material is required.[22−27] Mamidanna et al.[28] fabricated a PDMS-based microfluidic mixer by inkjet printing, including the fluid channels and sensing electrodes.

This work presents a straightforward fabrication strategy for multilayered, all-inkjet-printed soft electrical systems in an elastomeric matrix. In contrast to the previous approaches,[14,20] we printed the whole functional structure, including the conductive material and the dielectric material, with a single material printer. The key component of this approach is our PDMS (Sylgard 184) ink, which is used as a dielectric between

the conductive tracks. The work herein includes the characterization of silicone ink properties, such as viscosity and surface tension measurements, and printing trials for optimization of jetting stability and patterning of the dielectric ink. The ink was tuned to be compatible with the Fujifilm Dimatix DMP inkjet printers, which are widely used to print patterns for printed electronic applications.[29−33]

Printing of our PDMS ink was allowed at 30 °C temperature for at least 2 days with one cartridge, when stored in a refrigerator overnight, even though the polymer was mixed in advance. This is a significant improvement to the previous work, where the ink with a premixed PDMS component was reported to remain printable for only 2 h.[28] Even though the reactive printing strategy, where the two PDMS components are printed separately and mixed in situ, would allow an even longer shelf-life for the inks, using more than one ink cartridge to print one material will add steps to the fabrication process and make it both slower and less convenient.

Together with a highly conductive Ag NP ink, the optimized dielectric ink was used to print conductive lattice structures as a demonstration of an all-inkjet-printed, multilayered system. The results indicate that the printing of the elastomeric dielectric layers enables the additive and digital manufacturing of complex electrical devices. This is a great benefit in comparison to the processes, which are based on a PDMS casting process, where the fabrication of multilayered electronics will require using stencils, via structures and punching tools.[34,35] With sufficient patterning geometry and material selection, this process is easily applicable to the manufacturing of soft, biocompatible, and skin-conformable electrical devices entirely by inkjet printing, with only a few process steps.

■ RESULTS AND DISCUSSION

Herein, two ink solvents were used. Isobutyl acetate (IBA) was selected as a less hazardous substitute for toluene used by Mamidanna et al.[28] Peng et al.[21] used *n*-butyl acetate successfully with a 50 μm nozzle diameter in a Microfab jetlab II-printer. Here, the performance of the solvent was studied using a Dimatix DMP 2800-printer with a 21 μm nozzle diameter. Octyl acetate (OA) was selected as a slower-evaporating, nonhazardous alternative. It has been previously found to be a promising PDMS solvent by Sturgess et al.[14] The mixed Sylgard 184 (1:10) was diluted in both OA and IBA. The objective was to produce a well-working ink for the DMP-2800 inkjet printer, and therefore, the target viscosity was set to 10−20 mPa·s and the target surface tension to 20−35 mN/m.

First, the viscosities of different silicone inks were measured as a function of the shear rate from 1 to 1000 1/s (Figure 1a) to estimate inks' jettability at the printing frequency. The shear rate of the liquid in the nozzle is dependent on the piezoelectric actuator's motion and may reach values up to 40 kHz.[36] Therefore, the ink viscosity's response to higher shear rates is crucial to understand, when the ink jettability is estimated. Ink viscosities were also measured as a function of increasing temperature from 25 to 70 °C (Figure 1b). Even though the cartridge temperature is set to a low value, information on the viscosity at elevated temperatures is beneficial. When the height distance between the nozzles and the substrate is only 0.8 mm, heating of the substrate (60 °C) will also elevate the cartridge temperature (approx. 5 °C)
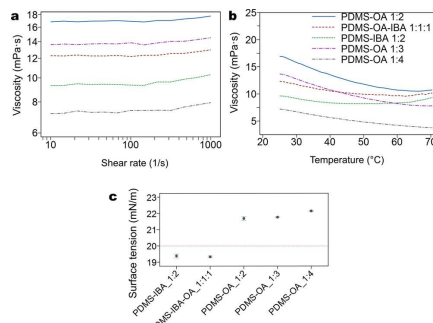
Figure 1. Summary of the fluid characteristics of all the ink solutions; the data labels are the same for both (a,b). (a) Measured viscosities of different ink compositions as a function of the shear rate (1−1000 1/s). One measurement per ink is given. (b) Measured viscosities as a function of the temperature (25−70 °C). One measurement per ink is given. (c) Measured surface tensions (15 measurements, confidence interval CI 95% for the mean).

during printing because there is no cooling element in the cartridge.

All viscosities remained rather stable during the shear rate tests, indicating Newtonian behavior. Some differences were observed in the temperature tests: the viscosities of all inks decrease with increasing temperature; a deeper slope is observed with the OA-diluted inks, whereas the IBA solvent leads to a moderate decrease in the viscosity. Additionally, a moderation of the slope can be observed at the higher end of the temperature range (50−70 °C), and even an increment of the viscosity is observed. The significant viscosity slope moderation of the IBA-containing solutions and their clear viscosity increment at higher temperatures are suspected to be an outcome of the accelerated solvent evaporation of this relatively volatile solvent (vapor pressure 20 hPa at 20 °C and low boiling point 120 °C), resulting in a higher PDMS concentration, when the solution is heated. With lower polymer concentrations (20−25% by weight), the moderation of the viscosity slope is less significant at elevated temperatures or is not observed at all.

In addition to the viscosity measurements, the surface tensions of the ink solutions were measured (Figure 1c). We observed that only the surface tensions of the OA-based inks were in the theoretical printable range ($\gamma > 20$ mN/m) and that the ink surface tension increased with higher OA-content.

The results of viscosity and surface tension measurements were clearly observed in the ink-jetting trials: Either of the IBA-containing inks could not be jetted successfully, which is most likely due to both the inadequate surface tension and the relatively high evaporation rate of the solvent, in comparison to the OA-diluted solutions. Droplets could be jetted for a short time, but the nozzles were clogging too quickly, preventing a reliable and reproducible jetting. Interestingly, the Z-numbers, which are commonly used to evaluate the printability of the inkjet inks,[20,37] were all in the range of $1 < Z < 3$ for our inks (Table S1).

However, it has been argued in the literature that there are many other parameters affecting the final jetting behavior and

printability, especially in the case of polymer inks. These parameters include, for example, the solvent vapor pressure, the molecular weight, and the concentration of the polymer.[38−40] Nevertheless, Peng et al. used *n*-butyl acetate successfully to dilute PDMS for inkjet printing in a 1:3 ratio (PDMS to solvent).[21] To investigate IBA jetting further, we prepared a 1:3 PDMS−IBA solution for jetting trials. The droplet firing was better than that with the 1:2 solution, but the nozzles still clogged very quickly. Only a frequent cleaning cycle could keep the nozzles firing, but even then, the droplets were heavily misdirected. Therefore, this ink was declared to be not stable enough for printing. A 1:4 solution was not prepared because the measurement results (Figure 1a−c) indicate that the viscosity will decrease far below 10 mPa·s, and the surface tension of the ink will not increase significantly with a higher solvent concentration, meaning no improvement in the ink's properties. The main difference between our approach and that of Peng et al. is the ink volume in the printhead: our nozzle diameter is only 21 μm, whereas their nozzle diameter was 50 μm.[21] Therefore, the ink volume in our printhead is significantly smaller, and the ink is likely to be more sensitive to the effects of surface tension, viscosity, or solvent vapor pressure.

The jetting of the octyl acetate-based inks was found to be sufficient for further trials. However, because the two components of Sylgard 184 were mixed in advance to the printing, it was necessary to keep the cartridge temperature as low as possible, thus hindering the cross-linking of the PDMS component. The 1:2 PDMS−OA solution required heating the cartridge to temperatures above 35 °C, and therefore it was discarded before further experiments. Both the 1:3 and 1:4 PDMS−OA solutions could be printed without heating the cartridge above 30 °C. To maximize the PDMS-content of the ink, we chose to use the 1:3 PDMS−OA solution instead of the 1:4 PDMS−OA solution. This solution remained printable for at least 2 days without the need to modify the cartridge settings, when the ink cartridge was stored in the refrigerator overnight.

The contact angles of the 1:3 PDMS−OA solution were measured on the spin-coated PDMS and on the printed silver surface to estimate its printability as a dielectric layer. The ink contact angles were 46 ± 1 and ≤15°, respectively. In the printing trials, it was observed that the droplet size on the substrate, which is equal to one pixel of a raster image, was approximately 45 μm, and that the well-defined, continuous lines could be printed on the PDMS substrate using a drop spacing (DS) of 20 μm. In Figure 2a, the measured line widths are presented for 2-pixel (2px), 4-pixel (4px), and 6-pixel (6px) lines from top to bottom, respectively.

The Raman data on the prints against the spectra of the cast reference PDMS and octyl acetate are shown in Figure 2b. In both the printed and cast reference PDMS spectra, strong characteristic peaks can be seen at 2904 and 2965 cm^{-1}, indicating CH$_3$ stretching.[41] Other strong PDMS peaks can be seen at 1410 and 1264 cm^{-1}, indicating asymmetric and symmetric CH$_3$ bending.[41] A PDMS peak at 862 cm^{-1} corresponds to symmetric CH$_3$ rocking, whereas a peak at 786 cm^{-1} indicates asymmetric CH$_3$ rocking and asymmetric Si−C stretching. Another characteristic peak of PDMS can be found at 710 cm^{-1}, corresponding to Si−C symmetric stretching. Finally, a peak at 490 cm^{-1} indicates the symmetric stretching of Si−O−Si. These peaks are visible in the spectra of both the ink-jetted PDMS and the reference PDMS. The
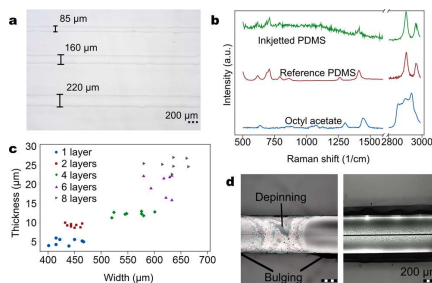
Figure 2. Properties of the printed PDMS. (a) Lines (width: 2 pixels (px), 4 pixels (px), and 6 pixels (px)) on a PDMS substrate, DS 20 μm. (b) Raman spectra of the printed sample (8 layers, DS 20 μm, 120 °C/20 min) against the cast reference PDMS and octyl acetate. (c) Thickness as a function of the pattern width, one to eight layer square patterns printed on the spin-coated PDMS. (d) Left: dielectric ink depinning from the silver surface, direct printing, right: dielectric ink covering the bottom trace, an improved printing strategy.

strong peaks in the octyl acetate spectrum can be found at 2859−2941 cm^{-1}, where a wide peak is shown. Additional peaks are at 637, 660, 1129, 1307, and 1743 cm^{-1}. Even though the background signal adds some noise to the spectrum of the thin printed PDMS sample, none of these octyl acetate's characteristic peaks are clearly visible. Therefore, it can be concluded that the final printed and cured PDMS is free of solvent residues and resembles the cast PDMS. Thus, similar curing conditions as in the traditional casting process can be used.

Printing with the 1:3 PDMS−OA solution led to an approximately 5 μm dry layer thickness, and printing with eight passes led to a 25 μm thickness, when printed on the PDMS substrate (Figure 2c). Ink spreading is well controlled on a hydrophobic PDMS substrate, and when small enough volumes of ink are added on top of the existing layers (Figure 2c: 1 layer and 2 layers), the pattern will not spread and the thickness can be built effectively. When the volume of the wet ink is high enough, the pattern will spread and only a moderate increment in thickness is observed, as shown in Figure 2c with four layers. When more layers are printed, the thickness is again built effectively, but the pattern does not spread significantly (Figure 2c, six layers and eight layers).

On the other hand, printing the PDMS ink on silver was prevented as such due to ink depinning and uncontrolled coalescence (Figure 2d). To control the ink coalescence on the silver surface, the PDMS ink was first printed next to the silver track to form borderlines and to act as contact points. After drying the ink, we filled the enclosed silver surface with the PDMS ink (Figure 2e). Printing five to eight layers of the PDMS resulted in uniform lines, insulating the underlying silver. To ensure the best possible electrical insulation between the conductive tracks, eight-layer PDMS prints were used in further printing trials.

To demonstrate the functionality of the developed PDMS ink, we fabricated a silicone elastomer-based two-layered conductive lattice structure with an electrically insulating PDMS layer. The hydrophobicity of the PDMS surface prevented printing of the Ag NP ink on top of the native PDMS substrate as such. As reported in the literature, it is

necessary to treat the hydrophobic PDMS surface at least with plasma or UV-ozone before coatings can be applied.[42−46] We chose nitrogen plasma for the pretreatment for conductive track printing. Previously, it has been found to enable slower hydrophobic recovery of the treated PDMS in comparison to the oxygen plasma treatment.[46,47] Here, the nitrogen plasma treatment also provided better wetting of the Ag NP ink on the PDMS substrate in comparison to the oxygen plasma. Because the printed PDMS's hydrophobicity was observed to be similar to that of the cast PDMS, an additional plasma treatment was applied to the structure after printing the dielectric layer.

In addition to the ink-wetting challenges, the interface behavior between the PDMS layers and the silver tracks at elevated temperatures proved to be another challenge. The silver tracks tended to wrinkle and crack (Figure 3a−c). This
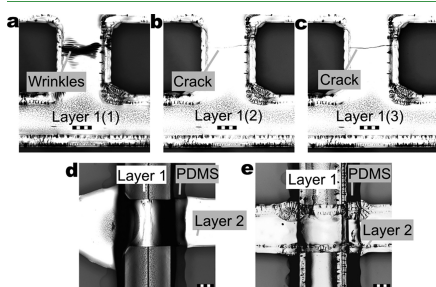
Figure 3. (a) Wrinkling of the bottommost silver track after curing [Layer1 (1)]. (b) Cracking of the wrinkled area after the dielectric printing and curing [Layer 1(2)]. (c) Crack propagation of the previous area after the topmost silver track printing and curing [Layer 1(3)]. (d) Ink flooding into the intersection of the conductive tracks, one printing pass. (e) Well-defined intersection of the conductive tracks, improved patterning strategy. Scale bar 200 μm.

behavior is most likely caused by the mismatch of the material coefficients of thermal expansion (CTE) and the Ag NP densification upon curing.[48−51] Another challenge was the flooding of the Ag NP ink at the intersection of the silver tracks, when the topmost track was printed in one pass (Figure 3d).

The optimized curing conditions for the Ag NP ink (120 °C/30 min) together with an improved printing strategy enabled the fabrication of pristine conductive lines (Figure 3e). We used here a similar patterning strategy as with the PDMS layer: first, we printed the outlines of the conductive tracks, let the print dry and settle, and followed it with pattern filling. This strategy also enabled the printing of well-defined tracks on top of the 3D surface formed by the insulated silver track (Figure 3e).

Once both the surface treatment parameters and printing strategy were optimized, we fabricated the final multilayered lattice structures (Figure 4a,b). The cross-sectional images of the topmost trace (Figure 4d), the intersection of the conductive tracks (Figure 4e−g), and the encapsulated bottommost trace (Figure 4h) show that the thickness of the printed dielectric on the silver surface is approximately 20−25 μm in the middle of the dielectric layer. The cross-sectional images revealed that the thickness of the dielectric was the highest in the center of the line, and was found to decrease
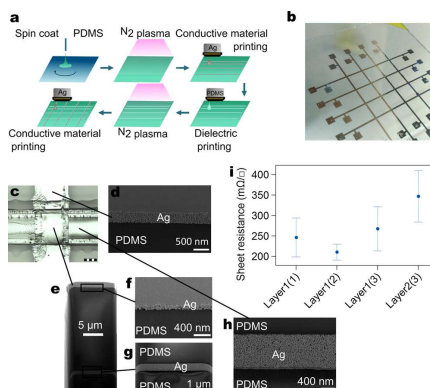
Figure 4. (a) Schematics of the fabrication process. (b) Photograph of the fabricated multilayered structure. (c) Microscopy image of a track intersection. Scale bar 200 μm. (d) Cross-sectional image of the topmost silver layer. (e) Cross-sectional image of the track intersection. (f) Cross-sectional image of the topmost silver layer at the intersection. (g) Cross-sectional image of the bottommost silver layer at the intersection. (h) Cross-sectional image of the bottommost silver layer. (i) Measured sheet resistances of the bottommost silver tracks after silver ink curing [Layer 1(1)], after dielectric curing [Layer 1(2)], and after topmost silver ink curing [Layer 1(3)] and the sheet resistances of the topmost silver tracks after curing [Layer 2(3)]. 24 measurements, confidence interval for the mean is 95 %.

toward the side, where the dielectric thickness was only approximately 10 μm, leading to a dome-like profile. The thickness of the conductive tracks was 500 nm−1 μm at the bottom conductor layer (Figure 4e−h) and 100−500 nm at the top conductor layer (Figure 4d−f). A partial delamination of the bottom silver layer from the substrate was observed in some cross-sectional images (Figure 4g,h). This is suspected to be a combination of the stresses from the cross-section sample fabricated by focused ion beam (FIB) and adhesion issues of the Ag NP−PDMS interface, making it more vulnerable to the stresses caused by the FIB process.

On the other hand, the printed PDMS layer seems to adhere better to the porous Ag NP structure above (Figure 4g,h). This finding is in line with previous literature reports, which suggest that casting the liquid PDMS over conductive Ag structures (NPs, flakes, nanowires, etc.) with a consequent curing step can provide better adherence of the metal layer to the elastomer in comparison to the metal coating of the hard-cured PDMS.[34,35,52−54]

In the resistance measurements, the inevitable degrading effect of the CTE mismatch during the repeated heat-curing steps was observed (Figure 4i). We observed that the annealing of the conductive tracks continues when the dielectric is thermally cured; whereas the sheet resistances of the tracks still continued to decrease. Additionally, the cracking of the tracks starts to affect the measured resistances in a few samples. After the printing and curing of the topmost silver tracks, the resistance increment of the bottommost tracks is more significant due to the crack propagation.

Despite the structural degradation, over 80% of the tracks were still conductive after curing the topmost silver tracks, and

the mean sheet resistance was only 8% higher than the initial value. Out of the 96 measured track intersections, only five short circuits were detected in total. This result confirms the effective electrical insulation ability of the dielectric PDMS ink layer.

The resistances of the topmost silver tracks (Layer 2) tend to be slightly higher, which is most likely due to the thinning of the topmost track in the intersections. As shown in the cross-sectional scanning electron microscopy (SEM) images, the thickness of the topmost track was only 100–400 nm at the intersections (Figure 4f), which not only increases the resistance but also makes it vulnerable to the mechanical stresses. Nevertheless, most measured sheet resistance values were still under 0.3 Ω/□.

Further studies of metal cracking mechanisms would be beneficial because track cracking was observed after the repeated curing steps, even though it was decreased significantly through optimization of both the plasma parameters and ink curing conditions. When the metal NP-based systems are heated, the conductive particles form a dense, sintered structure, enabling very high conductivity at relatively low temperatures, in comparison to a bulk metal. The disadvantage of the sintered nanoscale features is that they are more vulnerable to the thermal and mechanical stresses in comparison to, for example, flake inks, where the particle size is on a macroscale.[55] To improve the stability of our ink-jetted system under stresses, the substrate could be stretched in advance to the printing steps[56] or the pattern geometry could be adjusted.[42,57] A primer layer between the elastomeric substrate and the conductive tracks could enable the deposition of crack-free metal films on PDMS, as shown recently by Ryspayeva et al.[58]

When aiming for stretchable electronics used in, for example, e-skin applications, the conductive interconnects should also be stretchable. Even though the metal tracks in our work are not stretchable as such, several, directly applicable strategies for improved conductor elongation have been presented before. In the work of Xiang et al.,[59] it was shown that the optimization of the adhesion strength of the metal film to the PDMS can improve the stretchability of the devices up to 30%. Additionally, it has been reported in the literature that by simply changing the pattern geometry from a straight line to a horse shoe-like meander line, the stretchability of the inkjet-printed nanoparticle features will increase further by 10%.[60] Recently, Abu-Khalaf et al.[42] showed that inkjet-printed meander lines on PDMS are able to withstand 19% strain, even when a radial stretching load is used. To improve the stretching of the interconnects even further, inkjet printable silver nanowires could be used instead of spherical nanoparticles.[52] Inkjet printing of silver nanowires has been shown to be possible with the Dimatix printers.[61]

Because all of these strategies demonstrate either pattern geometries or materials for inkjet-printed electronics, they are directly applicable to our approach, highlighting the applicability of the proposed multilayered fabrication process. Other compatible functional materials include, but are not limited to, inkjettable graphene, poly(3,4-ethylenedioxythiophene):poly-(styrenesulfonate), and polyvinylidene fluoride–trifluoroethylene.[62,63] These materials can be used to replace metallic conductors or to add sensing functions. Printed PDMS itself has shown interesting performance as a dielectric in, for example, actuators and pressure sensors.[20,21] Therefore, the

proposed multilayer process holds a great promise to the future printed electronics applications.

■ CONCLUSIONS

Herein, an approach for all-inkjet-printed PDMS–based electrical multilayered structures was proposed. Optimization of the solvent type and concentration was shown to have a significant effect on the PDMS printability and the shelf-life of the ink. Herein, the ink cartridge remained functional for at least 2 days, even though the silicone elastomer was mixed in advance with the cartridge filling.

The outcome was an inkjet-printable PDMS solution, which is compatible with the widely used commercial printers. Thus, a single material printer can be used to print all the functional material layers of a soft multilayered electrical system, including both the elastomeric dielectric and other functional material layers, here, the highly conductive Ag NP tracks.

We have shown that not only the fabrication of elastomer-based devices by printing is possible, but also it outstandingly simplifies the fabrication process of multilayered devices, in contrast to the conventional lithography and mold-casting processes used for PDMS patterning, which often require additional equipment, such as punching tools or stencils. Furthermore, the digital nature of inkjet printing enables the fabrication of elastic interconnects simply by modifying the patterning geometries. Therefore, this approach has great potential for any biocompatible or skin-conformable application, where selective additive patterning of silicones is desirable.

■ EXPERIMENTAL METHODS

Silicone Ink Preparation. Sylgard 184 (Dow Corning) was used here both as the substrate and the dielectric material. The PDMS base and the curing agent were mixed in a 10:1 ratio (base to catalyst) in all experiments. The ink solvents were IBA (98%) and octyl acetate (OA, ≥99%) (Sigma-Aldrich). The PDMS was diluted in the solvents at various weight ratios, and the solutions were stirred for 15 min at 1500 rpm before injecting them into the ink cartridges.

Silicone Ink Characterization. The viscosities of the ink components were studied using a rotational rheometer (MCR301, Anton Paar). A concentric cylinder geometry, which is suitable for low-viscosity fluids, was chosen for the measurements. The viscosity of the ink components as a function of shear rate was measured at a constant temperature of 25 °C by increasing the shear rate in logarithmic steps (6 steps/decade) from 1 to 1000 1/s. The effect of the temperature on the viscosity was studied by temperature sweep measurements, where the shear rate was a constant 10 1/s, and the temperature was increased linearly from 25 to 70 °C at a rate of 1 °C/min.

The surface tensions of the ink components were measured by the pendant drop method (Drop Shape Analyzer DSA100, Krüss GmbH). First, ultrapure water was used as a reference substance for all measurements. Surface tensions were measured using the software's Young–Laplace equation for the extracted droplet profile. Measurements were repeated for all the prepared inks.

The composition of the printed and cured elastomer inks was determined using a confocal Raman microscope (532 nm, inVia Qontor, Renishaw). An optical interferometer (Wyko NT1100, Veeco) was used to measure the thickness of the printed silicone ink, when printed on the spin-coated PDMS substrate (Sylgard 184). A thin carbon coating was sputtered onto the surface (JEOL-530, JEOL) to improve the imaging of the otherwise transparent samples.

Device Fabrication. Glass slides were cleaned by ultrasonication in a deionized water bath for 15 min, followed by an acetone bath for 15 min at 50 °C. Then, the samples were placed in a 2-propanol bath for 10 min. Finally, the slides were rinsed with deionized water, dried

with compressed air, and exposed to UV light for 15 min. We then spin-coated the samples (2000 rpm, 60 s) with a 1% (by weight) polytetrafluoroethylene (PTFE) solution in Fluorinert FC-40 (Sigma-Aldrich) and cured the samples at 150 °C for 10 min. Teflon coating was used to enable peeling of the PDMS samples from the glass carrier after the fabrication process was completed.

To fabricate the PDMS substrates, we first spin-coated an approximately 20 μm-thick PDMS layer on a PTFE-coated glass slide (60 s, 1600 rpm) and cured it at 120 °C for 25 min. After that, the substrate was surface-treated with nitrogen plasma (exposure power 100 W, duration 1 min, pressure 0.6 mbar, and gas flow 700 sccm) in a plasma chamber (Diener Atto, Diener electronic GmbH).

We then inkjet-printed the first conductive pattern with an Ag NP ink (Silverjet DGP-10LT-15C, Advanced Nano Products) on the substrate directly after the surface pretreatment with a commercial inkjet printer (Dimatix DMP-2800, Fujifilm). The printer platen temperature was kept at 60 °C to let the inks dry and set before curing in the oven. This two-layer print was then annealed at 120 °C for 30 min, followed by the printing of the PDMS ink on the PDMS substrate and on top of the conductive tracks, sealing the conductors. Up to eight layers of the dielectric ink were printed directly on the underlying surfaces, without any additional surface treatments. The printer platen temperature was again kept at 60 °C to prevent excessive spreading of the wet ink. When all layers had been printed, we used a hot plate to cure the elastomer ink at 120 °C for 20 min, allowing the solvent to evaporate properly and to cross-link the PDMS.

After the dielectric printing, our device was again treated with the nitrogen plasma. To prevent the plasma exposure of the nonsealed measurement pads at both ends of the cured conductive tracks, a polyethylene terephthalate (PET) foil was used as a temporary protective mask during the surface treatment.

Then, we printed an additional set of Ag tracks on top of the PDMS layer. The topmost tracks were printed perpendicular to the first silver layer, thus making the PDMS an electrically insulating layer of the multilayered lattice structure. After that, the whole system was again cured at 120 °C for 30 min to anneal the topmost Ag NPs.

Device Characterization. An optical microscope was used to measure the line widths of the printed PDMS and the silver tracks and to detect the possible cracks. The resistances of the conductive tracks were measured using a 4-wire sensing mode of a source measure unit (Keithley 2425). The sheet resistance of each track was then calculated by dividing the total resistance by the ratio of track length (36 mm) to track width (0.5 mm). These resistance measurements were repeated after printing and curing of (1) the bottommost silver tracks, (2) the dielectric PDMS ink, and (3) the topmost silver tracks. A high-resolution scanning electron microscope with a FIB (Cross-beam 540, Zeiss) was used for the cross-sectional imaging of the devices.

■ ASSOCIATED CONTENT

⑤ Supporting Information

The Supporting Information is available free of charge at https://pubs.acs.org/doi/10.1021/acsami.9b19632.

Calculated Z-numbers for each PDMS ink (PDF)

■ AUTHOR INFORMATION

Corresponding Author

Riikka Mikkonen − Unit of Electrical Engineering, Faculty of Information Technology and Communication Sciences, Tampere University, 33720 Tampere, Finland; ● orcid.org/0000-0003-2961-6821; Email: riikka.mikkonen@tuni.fi

Authors

Paula Puistola − Unit of Electrical Engineering, Faculty of Information Technology and Communication Sciences, Tampere University, 33720 Tampere, Finland

Ilari Jönkkäri − Unit of Materials Science and Environmental Engineering, Faculty of Engineering and Natural Sciences, Tampere University, 33720 Tampere, Finland

Matti Mäntysalo − Unit of Electrical Engineering, Faculty of Information Technology and Communication Sciences, Tampere University, 33720 Tampere, Finland

Complete contact information is available at:
https://pubs.acs.org/10.1021/acsami.9b19632

■ REFERENCES

(1) Kim, J.-H.; Kim, S.-R.; Kil, H.-J.; Kim, Y.-C.; Park, J.-W. Highly Conformable, Transparent Electrodes for Epidermal Electronics. *Nano Lett.* **2018**, *18*, 4531−4540.

(2) Backman, D. E.; LeSavage, B. L.; Shah, S. B.; Wong, J. Y. A Robust Method to Generate Mechanically Anisotropic Vascular Smooth Muscle Cell Sheets for Vascular Tissue Engineering. *Macromol. Biosci.* **2017**, *17*, 1600434.

(3) Drupitha, M. P.; Bankoti, K.; Pal, P.; Das, B.; Parameswar, R.; Dhara, S.; Nando, G. B.; Naskar, K. Morphology-Induced Physico-Mechanical and Biological Characteristics of TPU−PDMS Blend Scaffolds for Skin Tissue Engineering Applications. *J. Biomed. Mater. Res. Part B Appl. Biomater.* **2019**, *107*, 1634−1644.

(4) Shuai, X.; Zhu, P.; Zeng, W.; Hu, Y.; Liang, X.; Zhang, Y.; Sun, R.; Wong, C.-p. Highly Sensitive Flexible Pressure Sensor Based on Silver Nanowires-Embedded Polydimethylsiloxane Electrode with Microarray Structure. *ACS Appl. Mater. Interfaces* **2017**, *9*, 26314−26324.

(5) Qin, D.; Xia, Y.; Whitesides, G. M. Soft Lithography for Micro- and Nanoscale Patterning. *Nat. Protoc.* **2010**, *5*, 491.

(6) Grosberg, A.; Alford, P. W.; McCain, M. L.; Parker, K. K. Ensembles of Engineered Cardiac Tissues for Physiological and Pharmacological Study: Heart on a Chip. *Lab Chip* **2011**, *11*, 4165−4173.

(7) O'Bryan, C. S.; Bhattacharjee, T.; Hart, S.; Kabb, C. P.; Schulze, K. D.; Chilakala, I.; Sumerlin, B. S.; Sawyer, W. G.; Angelini, T. E. Self-Assembled Micro-Organogels for 3D Printing Silicone Structures. *Sci. Adv.* **2017**, *3*, No. e1602800.

(8) Hinton, T. J.; Hudson, A.; Pusch, K.; Lee, A.; Feinberg, A. W. 3D Printing PDMS Elastomer in a Hydrophilic Support Bath via Freeform Reversible Embedding. *ACS Biomater. Sci. Eng.* **2016**, *2*, 1781−1786.

(9) Holländer, J.; Hakala, R.; Suominen, J.; Moritz, N.; Yliruusi, J.; Sandler, N. 3D Printed UV Light Cured Polydimethylsiloxane Devices for Drug Delivery. *Int. J. Pharm.* **2018**, *544*, 433−442.

(10) Ozbolat, V.; Dey, M.; Ayan, B.; Povilianskas, A.; Demirel, M. C.; Ozbolat, I. T. 3D Printing of PDMS Improves Its Mechanical and Cell Adhesion Properties. *ACS Biomater. Sci. Eng.* **2018**, *4*, 682−693.

(11) Patel, D. K.; Sakhaei, A. H.; Layani, M.; Zhang, B.; Ge, Q.; Magdassi, S. Highly Stretchable and UV Curable Elastomers for Digital Light Processing Based 3D Printing. *Adv. Mater.* **2017**, *29*, 1606000.

(12) Abbel, R.; Teunissen, P.; Rubingh, E.; Lammeren, T. v.; Cauchois, R.; Everaars, M.; Valeton, J.; Geijn, S. v. d.; Groen, P. Industrial-Scale Inkjet Printed Electronics Manufacturing-{\textemdash}production up-Scaling from Concept Tools to a Roll-to-Roll Pilot Line. *Transl. Mater. Res.* **2014**, *1*, 015002.

(13) Wu, J.; Wang, R.; Yu, H.; Li, G.; Xu, K.; Tien, N. C.; Roberts, R. C.; Li, D. Inkjet-Printed Microelectrodes on PDMS as Biosensors for Functionalized Microfluidic Systems. *Lab Chip* **2015**, *15*, 690–695.

(14) Sturgess, C.; Tuck, C. J.; Ashcroft, I. A.; Wildman, R. D. 3D Reactive Inkjet Printing of Polydimethylsiloxane. *J. Mater. Chem. C* **2017**, *5*, 9733–9743.

(15) Tavakoli, M.; Malakooti, M. H.; Paisana, H.; Ohm, Y.; Green Marques, D.; Alhais Lopes, P.; Piedade, A. P.; de Almeida, A. T.; Majidi, C. EGaIn-Assisted Room-Temperature Sintering of Silver Nanoparticles for Stretchable, Inkjet-Printed, Thin-Film Electronics. *Adv. Mater.* **2018**, *30*, 1801852.

(16) Gao, M.; Li, L.; Li, W.; Zhou, H.; Song, Y. Direct Writing of Patterned, Lead-Free Nanowire Aligned Flexible Piezoelectric Device. *Adv. Sci.* **2016**, *3*, 1600120.

(17) Thuau, D.; Kallitsis, K.; Dos Santos, F. D.; Hadziioannou, G. All Inkjet-Printed Piezoelectric Electronic Devices: Energy Generators, Sensors and Actuators. *J. Mater. Chem. C* **2017**, *5*, 9963–9966.

(18) Su, M.; Li, F.; Chen, S.; Huang, Z.; Qin, M.; Li, W.; Zhang, X.; Song, Y. Nanoparticle Based Curve Arrays for Multirecognition Flexible Electronics. *Adv. Mater.* **2016**, *28*, 1369–1374.

(19) Wang, S.; Xu, J.; Wang, W.; Wang, G.-J. N.; Rastak, R.; Molina-Lopez, F.; Chung, J. W.; Niu, S.; Feig, V. R.; Lopez, J.; Lei, T.; Kwon, S.-K.; Kim, Y.; Foudeh, A. M.; Ehrlich, A.; Gasperini, A.; Yun, Y.; Murmann, B.; Tok, J. B.-H.; Bao, Z. Skin Electronics from Scalable Fabrication of an Intrinsically Stretchable Transistor Array. *Nature* **2018**, *555*, 83.

(20) McCoul, D.; Rosset, S.; Schlatter, S.; Shea, H. Inkjet 3D Printing of UV and Thermal Cure Silicone Elastomers for Dielectric Elastomer Actuators. *Smart Mater. Struct.* **2017**, *26*, 125022.

(21) Peng, Y.; Xiao, S.; Yang, J.; Lin, J.; Yuan, W.; Gu, W.; Wu, X.; Cui, Z. The Elastic Microstructures of Inkjet Printed Polydimethylsiloxane as the Patterned Dielectric Layer for Pressure Sensors. *Appl. Phys. Lett.* **2017**, *110*, 261904.

(22) Lopes, P. A.; Paisana, H.; De Almeida, A. T.; Majidi, C.; Tavakoli, M. Hydroprinted Electronics: Ultrathin Stretchable Ag–In–Ga E-Skin for Bioelectronics and Human–Machine Interaction. *ACS Appl. Mater. Interfaces* **2018**, *10*, 38760–38768.

(23) Mohammed, M. G.; Kramer, R. All-Printed Flexible and Stretchable Electronics. *Adv. Mater.* **2017**, *29*, 1604965.

(24) Kong, Y. L.; Tamargo, I. A.; Kim, H.; Johnson, B. N.; Gupta, M. K.; Koh, T.-W.; Chin, H.-A.; Steingart, D. A.; Rand, B. P.; McAlpine, M. C. 3D Printed Quantum Dot Light-Emitting Diodes. *Nano Lett.* **2014**, *14*, 7017–7023.

(25) Wang, C.; Sim, K.; Chen, J.; Kim, H.; Rao, Z.; Li, Y.; Chen, W.; Song, J.; Verduzco, R.; Yu, C. Soft Ultrathin Electronics Innervated Adaptive Fully Soft Robots. *Adv. Mater.* **2018**, *30*, 1706695.

(26) Markvicka, E. J.; Bartlett, M. D.; Huang, X.; Majidi, C. An Autonomously Electrically Self-Healing Liquid Metal–Elastomer Composite for Robust Soft-Matter Robotics and Electronics. *Nat. Mater.* **2018**, *17*, 618–624.

(27) You, I.; Kong, M.; Jeong, U. Block Copolymer Elastomers for Stretchable Electronics. *Acc. Chem. Res.* **2019**, *52*, 63–72.

(28) Mamidanna, A.; Lefky, C.; Hildreth, O. Drop-on-Demand Printed Microfluidics Device with Sensing Electrodes Using Silver and PDMS Reactive Inks. *Microfluid. Nanofluid.* **2017**, *21*, 1–9.

(29) Lee, J.; Kim, J.; Park, J.; Lee, C. Characterization of in Situ Sintering of Silver Nanoparticles on Commercial Photo Papers in Inkjet Printing. *Flexible Printed Electron.* **2018**, *3*, 025001.

(30) Su, W.; Cook, B. S.; Fang, Y.; Tentzeris, M. M. Fully Inkjet-Printed Microfluidics: A Solution to Low-Cost Rapid Three-Dimensional Microfluidics Fabrication with Numerous Electrical and Sensing Applications. *Sci. Rep.* **2016**, *6*, 35111.

(31) Angelo, P. D.; Farnood, R. R. Photoluminescent Inkjet Ink Containing ZnS:Mn Nanoparticles as Pigment. *J. Exp. Nanosci.* **2011**, *6*, 473–487.

(32) Wang, Y.; Zhu, C.; Pfattner, R.; Yan, H.; Jin, L.; Chen, S.; Molina-Lopez, F.; Lissel, F.; Liu, J.; Rabiah, N. I.; Chen, Z.; Chung, J. W.; Linder, C.; Toney, M. F.; Murmann, B.; Bao, Z. A Highly Stretchable, Transparent, and Conductive Polymer. *Sci. Adv.* **2017**, *3*, No. e1602076.

(33) Grubb, P. M.; Subbaraman, H.; Park, S.; Akinwande, D.; Chen, R. T. Inkjet Printing of High Performance Transistors with Micron Order Chemically Set Gaps. *Sci. Rep.* **2017**, *7*, 1202.

(34) Huang, Q.; Al-Milaji, K. N.; Zhao, H. Inkjet Printing of Silver Nanowires for Stretchable Heaters. *ACS Appl. Nano Mater.* **2018**, *1*, 4528–4536.

(35) Sun, J.; Jiang, J.; Bao, B.; Wang, S.; He, M.; Zhang, X.; Song, Y. Fabrication of Bendable Circuits on a Polydimethylsiloxane (PDMS) Surface by Inkjet Printing Semi-Wrapped Structures. *Materials* **2016**, *9*, 253.

(36) Woo, K.; Jang, D.; Kim, Y.; Moon, J. Relationship between Printability and Rheological Behavior of Ink-Jet Conductive Inks. *Ceram. Int.* **2013**, *39*, 7015–7021.

(37) Reis, N.; Ainsley, C.; Derby, B. Ink-Jet Delivery of Particle Suspensions by Piezoelectric Droplet Ejectors. *J. Appl. Phys.* **2005**, *97*, 094903.

(38) de Gans, B.-J.; Kazancioglu, E.; Meyer, W.; Schubert, U. S. Ink-Jet Printing Polymers and Polymer Libraries Using Micropipettes. *Macromol. Rapid Commun.* **2004**, *25*, 292–296.

(39) de Gans, B.-J.; Duineveld, P. C.; Schubert, U. S. Inkjet Printing of Polymers: State of the Art and Future Developments. *Adv. Mater.* **2004**, *16*, 203–213.

(40) Tekin, E.; Smith, P. J.; Schubert, U. S. Inkjet Printing as a Deposition and Patterning Tool for Polymers and Inorganic Particles. *Soft Matter* **2008**, *4*, 703–713.

(41) Bae, S. C.; Lee, H.; Lin, Z.; Granick, S. Chemical Imaging in a Surface Forces Apparatus: Confocal Raman Spectroscopy of Confined Poly(Dimethylsiloxane). *Langmuir* **2005**, *21*, 5685–5688.

(42) Abu-Khalaf, J.; Al-Ghussain, L.; Al-Halhouli, A. a. Fabrication of Stretchable Circuits on Polydimethylsiloxane (PDMS) Pre-Stretched Substrates by Inkjet Printing Silver Nanoparticles. *Materials* **2018**, *11*, 2377.

(43) Belsey, K. E.; Parry, A. V. S.; Rumens, C. V.; Ziai, M. A.; Yeates, S. G.; Batchelor, J. C.; Holder, S. J. Switchable Disposable Passive RFID Vapour Sensors from Inkjet Printed Electronic Components Integrated with PDMS as a Stimulus Responsive. *J. Mater. Chem. C* **2017**, *5*, 3167–3175.

(44) Ko, E.-H.; Kim, H.-J.; Lee, S.-M.; Kim, T.-W.; Kim, H.-K. Stretchable Ag Electrodes with Mechanically Tunable Optical Transmittance on Wavy-Patterned PDMS Substrates. *Sci. Rep.* **2017**, *7*, 46739.

(45) Hemmilä, S.; Cauich-Rodríguez, J. V.; Kreutzer, J.; Kallio, P. Rapid, Simple, and Cost-Effective Treatments to Achieve Long-Term Hydrophilic PDMS Surfaces. *Appl. Surf. Sci.* **2012**, *258*, 9864–9875.

(46) Li, C.-Y.; Liao, Y.-C. Adhesive Stretchable Printed Conductive Thin Film Patterns on PDMS Surface with an Atmospheric Plasma Treatment. *ACS Appl. Mater. Interfaces* **2016**, *8*, 11868–11874.

(47) Jokinen, V.; Suvanto, P.; Franssila, S. Oxygen and Nitrogen Plasma Hydrophilization and Hydrophobic Recovery of Polymers. *Biomicrofluidics* **2012**, *6*, 016501.

(48) Kim, Y.; Ren, X.; Kim, J. W.; Noh, H. Direct Inkjet Printing of Micro-Scale Silver Electrodes on Polydimethylsiloxane (PDMS) Microchip. *J. Micromech. Microeng.* **2014**, *24*, 115010.

(49) Moon, K.-S.; Dong, H.; Maric, R.; Pothukuchi, S.; Hunt, A.; Wong, C. P. Thermal Behavior of Silver Nanoparticles for Low-Temperature Interconnect Applications. *J. Electron. Mater.* **2005**, *34*, 168–175.

(50) Li, J.-H.; Jang, K.-L.; Ahn, K.; Yoon, T.; Lee, T.-I.; Kim, T.-S. Thermal Expansion Behavior of Thin Films Expanding Freely on Water Surface. *Sci. Rep.* **2019**, *9*, 7071.

(51) Greer, J. R.; Street, R. A. Thermal Cure Effects on Electrical Performance of Nanoparticle Silver Inks. *Acta Mater.* **2007**, *55*, 6345−6349.

(52) Amjadi, M.; Pichitpajongkit, A.; Lee, S.; Ryu, S.; Park, I. Highly Stretchable and Sensitive Strain Sensor Based on Silver Nanowire−Elastomer Nanocomposite. *ACS Nano* **2014**, *8*, 5154−5163.

(53) Huang, G.-W.; Xiao, H.-M.; Fu, S.-Y. Wearable Electronics of Silver-Nanowire/Poly(Dimethylsiloxane) Nanocomposite for Smart Clothing. *Sci. Rep.* **2015**, *5*, 13971.

(54) Hilbich, D.; Gray, B. L.; Shannon, L. A Low-Cost, Micropattern Transfer Process for Thick-Film Metallization of PDMS. *J. Electrochem. Soc.* **2017**, *164*, B3067−B3076.

(55) Cronin, H. M.; Stoeva, Z.; Brown, M.; Shkunov, M.; Silva, S. R. P. Photonic Curing of Low-Cost Aqueous Silver Flake Inks for Printed Conductors with Increased Yield. *ACS Appl. Mater. Interfaces* **2018**, *10*, 21398−21410.

(56) Lee, J.; Chung, S.; Song, H.; Kim, S.; Hong, Y. Lateral-Crack-Free, Buckled, Inkjet-Printed Silver Electrodes on Highly Pre-Stretched Elastomeric Substrates. *J. Phys. D: Appl. Phys.* **2013**, *46*, 105305.

(57) Fan, J. A.; Yeo, W.-H.; Su, Y.; Hattori, Y.; Lee, W.; Jung, S.-Y.; Zhang, Y.; Liu, Z.; Cheng, H.; Falgout, L.; Bajema, M.; Coleman, T.; Gregoire, D.; Larsen, R. J.; Huang, Y.; Rogers, J. A. Fractal Design Concepts for Stretchable Electronics. *Nat. Commun.* **2014**, *5*, 3266.

(58) Ryspayeva, A.; Jones, T. D. A.; Esfahani, M. N.; Shuttleworth, M. P.; Harris, R. A.; Kay, R. W.; Desmulliez, M. P. Y.; Marques-Hueso, J. A Rapid Technique for the Direct Metallization of PDMS Substrates for Flexible and Stretchable Electronics Applications. *Microelectron. Eng.* **2019**, *209*, 35−40.

(59) Xiang, Y.; Li, T.; Suo, Z.; Vlassak, J. J. High Ductility of a Metal Film Adherent on a Polymer Substrate. *Appl. Phys. Lett.* **2005**, *87*, 161910.

(60) Jablonski, M.; Lucchini, R.; Bossuyt, F.; Vervust, T.; Vanfleteren, J.; De Vries, J. W. C.; Vena, P.; Gonzalez, M. Impact of Geometry on Stretchable Meandered Interconnect Uniaxial Tensile Extension Fatigue Reliability. *Microelectron. Reliab.* **2015**, *55*, 143−154.

(61) Finn, D. J.; Lotya, M.; Coleman, J. N. Inkjet Printing of Silver Nanowire Networks. *ACS Appl. Mater. Interfaces* **2015**, *7*, 9254−9261.

(62) Vuorinen, T.; Niittynen, J.; Kankkunen, T.; Kraft, T. M.; Mäntysalo, M. Inkjet-Printed Graphene/PEDOT:PSS Temperature Sensors on a Skin-Conformable Polyurethane Substrate. *Sci. Rep.* **2016**, *6*, 35289.

(63) Haque, R. I.; Vié, R.; Germainy, M.; Valbin, L.; Benaben, P.; Boddaert, X. Inkjet Printing of High Molecular Weight PVDF-TrFE for Flexible Electronics. *Flexible Printed Electron.* **2015**, *1*, 015001.

PUBLICATION
IV

Inkjettable, polydimethylsiloxane based soft electronics

R. Mikkonen, M. Mäntysalo

Inkjettable, polydimethylsiloxane based soft electronics

Riikka Mikkonen
Faculty of Information Technology and Communication
Sciences
Tampere University
Tampere, Finland
riikka.mikkonen@tuni.fi

Matti Mäntysalo
Faculty of Information Technology and Communication
Sciences
Tampere University
Tampere, Finland
matti.mantysalo@tuni.fi

Abstract— In this paper, we report our recent work with an inkjettable polydimethylsiloxane (PDMS) solution, which is intended for multilayer printing of soft electronics. Here, we present optimized printing parameters for the PDMS ink, and the surface treatment modification methods of PDMS for conductive track printing are discussed in further detail. In this paper, processing parameters are described for successful multilayer printing of soft electronics, such as sensors.

Keywords—PDMS, inkjet printing, soft electronics

I. INTRODUCTION

PDMS is known as an inexpensive, optically transparent and biocompatible soft elastomer. For these reasons, it is widely used in applications like tissue mimicking, electronic skin (e-skin) and microfluidics [1-3]. Unfortunately, the traditional manufacturing methods (lithography, mold casting) make PDMS fabrication both time-consuming and inconvenient. Therefore, approaches for additive manufacturing of PDMS have been presented in the recent years [4-6].

An example of additive manufacturing methods is inkjet printing. This digital technique is already utilized in the printed electronics fabrication, where it can be used to build soft, large area flexible and stretchable electronics, such as piezoelectric devices, and skin-conformable systems [7,8]. Combining inkjet printing of soft materials with other jettable materials would simplify building of these complex devices, when less process steps are required.

Earlier, we presented an approach for multilayer printing of PDMS based soft electronics [9]. This paper reports our recent work with the printed PDMS. In addition to PDMS jetting parameters, alternative surface modification methods of PDMS for silver printing were studied.

II. MATERIALS & METHODS

A. inkjettable PDMS

Here, a two-component PDMS (Sylgard 184, Dow) was used in a 1:10 ratio (catalyst to base). To create a jettable solution, it was mixed in a 1:3 ratio with octyl acetate. The details of the solvent selection have been discussed in [9]. The solution was stirred for 15 min at 1500 rpm before injecting it to an ink cartridge. A Dimatix DMP 2800 inkjet printer was used to print the PDMS ink solution, using 10 pl-volume liquid crystal polymer (LCP) cartridges. The ink was cured at 120 ºC temperature for 25 min.

B. PDMS surface treatments

Spin coated (1600 rpm, 60 s), 20 µm thick Sylgard 184 (1:10 ratio) layers were used as substrates for silver printing. The PDMS surface was treated before silver printing with several surface modification methods: First, with a flame-pyrolytic surface silicating method (NanoFlame, Polytec PT GmbH), where a thin silicon oxide layer is formed on the substrate surface. The precursor particles are separated thermally, dividing the tool's flame to a reducing inner part, and an oxidizing outer part.

Another method was a chemical modification with a (3-mercaptopropyl)trimethoxysilane (MPTMS) solution that was spin coated on a plasma treated PDMS surface (1600 rpm, 2 min) and baked for 30 min at 120 ºC. These methods were compared to the nitrogen plasma modification (Diener Atto, Diener Electronic GmbH) reported in [9].

C. Conductor printing

An inkjettable silver nanoparticle (Ag np) ink (Silverjet DGP-40LT-15C, Advanced Nano Products Co., Ltd.) was used to print the conductive tracks with the Dimatix printer. A 10 pl standard DMP cartridge was used. The cartridge temperature was 40 ºC, and the substrate temperature was kept at 60 ºC. After printing, all samples were cured at 120 ºC for 30 minutes.

III. RESULTS

A. PDMS printing

As discussed already in [9], it is necessary to minimize the temperature during PDMS printing. Lower temperature will help to prevent elastomer crosslinking and thus, to increase the cartridge's shelf life. Here, we studied the printing parameters further.

It was concluded that a waveform, where a strong and long firing pulse is used, improved ink jetting significantly from the previous results. This waveform shape is typical for high viscosity inks, and it was clearly enhancing the jetting stability, when the cartridge was used on several days in a row, in comparison to other waveforms. The nozzles could be kept firing by simply elevating the cartridge temperature by a few degrees at the time. Thus, small temperature increments allow printing for several days, if the cartridge is stored in a refrigerator overnight. summary of the printing parameters for the PDMS ink is given in Table I.

Test substrates with each surface treatment were prepared for Ag np inkjet printing. A summary of the optimized treatment parameters is given in Table II. The alternative treatments were studied and compared to the nitrogen plasma, as it has been reported that the plasma treatment may not provide a permanent surface modification of PDMS, causing it to recover its native hydrophobicity over time, even though differences between plasma gases have been reported [10].

Parameter	Value
Substrate temperature	60 ºC
Cartridge temperature	30 ºC (elevated over time)
Max. jetting frequency	2.0 kHz
Jetting pulse duration	69.76 µs
Firing voltage	24 V
Firing pulse level	100 %
Slew rate	0.54 (Rising and falling edge)
Non-jetting time	89.024 µs

TABLE II.   SURFACE TREATMENT SPECIFICATIONS

Method	Specifications
Nitrogen plasma	Exposure power: 100 W, time: 1 min, chamber pressure 0.6 mbar, gas flow 700 sccm [1]
MPTMS	A 6 % solution in ethanol, spin coat for 2 min at 1600 rpm on plasma treated PDMS, bake for 30 min at 120 ºC
Pyrolytic coating	Treat substrate with a steady back-and-forth movement for 4 times

B. Surface treatments and Ag np printing

Once the substrates had been prepared, the printing trials were started by drop matrix printing, to determine the suitable drop spacing for each ink-substrate combination. When the drop spacings were calculated from the droplet diameters, we tried line printing on each substrate. Smooth, well-defined lines could be printed on the nitrogen plasma-treated substrate (Fig 1b), whereas the line prints on both PDMS with pyrolytic coating, and MPTMS-coated PDMS had rougher edges (Fig. 1d & Fig. 1f).

The MPTMS-coated PDMS was observed to be rough, and it seems that the substrate's surface roughness affects the print quality on this substrate. Kirikova et al found in [11] that this treatment type is well suited as an ink primer for improved wetting and adhesion of screen printed silver patterns on PDMS. Since the inkjet printed lines tend to be an order of magnitude thinner than the screen printed lines, it is likely that the Ag np ink is more sensitive to the variations in the surface roughness.

In addition to the wetting experiments, we did a simple peeling test of the printed lines with each ink-substrate combination using a scotch tape. Some ink was removed from the nitrogen plasma- and MPTMS-treated samples, but the samples with the pyrolytic coating could withstand these peeling tests outstandingly (Fig. 2).
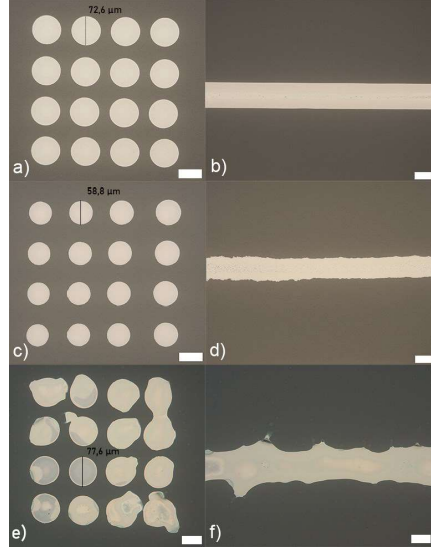
Fig. 1. a) A drop matrix on plasma treated PDMS, b) a line on plasma treated PDMS, c) A drop matrix on PDMS with pyrolytic coating, d) a line on PDMS with pyrolytic coating, d) a drop matrix on MPTMS-coated PDMS, d) A line on MPTMS-coated PDMS. Scale bar: 50 µm.
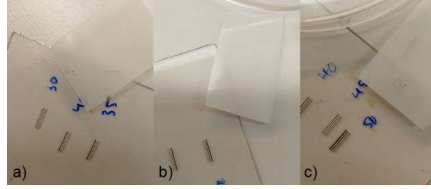

Fig. 2. Peeling test results of Ag np ink on a) plasma treated PDMS, b) PDMS with pyrolytic coating, c) MPTMS-coated PDMS.

Based on the results of line printing trials and peeling tests, the pyrolytic coating was selected for the multilayer printing experiments. The process flow for the multilayer printing is illustrated in Fig. 3. First, the PDMS substrate is modified with the chosen surface treatment method. Secondly, a layer of conductive tracks is printed with the Ag np ink, followed by the elastomeric dielectric printing. After that, the PDMS surface is modified again, including the printed elastomer. Then, the second layer of conductive tracks is printed. Each layer is cured after printing.

In comparison to the previously used, nitrogen plasma-based process, a pyrolytic coating process is both faster and simpler, since only a handheld tool and gas refill are required. On the other hand, since this treatment is more dependent on the user, it is harder to achieve a repeatable surface modification process. For example, the distance of the flame to the sample may vary between samples, and the treatment time is hard to control with the manual back-and-forth movement.

However, we managed to fabricate similar 2-layer structures as before in [9] with the nitrogen plasma, as illustrated in Fig. 4. Furthermore, we observed that despite the challenges with the pyrolytic coating stability, less cracks and wrinkling of the conductive tracks were observed than before, when the treatment was successful (Fig. 4). This is assumed to be due to the silicon oxide layer that is formed on the PDMS surface, protecting the underlying elastomer from the chemical exposure and making it more stable during the thermal curing phase.
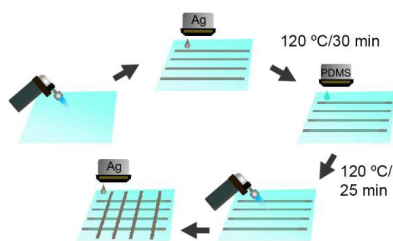
Fig. 3. Process flow of PDMS based multilayer printing.
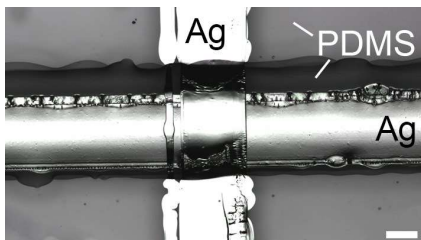
Fig. 4. A multilayer print on PDMS with pyrolytic coating, including two layers of conductive tracks, and a printed PDMS layer as a dielectric between them. Scale bar: 200 µm.
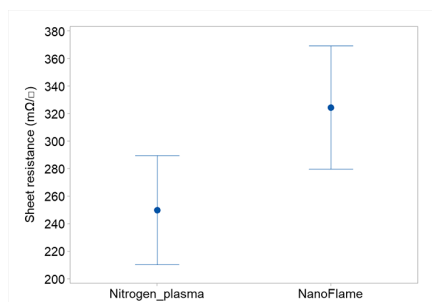
Fig. 5. The measured sheet resistances of the nitrogen plasma samples and the samples with pyrolytic coating (NanoFlame). 16 measurements, confidence interval for the mean is 95 %. The nitrogen plasma results are adapted from [9].

To compare the electrical properties of the samples with the previous results from [9], the sheet resistances of the samples were measured. The results are illustrated in Fig. 5. The measured sheet resistances of the samples with the pyrolytic coating were approximately 40 % higher than the previous results. Still, the sheet resistances are well below 0.5 $\Omega/\square$.

IV. Conclusions

In this paper, we reported our recent work towards all inkjet printed, PDMS based soft electronics. Here, PDMS jetting parameters were discussed, and alternative surface treatments for plasma were studied. The results show that a silicon oxide layer, which can be formed on the PDMS surface by a straightforward and fast, flame pyrolytic silicating method, improves the adhesion of the conductive inks significantly in comparison to the previously used plasma treatment.

Our process is designed for the widely used Dimatix material printers, and thus, the results are readily applicable. Therefore, these findings could be used in electronics manufacturing to build, for example, soft sensors and other complex devices, where multilayer printing of more than one material is required, in order to achieve the desired functionalities.

References

[1] J.-H. Kim, S.-R. Kim, H.-J. Kil, Y.-C. Kim, J.-W. Park, "Highly conformable, transparent electrodes for epidermal electronics", Nano Lett. 2018, vol. 18, pp. 4531–4540.

[2] D. E. Backman, B. L. LeSavage, S. B. Shah, and J. Y. Wong, "A robust method to generate mechanically anisotropic vascular smooth muscle cell sheets for vascular tissue engineering", Macromol. Biosci., 2017, 17, 1600434.

[3] M.P. Drupitha et al, "Morphology-induced physico-mechanical and biological characteristics of TPU–PDMS blend scaffolds for skin tissue engineering applications", J. Biomed. Mater. Res. Part B Appl. Biomater., 2019, 107, pp. 1634–1644.

[4] C.S. O'Bryan, et al, "Self-assembled micro-organogels for 3D printing silicone structures", Sci. Adv. 2017, 3, e1602800.

[5] V. Ozbolat, M. Dey, B. Ayan, A. Povilianskas, M. C. Demirel, and I. T. Ozbolat, "3D printing of PDMS improves its mechanical and cell adhesion properties", ACS Biomater. Sci. Eng. 2018, 4, pp. 682–693.

[6] C. Sturgess, C. J. Tuck, I. A. Ashcroft, and R. D. Wildman, "3D reactive inkjet printing of polydimethylsiloxane", J. Mater. Chem. C., 2017, 5, pp. 9733–9745.

[7] D. Thuau, K. Kallitsis, F. D. Dos Santos, and G. Hadziioannou, "All inkjet-printed piezoelectric electronic devices: energy generators, sensors and actuators" J. Mater. Chem. C., 2017, 5, pp. 9963–9966.

[8] S. Wang et al, "Skin electronics from scalable fabrication of an intrinsically stretchable transistor array" Nature, 2018, vol. 555, 83.

[9] R. Mikkonen, P. Puistola, I. Jönkkäri, and M. Mäntysalo, "Inkjet printable polydimethylsiloxane for all-inkjet-printed multilayered soft electrical applications", ACS Appl. Mater. Interfaces, 2020, vol. 12, pp. 11990-11997.

[10] V. Jokinen, P. Suvanto, and S. Franssila, "Oxygen and nitrogen plasma hydrophilization and hydrophobic recovery of polymers", Biomicrofluidics, 2012, vol 6, 016501.

[11] M. N. Kirikova et al, "Direct-write printing of reactive oligomericalkoxysilanes as an affordable and highly efficientroute for promoting local adhesion of silver inks polymer substrates", J. Mater. Chem. C., 2016, vol 4, pp. 2211-2218.

PUBLICATION
V

Inkjet-printed, nanofiber-based soft capacitive pressure sensors for tactile sensing

R. Mikkonen, A. Koivikko, T. Vuorinen, V. Sariola, M. Mäntysalo

IEEE Sensors Council

Inkjet-Printed, Nanofiber-Based Soft Capacitive Pressure Sensors for Tactile Sensing

Riikka Mikkonen, Anastasia Koivikko, Tiina Vuorinen, Veikko Sariola, *Member, IEEE*,
and Matti Mäntysalo, *Member, IEEE*

Abstract—The development of soft electronics is critical to the realization of artificial intelligence that comes into direct contact with humans, such as wearable devices, and robotics. Furthermore, rapid prototyping and inexpensive processes are essential for the development of these applications. We demonstrate here an additive, low-cost method for fabricating polydimethylsiloxane based soft electronics by inkjet printing. Herein, a novel approach using a water-soluble polyvinyl alcohol layer as the substrate, inexpensive, fully digital fabrication of capacitive pressure sensors is enabled by sandwiching mesh-like conductive layers and microstructured dielectric in a straightforward, convenient manner. These sensors exhibit improved sensitivity (4 MPa^{-1}) at low

pressures (<1 kPa) in contrast to sensors with a flat elastomer dielectric and can still detect large pressures around 50 kPa, having excellent long-term repeatability over 2000 cycles, without significant hysteresis (≤8.5 %). The tactile sensing ability of the fabricated devices was demonstrated in a practical application. Moreover, sensor characteristics are easily adjustable, simply by changing printing parameters or tuning the ink solution. The proposed approach provides scalable solution for fabricating high-sensitivity printed sensors for e-skin and human-machine interfaces.

Index Terms—Polydimethylsiloxane, capacitive pressure sensor, inkjet printing, printed electronics, soft electronics, polyvinyl alcohol.
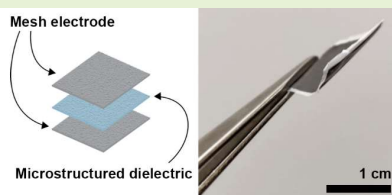
I. INTRODUCTION

SOFT and flexible electronics have been of interest in the recent years for their promising applications in human-machine interfaces, skin prosthetics, soft robotics, and wearable electronics [1]–[6]. These devices should be both flexible and lightweight. Additionally, high sensitivity, robustness and ease of fabrication are desirable characteristics for soft electronics.

In the skin-like electronics and other wearable applications, pressure sensing is one important function. Typical pressure sensors are often capacitive [7], piezoresistive [8], piezoelectric [9] or triboelectric [10]. The capacitive sensors are a popular choice for their structural simplicity, ease of fabrication, tunability and low power consumption [11]–[13]. A typical structure of the capacitive-type soft sensor consists of a dielectric layer, typically an elastomer, sandwiched between two flexible electrodes. Such sensors are essentially plate capacitors, and thus their performance is heavily influenced by choice of the dielectric material. Therefore, great attention has been paid to the dielectric characteristics.

Among elastic materials, soft silicone elastomers, especially polydimethylsiloxane (PDMS) is an interesting option for many wearable applications for being inexpensive, transparent, inert, biocompatible with human tissues and mechanically resilient [14]–[17]. Furthermore, PDMS properties can be tuned simply by changing the cross-linking ratio of the prepolymer and the curing agent; a low cross-linking density makes the elastomer more gel-like, whereas the elastic properties are more dominant with a higher cross-linking density. However, it has been shown that the viscoelastic characteristics of the soft elastomer also might have a significant effect on, for example, the hysteresis and sensitivity of soft sensors [18].

Dielectric layers with microstructures, such as pores and pyramids, have been used to improve the sensitivity and to

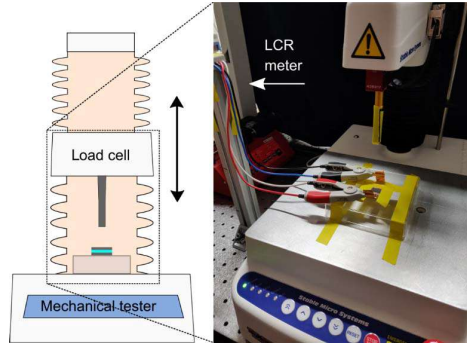Fig. 1. Schematic illustration of sensor fabrication process.

Fig. 2. Experimental setup for measuring the change in capacitance in response to applied pressure, including a schematic illustration of the sample placed to a mechanical tester, together with a photograph of a sample attached to the tester and connected to the LCR meter.
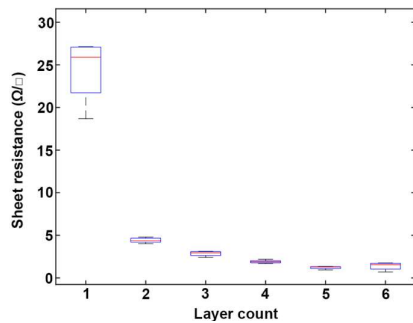

Fig. 3. Sheet resistances of the Ag NP prints as a function of layer count. Boxplot is showing the interquartile range of 5 measurements, and the whiskers show the whole range of the measured values.

reduce hysteresis of the sensor, because these microstructures may be more easily compressed than flat films [14], [19]–[23]. Many such microstructures are fabricated by using lithographic methods, in which cumbersome, time-consuming processes and hazardous chemicals are used [13], [20], [21].

To address these issues, additive fabrication techniques, like printing technologies have been used [7], [24]–[26]. Printed electronics have attracted increasing attention in recent years as an alternative to conventional microfabrication technologies to realize a range of low-cost, large-area, and flexible functional devices. Especially the fully additive methods, such as inkjet printing, offer mask-free, cost-effective, and digital methods to fabricate functional patterns in large scale, in comparison with other methods used to assemble material layers into electronic devices, such as spin-coating and lithographic patterning [27]–[29].

In this work, we report a facile method for fabricating fully printed, elastomeric capacitive sensors with high flexibility and great sensitivity at a wide pressure range. Earlier, we developed an inkjet printable PDMS solution for multilayer printing of soft electronics [30], and the process was further studied in [31]. However, challenges remained in the realization of uniform conductive layer with good adhesion on top of the printed PDMS layer in these studies. In addition, fabrication of self-standing printed PDMS layers, or the options for transferring the printed structures to the target substrate were not addressed before.

Here, we have solved these issues by using water-soluble, electrospun polyvinyl alcohol (PVA) fibers both as a temporary carrier and a functional layer, to realize fully inkjet printed tactile pressure sensors. It has been shown earlier that this material can be used to improve not only the mechanical strength and elasticity of soft, skin-like electronics, but also skin-mountability and wear comfort [32]–[34].

We fabricated conductive mesh electrodes by inkjet printing silver nanoparticles (Ag NP) on PVA, while a dielectric layer, consisting of a PVA mesh layer embedded in an inkjet printed PDMS layer, was placed between the mesh electrodes to form a capacitive tactile pressure sensor. Two different PDMS cross-linking densities were used to compare the impact of

the viscoelasticity on the sensor performance. These printed sensors were characterized in comparison to reference sensors with conventional, spin-coated dielectric layers.

II. MATERIALS AND METHODS

A. Sensor Fabrication Process

1) The PVA-Layer: PVA solution was prepared by dissolving PVA granules in deionized (DI) water. The used PVA material had molecular weight of 47000 with a degree of hydrolysis of 98.0 – 98.8 mol% (Fluka, Germany). Then, the PVA-layer was electrospun using KDS 100 syringe infusion pump (kdScientific, USA) together with Chargemaster high voltage supply (SIMCO, USA). Electrospinning was done with 2 ml/h feeding speed and 25 cm distance and 25 kV voltage between the needle and the substrate.

2) Inkjet-Printing of the Mesh Electrodes: The PVA layer was carefully peeled from the electrospinning substrate and placed on a hydrophobic ethylene tetrafluoroethylene (ETFE)-substrate (Novoflon ET 6235 EZ, NOVOFOL Kunststoffprodukte GmbH & Co, Germany). Ag NP ink (DGP 40LT-15C, Advanced Nanoproducts, Korea) was used for
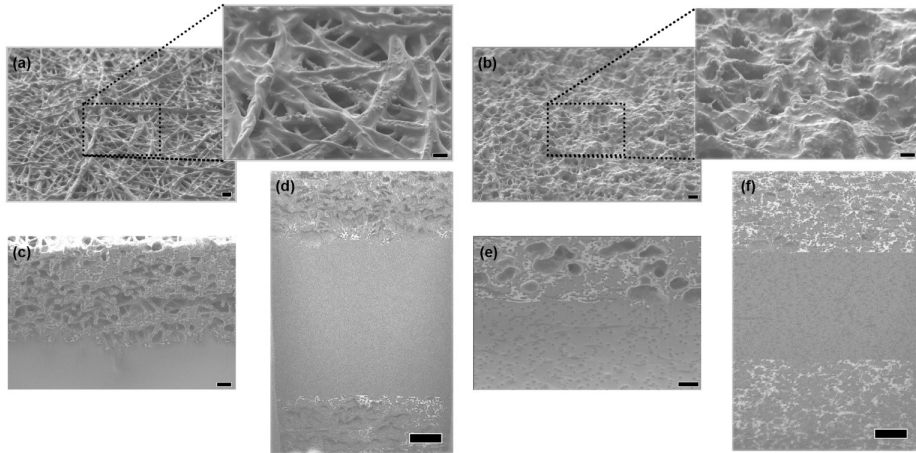
Fig. 4. SEM-images of the fabricated sensors showing (a) the surface of the reference sensor's mesh electrode, scale bar 1 μm (inset 500 nm), (b) surface of the printed sensor's mesh electrode, scale bar 1 μm (inset 500 nm), (c) interface between the reference sensor's electrode and the spin-coated dielectric, scale bar 1 μm, (d) cross-section of the reference sensor: the spin-coated dielectric is sandwiched between the electrodes, scale bar 3 μm (e) interface between the printed sensor's electrode and the printed PVA-PDMS dielectric, scale bar 1 μm, (f) cross-section of the printed sensor: the printed PVA-PDMS dielectric is sandwiched between the electrodes, scale bar 3 μm.

inkjet printing the electrode pattern on the PVA mesh with a Dimatix DMP-2831 material printer (Fujifilm, USA). After printing, the electrodes were thermally cured at 120 °C for 60 min.

3) Inkjet Printing of the PDMS Dielectric: The sensor dielectric was fabricated by inkjet printing PDMS onto the PVA mesh. Sylgard 184 (Dow, USA) was selected as the dielectric material since its printability has been demonstrated in our earlier work [30]. Here, two cross-linking densities of the PDMS were used: stiffer (1:10), and softer (1:20) (curing agent to base-ratio). The PDMS was diluted in octyl acetate in a 1:3 weight ratio to allow printing without cartridge heating using the Dimatix DMP-2831 material printer. These freshly printed dielectric layers were thermally cured at 120 °C for 25 min. For comparison, reference dielectrics were fabricated by spin-coating (4000 rpm, 60 s) thin foils of Sylgard 184 in both 1:10 and 1:20 ratio on top of an ETFE substrate.

4) Stacking the Device: After curing the dielectric, additional PDMS layers were printed to make a wet, glue-like layer, onto which the bottom electrode was placed and gently pressed to bond the layers. Excessive ink was wiped from the surface, and the whole structure was thermally cured at 120 °C for 25 min. After attaching the bottom electrode, the whole device was turned upside down, and the process was repeated to add the top electrode. Again, the device was cured at 120 °C for 25 min to bond the material layers. Finally, the remnants of the PVA layers were dissolved with DI water. A similar process was used to stack the reference devices with the spin-coated PDMS dielectrics, but instead of printing, 1 μl of the ink solution was dispensed with a pipette to form the glue-like layer for bonding the electrodes. A visual presentation of the sensor fabrication process is given in Fig. 1.

B. Characterization

1) Electrical Properties of the Mesh Electrode: The resistance of the Ag NP mesh with increasing layer count was measured with a multimeter. The sheet resistance R_s of each sample was calculated from the measured resistance value with the following formula:

$$R_S = R\frac{w}{l} \tag{1}$$

where l is the line length and w is the width of the conductive line.

2) Cross-Sectional Imaging (FIB SEM): A high-resolution scanning electron microscope with a FIB (Crossbeam 540, Zeiss) was used for the cross-sectional imaging of the devices.

3) Pressure-Capacitance Measurements: To evaluate the sensitivity and pressure range of the fabricated capacitive sensors, both electrodes were connected to the alligator clips of an LCR meter (ST2827A, Sourcetronics, Germany) with copper tape. We used a mechanical tester (TA.XTplus, Stable Micro Systems, UK) with a 10 mm diameter cylindrical probe to apply pressure on the sensor. A small piece of Ecoflex 00-50 (Smooth-On Inc., USA) was placed on the probe tip to mimic tissue-like force source. The measurement setup is shown in Fig. 2.

In each experiment, the mechanical tester lowered the probe in contact with the sensor until a predetermined pressure (force divided by the probe surface area) was reached. The probe was held steady for a given contact time (0 s or 10 s, depending on the experiment), after which the load was removed. Pressures ranging from 0.1 to 50 kPa were tested. While different loads were being applied, the capacitance of the sensor was
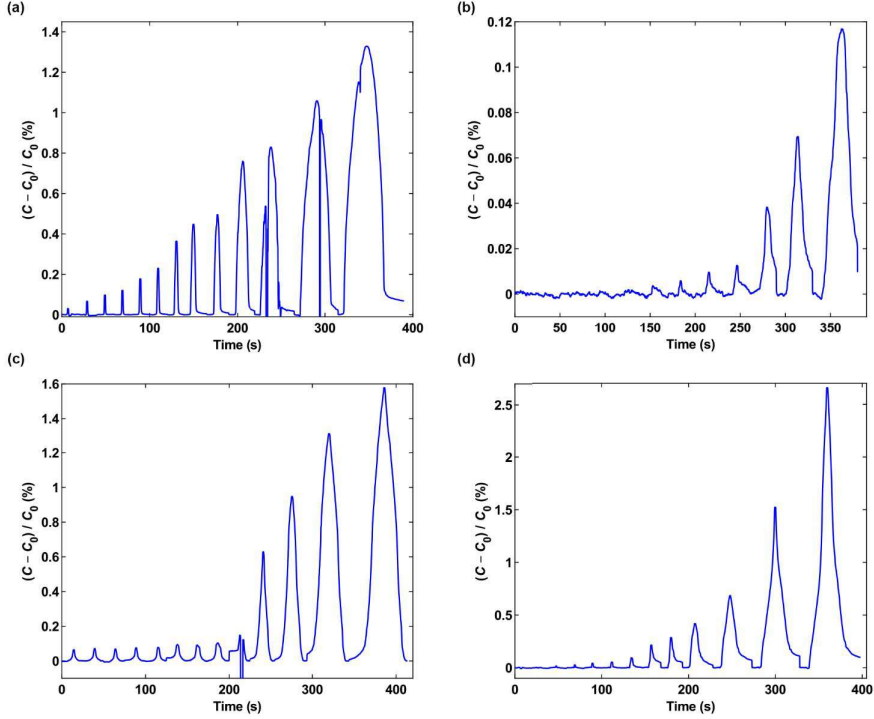
Fig. 5. Relative change in capacitance over time with different pressures from 0.1 kPa to 50 kPa (1 s load) for (a) softer PVA-PDMS sensor, b) stiff PVA-PDMS sensor, c) soft reference sensor, and d) stiff reference sensor.

measured using the LCR meter, with a bias voltage of 1 V at a 10 kHz frequency.

The relative capacitance change $\tilde{C}$ was calculated with:

$$\tilde{C} = \frac{C - C_0}{C}, \tag{2}$$

where C is the measured capacitance, and C_0 is the initial capacitance at zero pressure. The sensitivity S of the sensor was calculated according to the following formula:

$$S = \frac{\Delta \tilde{C}}{\Delta P}, \tag{3}$$

where P is the applied pressure.

III. RESULTS

A. Inkjet Printing Materials on PVA

The print resolution of the Ag NP ink was set to 770 dpi, and the printing parameters were optimized to allow the print to dry for 240 s before printing additional layers, and thus to avoid ink flooding. Ink drying was aided by keeping the plate temperature at 60 °C.

The electrical measurements showed that adding only a few layers of ink to the structure decreased the resistance of the silver prints significantly (Fig. 3). The initial decrease is a lot faster than a simple inverse of the number of layers: the resistance of the 2-layer prints is only 20 % of the resistance of the 1-layer print. Additionally, the resistance values seemed to saturate at approximately 1-2 $\Omega/\square$ after 4-6 layers.

Furthermore, the mechanical toughness of the prints improved when higher ink volumes are used. The 1-layer prints were very fragile and tended to break after the dissolving of the PVA layer, but such behavior was not seen any more in the 2-layer prints. Based on these observations, we chose the 4-layer prints for further experiments.

The spreading of the PDMS ink was affected by the ink volume and drying time between layers. However, well-defined patterns could be obtained at an 876-dpi printing resolution, when a delay of 60 s was used between layers, and the plate temperature was kept at 60 °C.

To obtain a uniform dielectric, 4 layers of PDMS ink were jetted on the PVA film, resulting in an approximately 10 μm thick dielectric layer. Even though the printed dielectric layer was rather thin, we observed it to be surprisingly convenient to handle with tweezers, at least in comparison
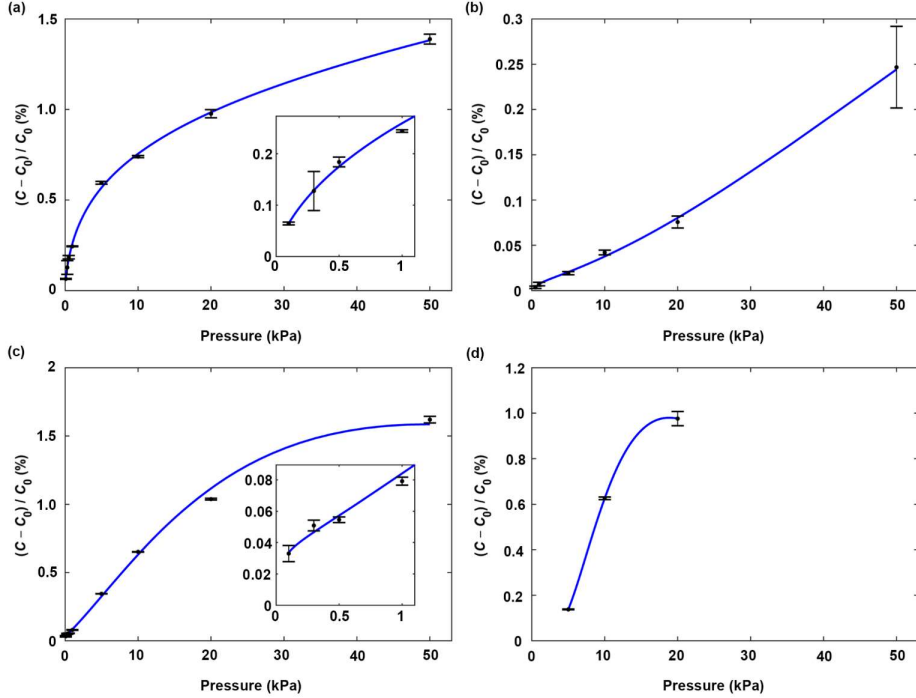
Fig. 6. Relative change in capacitance as a function of the applied pressures from 0.1 kPa to 50 kPa (10 s load) for (a) soft PVA-PDMS sensor, (b) stiff PVA-PDMS sensor, (c) soft reference sensor, (d) stiff reference sensor. Error bars show the standard deviation from the mean of 5 measurements.

to the spin-coated reference dielectric, despite the higher thickness of the latter (15 μm).

The stacked material layers of the sensors having either the spin-coated reference dielectric or the printed dielectric, are shown in Fig. 4. Both the surface SEM images, and cross-sectional images show that in the spin-coated version, the surface of the electrode (Fig. 4a) is more porous than that of the printed sensor (Fig. 4b). This is related to the fabrication process: since the bonding layer between the dielectric and the electrode is printed already before applying the electrode, the PDMS ink is penetrating the porous Ag NP mesh. In contrast, when the reference electrode is first attached to the dielectric, and the bonding layer is formed after that, the PDMS volume is smaller in the interface. This conclusion is supported by the cross-sectional images (Fig. 4c-f): although the mesh electrode in both sensor types is sponge-like, there are more cavities in the electrode of the reference sensor, even though traces of PDMS can be seen in this layer also.

The less porous composition of the printed mesh electrode is considered advantageous, since the electrode and the dielectric layer are more tightly attached to each other. It has been shown earlier, e.g. in [11], [35]–[37] that embedding the conductive material into PDMS is useful for the adhesion between the

material layers, and thus for the mechanical strength of the soft devices.

An interesting feature of the dielectric is seen in the cross-sectional images (Fig. 4c-f): the spin-coated dielectric has a uniform structure, whereas the printed dielectric is clearly porous. We assume this finding to correlate with the observed convenience of handling the printed PDMS foils: the PVA fibers are trapped inside the printed dielectric layer, and are therefore providing additional stiffness and mechanical support for the soft foils.

B. Printed Tactile Sensors

The relative changes in the measured capacitance for each sensor as a function of time are shown in Fig. 5. The probe approached the sensor until the desired pressure was reached, and the load was maintained for 1 s, before the probe was retracted. The probe velocity was set to 0.1 mm/s during both approach and retraction. The applied pressures ranged from 0.1 kPa to 50 kPa.

Fig. 5 shows that the softer sensors (Figs 5a & c) can detect smaller pressures (<1 kPa) than the stiffer sensors (Fig. 5b & d). Furthermore, comparing the response of soft
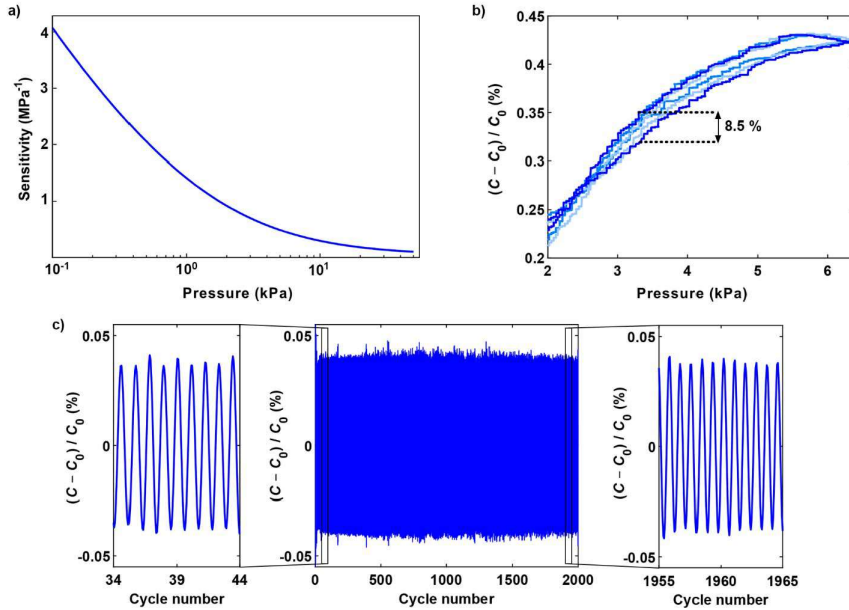
Fig. 7.   a) The calculated sensitivity of the softer printed sensor as a function of applied pressure from 0.1 kPa to 50 kPa, b) the measured response and recovery of the sensor (2-6.4 kPa), maximum hysteresis of 8.5 % shown, c) sensor performance in a cyclic test, where a loading-unloading cycle was repeated for 2000 cycles at a frequency of 0.5 Hz.

PVA-PDMS sensor to the response of the soft reference dielectric sensor, we see that the reference dielectric sensor does not reliably recognize the difference between the applied pressures, until before the pressure reaches 5 kPa (Figs 5a & c).

The sudden changes in the signals of Fig. 5a (20 & 35 kPa) and Fig. 5c (5 kPa) may be a result from the probe mounting, irregularities in the mounting table surface, or other inevitable nonlinearities. It is also possible that the connectors bend under the applied pressure and could cause interference to the signal.

Overall, we take these observations as an evidence that the soft PVA-PDMS sensor has the most desirable pressure response, especially for applications where measuring small pressures is required. The sensitivity of the stiff printed sensor (Fig. 5b) seems to be approximately one-tenth of the measured sensitivities for the rest of the sensors. These results indicate that the presence of the PVA fibers in the dielectric stiffens the dielectric, improving the response of the soft elastomer layer, but diminishing the sensitivity of the already stiff dielectric, especially at low pressures. The stiff reference sensor shows great sensitivity at the largest pressures but is not capable to detect the low pressures as well as the softer ones.

To further study the pressure response of the sensors, we measured the capacitance while the sensors were pressed for 10 s with different pressures varying from 0.1 kPa to 50 kPa. The measurements were repeated at least four times. The results are shown in Fig. 6, where the relative change in

capacitance versus the applied pressure is shown for each sensor type. The stiff reference dielectric sensor broke during the experiments, so the Fig. 6 only shows the portion of measurements completed before the catastrophic failure of the sensor.

In Fig. 6, it can be noticed that the soft PVA-PDMS and the soft reference sensors have a sub-linear response, their sensitivity decreasing with the increment of the applied pressure, while the stiff PDMS-PVA sensor showed a more linear response. For many applications, such a sub-linear response is desirable: it allows distinguishing between small pressures accurately, while the decreasing sensitivity allows also measuring larger pressures.

Of the sensors tested, the soft PVA-PDMS has the highest sensitivity in the small pressure range. Therefore, we calculated the sensitivity for the soft PVA-PDMS sensor, and it is shown in Fig. 7a. The highest sensitivity (4 MPa^{-1}) was achieved with the smallest pressures (0.1 kPa) and this further confirms that the soft PVA-PDMS sensor is suitable for measuring small pressures.

To further study the performance of this sensor, we measured its hysteresis by consecutively applying a load on the sensor and then removing the load. Maximum load applied was 6.4 kPa. In these experiments, the probe speed was set very slow (0.01 mm/s), to avoid dynamic effects from, e.g., viscoelasticity of the materials. The results are shown in Fig. 7b. The hysteresis of the soft PVA-PDMS sensor is low ($\leq$8.5 %) in the measured pressure range. Here, the measured

relative change in capacitance is presented as a function of pressure varying from 2 kPa to approx. 6.4 kPa. With smaller pressures (0-2 kPa), the force probe was not pressing the thin sensor evenly, causing severe signal interference, and the response in that area was therefore discarded from further analysis. Based on these results, we conclude that the sensor has a small, but not insignificant hysteresis, which should be considered in the practical applications of these sensors.

To study the long-term stability of the sensor, we conducted a cyclic experiment, where the probe was set to move sinusoidally up and down to apply load on the sensor. The frequency of the probe was 0.5 Hz. The experiment was conducted so that first a static load was applied on the sensor and then the amplitude of the sinusoidal displacement was chosen so that the load varied approximately 20 kPa peak-to-peak. This cycle was repeated for 2000 times, and the obtained capacitance data were band-pass filtered (lower half-power frequency 0.35 Hz, higher half-power frequency 0.65 Hz) for a better presentation of the dynamic response.

The results of this experiment are presented in Fig. 7c. As seen in Fig. 7c, the printed soft PVA-PDMS sensor can detect the dynamic pressure variation accurately even after 2000 cycles. Based on these results from cyclic experiments, we conclude that the sensor can work reliably and repeatably for long periods of time.

To demonstrate a practical application of our sensors, we attached one of the printed soft sensors to a glove-covered fingertip and recorded the capacitance of the sensor while the finger was touching the underlying surface with varying pressures and hold times. As seen in the recorded video (S1), the sensor can detect the physical interaction with the surrounding environment.

IV. Conclusion

We have developed here a straightforward method for inkjet printing of PDMS based, multilayered electronics. This method is based on material printing on a temporary, supportive PVA layer that is first used to make mesh-like conductive layers, and to tune the properties of the elastomer dielectric, without the need for complex processing or hazardous chemicals. The applicability of this method for fabrication of soft devices was demonstrated by creating tactile pressure sensors.

The results show that this approach can improve the sensor performance significantly: small pressures ($<$1 kPa) can be detected accurately, and the fabricated sensors can detect pressures still at 50 kPa. This range covers most activities of the skin-like systems [38]. Moreover, low hysteresis ($\leq$8.5 %) and long-term repeatability over 2000 cycles were obtained. We also demonstrated here the suitability of these devices for tactile sensing by using them to detect fingertip's physical interaction with its surroundings. Furthermore, the additive and digital nature of the process allows both rapid prototyping and tuning of different sensor configurations. Therefore, our work paves way towards low-cost and easily customizable soft electronics with applications in, for example, wearable devices and smart prosthetics.

References

[1] L. Zhou, J. Fu, Q. Gao, P. Zhao, and Y. He, "All-printed flexible and stretchable electronics with pressing or freezing activatable liquid-metal–silicone inks," *Adv. Funct. Mater.*, vol. 30, no. 3, Jan. 2020, Art. no. 1906683, doi: 10.1002/adfm.201906683.

[2] Y. Chen *et al.*, "Shape-adaptive, self-healable triboelectric nanogenerator with enhanced performances by soft solid–solid contact electrification," *ACS Nano*, vol. 13, no. 8, pp. 8936–8945, Jul. 2019, doi: 10.1021/acsnano.9b02690.

[3] J. Kim, B. Kang, and K. Cho, "Heat-assisted photoacidic oxidation method for tailoring the surface chemistry of polymer dielectrics for low-power organic soft electronics," *Adv. Funct. Mater.*, vol. 29, no. 11, Mar. 2019, Art. no. 1806030, doi: 10.1002/adfm.201806030.

[4] L. Zhu, B. Wang, S. Handschuh-Wang, and X. Zhou, "Liquid metal–based soft microfluidics," *Small*, vol. 16, no. 9, Mar. 2020, Art. no. 1903841, doi: 10.1002/smll.201903841.

[5] Y. Shi, C. Wang, Y. Yin, Y. Li, Y. Xing, and J. Song, "Functional soft composites as thermal protecting substrates for wearable electronics," *Adv. Funct. Mater.*, vol. 29, no. 45, Nov. 2019, Art. no. 1905470, doi: 10.1002/adfm.201905470.

[6] Y. Wang *et al.*, "Tough but self-healing and 3D printable hydrogels for E-skin, E-noses and laser controlled actuators," *J. Mater. Chem. A*, vol. 7, no. 43, pp. 24814–24829, Nov. 2019, doi: 10.1039/C9TA04248B.

[7] H. Shi *et al.*, "Screen-printed soft capacitive sensors for spatial mapping of both positive and negative pressures," *Adv. Funct. Mater.*, vol. 29, no. 23, Jun. 2019, Art. no. 1809116, doi: 10.1002/adfm.201809116.

[8] L. Lo, H. Shi, H. Wan, Z. Xu, X. Tan, and C. Wang, "Inkjet-printed soft resistive pressure sensor patch for wearable electronics applications," *Adv. Mater. Technol.*, vol. 5, no. 1, Jan. 2020, Art. no. 1900717, doi: 10.1002/admt.201900717.

[9] J. Jiang *et al.*, "Flexible piezoelectric pressure tactile sensor based on electrospun BaTiO$_3$/poly(vinylidene fluoride) nanocomposite membrane," *ACS Appl. Mater. Interfaces*, vol. 12, no. 30, pp. 33989–33998, Jul. 2020, doi: 10.1021/acsami.0c08560.

[10] V. Vivekananthan, A. Chandrasekhar, N. R. Alluri, Y. Purusothaman, and S.-J. Kim, "A highly reliable, impervious and sustainable triboelectric nanogenerator as a zero-power consuming active pressure sensor," *Nanosc. Adv.*, vol. 2, no. 2, pp. 746–754, Feb. 2020, doi: 10.1039/C9NA00790C.

[11] S. Kang *et al.*, "Highly sensitive pressure sensor based on bioinspired porous structure for real-time tactile sensing," *Adv. Electron. Mater.*, vol. 2, no. 12, Dec. 2016, Art. no. 1600356, doi: 10.1002/aelm.201600356.

[12] M. Han, J. Lee, J. K. Kim, H. K. An, S.-W. Kang, and D. Jung, "Highly sensitive and flexible wearable pressure sensor with dielectric elastomer and carbon nanotube electrodes," *Sens. Actuators A, Phys.*, vol. 305, Apr. 2020, Art. no. 111941, doi: 10.1016/j.sna.2020.111941.

[13] S. R. A. Ruth, L. Beker, H. Tran, V. R. Feig, N. Matsuhisa, and Z. Bao, "Rational design of capacitive pressure sensors based on pyramidal microstructures for specialized monitoring of biosignals," *Adv. Funct. Mater.*, vol. 30, no. 29, Jul. 2020, Art. no. 1903100, doi: 10.1002/adfm.201903100.

[14] J.-H. Kim, S.-R. Kim, H.-J. Kil, Y.-C. Kim, and J.-W. Park, "Highly conformable, transparent electrodes for epidermal electronics," *Nano Lett.*, vol. 18, no. 7, pp. 4531–4540, Jul. 2018, doi: 10.1021/acs.nanolett.8b01743.

[15] D. E. Backman, B. L. LeSavage, S. B. Shah, and J. Y. Wong, "A robust method to generate mechanically anisotropic vascular smooth muscle cell sheets for vascular tissue engineering," *Macromolecular Biosci.*, vol. 17, no. 6, Jun. 2017, Art. no. 1600434, doi: 10.1002/mabi.201600434.

[16] M. P. Drupitha *et al.*, "Morphology-induced physico-mechanical and biological characteristics of TPU–PDMS blend scaffolds for skin tissue engineering applications," *J. Biomed. Mater. Res. B, Appl. Biomaterials*, vol. 107, no. 5, pp. 1634–1644, Jul. 2019, doi: 10.1002/jbm.b.34256.

[17] X. Shuai *et al.*, "Highly sensitive flexible pressure sensor based on silver nanowires-embedded polydimethylsiloxane electrode with microarray structure," *ACS Appl. Mater. Interfaces*, vol. 9, no. 31, pp. 26314–26324, Jul. 2017, doi: 10.1021/acsami.7b05753.

[18] J. Hwang, S. G. Lee, S. Kim, J. S. Kim, D. H. Kim, and W. H. Lee, "Unveiling viscoelastic response of capacitive-type pressure sensor by controlling cross-linking density and surface structure of elastomer," *ACS Appl. Polym. Mater.*, vol. 2, no. 6, pp. 2190–2198, May 2020, doi: 10.1021/acsapm.0c00193.

[19] Y. Kim, S. Jang, and J. H. Oh, "Fabrication of highly sensitive capacitive pressure sensors with porous PDMS dielectric layer via microwave treatment," *Microelectronic Eng.*, vol. 215, Jul. 2019, Art. no. 111002, doi: 10.1016/j.mee.2019.111002.

[20] E. Thouti *et al.*, "Tunable flexible capacitive pressure sensors using arrangement of polydimethylsiloxane micro-pyramids for bio-signal monitoring," *Sens. Actuators A, Phys.*, vol. 314, Oct. 2020, Art. no. 112251, doi: 10.1016/j.sna.2020.112251.

[21] L. Ma *et al.*, "A highly sensitive and flexible capacitive pressure sensor based on a micro-arrayed polydimethylsiloxane dielectric layer," *J. Mater. Chem. C*, vol. 6, no. 48, pp. 13232–13240, Dec. 2018, doi: 10.1039/C8TC04297G.

[22] X. Zeng *et al.*, "Tunable, ultrasensitive, and flexible pressure sensors based on wrinkled microstructures for electronic skins," *ACS Appl. Mater. Interfaces*, vol. 11, no. 23, pp. 21218–21226, May 2019, doi: 10.1021/acsami.9b02518.

[23] V. Palaniappan *et al.*, "Laser-assisted fabrication of a highly sensitive and flexible micro pyramid-structured pressure sensor for E-skin applications," *IEEE Sensors J.*, vol. 20, no. 14, pp. 7605–7613, Jul. 2020, doi: 10.1109/JSEN.2020.2989146.

[24] X. Wang *et al.*, "Printed conformable liquid metal e-skin-enabled spatiotemporally controlled bioelectromagnetics for wireless multisite tumor therapy," *Adv. Funct. Mater.*, vol. 29, no. 51, Dec. 2019, Art. no. 1907063, doi: 10.1002/adfm.201907063.

[25] P. Wei *et al.*, "Flexible and stretchable electronic skin with high durability and shock resistance via embedded 3D printing technology for human activity monitoring and personal healthcare," *Adv. Mater. Technol.*, vol. 4, no. 9, Sep. 2019, Art. no. 1900315, doi: 10.1002/admt.201900315.

[26] S. Masihi *et al.*, "A novel printed fabric based porous capacitive pressure sensor for flexible electronic applications," in *Proc. IEEE SENSORS*, Oct. 2019, pp. 1–4, doi: 10.1109/SENSORS43011.2019.8956672.

[27] S. Wang *et al.*, "Skin electronics from scalable fabrication of an intrinsically stretchable transistor array," *Nature*, vol. 555, no. 7694, p. 83, 2018, doi: 10.1038/nature25494.

[28] M. Tavakoli *et al.*, "EGaIn-assisted room-temperature sintering of silver nanoparticles for stretchable, inkjet-printed, thin-film electronics," *Adv. Mater.*, vol. 30, no. 29, Jul. 2018, Art. no. 1801852, doi: 10.1002/adma.201801852.

[29] S. Su *et al.*, "Nanoparticle based curve arrays for multirecognition flexible electronics," *Adv. Mater.*, vol. 28, no. 7, pp. 1369–1374, Feb. 2016, doi: 10.1002/adma.201504759.

[30] R. Mikkonen, P. Puistola, I. Jönkkäri, and M. Mäntysalo, "Inkjet-printable polydimethylsiloxane for all-inkjet-printed multilayered soft electrical applications," *ACS Appl. Mater. Interfaces*, vol. 12, no. 10, pp. 11990–11997, 2020, doi: 10.1021/acsami.9b19632.

[31] R. Mikkonen and M. Mantysalo, "Inkjettable, polydimethylsiloxane based soft electronics," in *Proc. IEEE Int. Conf. Flexible Printable Sensors Syst. (FLEPS)*, Aug. 2020, pp. 1–3, doi: 10.1109/FLEPS49123.2020.9239558.

[32] A. Miyamoto *et al.*, "Inflammation-free, gas-permeable, lightweight, stretchable on-skin electronics with nanomeshes," *Nature Nanotechnol.*, vol. 12, no. 9, pp. 907–913, Sep. 2017, doi: 10.1038/nnano.2017.125.

[33] S. Lee *et al.*, "Nanomesh pressure sensor for monitoring finger manipulation without sensory interference," *Science*, vol. 370, no. 6519, pp. 966–970, Nov. 2020, doi: 10.1126/science.abc9735.

[34] Y. Wang *et al.*, "A durable nanomesh on-skin strain gauge for natural skin motion monitoring with minimum mechanical constraints," *Sci. Adv.*, vol. 6, no. 33, Aug. 2020, Art. no. eabb7043, doi: 10.1126/sciadv.abb7043.

[35] Q. Huang, K. N. Al-Milaji, and H. Zhao, "Inkjet printing of silver nanowires for stretchable heaters," *ACS Appl. Nano Mater.*, vol. 1, no. 9, pp. 4528–4536, Aug. 2018, doi: 10.1021/acsanm.8b00830.

[36] K.-H. Jung, J. Kim, B.-G. Park, C.-J. Lee, H.-J. Sung, and S.-B. Jung, "Fabrication of ag circuit embedded in PDMS substrate and its mechanical and electrical property with variations of photonic energy," *J. Alloys Compounds*, vol. 748, pp. 898–904, Jun. 2018, doi: 10.1016/j.jallcom.2018.03.171.

[37] H. Fan *et al.*, "Prepolymerization-assisted fabrication of an ultra-thin immobilized layer to realize a semi-embedded wrinkled AgNW network for a smart electrothermal chromatic display and actuator," *J. Mater. Chem. C*, vol. 5, no. 37, pp. 9778–9785, 2017, doi: 10.1039/C7TC03358C.

[38] Y. Zang, F. Zhang, C.-A. Di, and D. Zhu, "Advances of flexible pressure sensors toward artificial intelligence and health care applications," *Mater. Horizons*, vol. 2, no. 2, pp. 140–156, 2015, doi: 10.1039/C4MH00147H.

Riikka Mikkonen received the B.Sc. and M.Sc. degrees in electrical engineering from the Tampere University of Technology, Tampere, Finland, in 2015 and 2017, respectively. She is currently pursuing the D.Sc. degree in electronics with Tampere University, Tampere. Her research interests include printed electronics, especially printable materials, and their applications for soft and flexible devices.

Anastasia Koivikko received the B.Sc. and M.Sc. degrees in biomedical engineering from the Tampere University of Technology, Tampere, Finland, in 2015 and 2017, respectively, where she is currently pursuing the D.Sc. degree. In 2019, she worked a Guest Researcher with the Max Planck Institute for Intelligent Systems. Her research interests include fabrication of soft robots, especially soft grippers and integration of stretchable sensors into soft robotic systems.

Tiina Vuorinen received the B.Sc. and M.Sc. degree in electrical engineering from the Tampere University of Technology, Tampere, Finland, in 2013 and 2014, respectively. She is currently pursuing the D.Sc. degree in electronics with Tampere University, Tampere. Her research interests include printed electronics, materials in electronics and conformable electronics.

Veikko Sariola (Member, IEEE) received the D.Sc. (Tech.) degree in electrical engineering from Aalto University, Finland, in 2012. From 2013 to 2015, he was a Postdoctoral Researcher with Carnegie Mellon University. In 2016, he was appointed as a Research Fellow from the Academy of Finland. He is currently an Associate Professor of Biomedical Microsystems with Tampere University, Finland. His current research interests include bio-inspired materials and robotics.

Matti Mäntysalo (Member, IEEE) received the M.Sc. and D.Sc. (Tech.) degrees in electrical engineering from the Tampere University of Technology, Tampere, Finland, in 2004 and 2008, respectively. From 2011 to 2012, he was a Visiting Scientist with the iPack Vinn Excellence Center, School of Information and Communication Technology, KTH Royal Institute of Technology, Stockholm, Sweden. He is currently a Professor of Electronics Materials and Manufacturing with Tampere University. His current research interests include printed electronics materials, fabrication processes, stretchable electronics, and especially the integration of printed electronics with silicon-based technology (hybrid systems). He was a recipient of the Academy Research Fellow Grant from the Academy of Finland from 2015 to 2020.